Aalborg Universitet

AALBORG UNIVERSITY
DENMARK

Understanding and Expanding the Weldability of Plastics

Juhl, Thomas Brokholm

Publication date:
2013

Document Version
Publisher's PDF, also known as Version of record

Link to publication from Aalborg University

Citation for published version (APA):
Juhl, T. B. (2013). *Understanding and Expanding the Weldability of Plastics*. Institut for Mekanik og Produktion, Aalborg Universitet.

General rights
Copyright and moral rights for the publications made accessible in the public portal are retained by the authors and/or other copyright owners and it is a condition of accessing publications that users recognise and abide by the legal requirements associated with these rights.

- Users may download and print one copy of any publication from the public portal for the purpose of private study or research.
- You may not further distribute the material or use it for any profit-making activity or commercial gain
- You may freely distribute the URL identifying the publication in the public portal -

Take down policy
If you believe that this document breaches copyright please contact us at vbn@aub.aau.dk providing details, and we will remove access to the work immediately and investigate your claim.

Downloaded from vbn.aau.dk on: May 04, 2023

UNDERSTANDING AND EXPANDING THE WELDABILITY OF PLASTICS

THOMAS BROKHOLM JUHL

PHD THESIS

Internal Report no: 96
November 2013

Materials Science and Engineering Group
Department of Mechanical and Manufacturing Engineering
Faculty of Engineering and Science
Aalborg University
Denmark

PhD Thesis
Department of Mechanical and Manufacturing Engineering
Fibigerstræde 16
9220 Aalborg Ø
Telephone (+45) 9940 7117
Fax (+45) 9815 3030
http://www.m-tech.aau.dk

AALBORG UNIVERSITY
DENMARK

Title:

Understanding and Expanding the Weldability of Plastics

Program:

Mechanical Engineering

Period:

August 1, 2010 to July 31, 2013

Student:

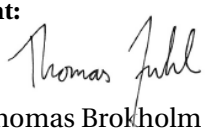

Thomas Brokholm Juhl

Supervisor:

Jesper deClaville Christiansen

Total page count:
170

Enclosures:

- One CD
- *"Investigation on High-Strength Laser Welds of Polypropylene and High-Density Polyethylene"* [Juhl et al., 2013a]
- *"Mechanical Testing of Polystyrene/Polystyrene Laser Welds"* [Juhl et al., 2013b]
- *"Predicting the Laser Weldability of Dissimilar Polymers"* [Juhl et al., 2013]

This thesis has been submitted for assessment in partial fulfillment of the PhD degree. The thesis is based on the submitted or published scientific papers which are listed above. Parts of the papers are used directly or indirectly in the extended summary of the thesis. As part of the assessment, co-author statements have been made available to the assessment committee and are also available at the Faculty. The thesis is not in its present form acceptable for open publication but only in limited and closed circulation as copyright may not be ensured.

PREFACE

This PhD thesis has been submitted to the Faculty of Engineering and Science, Aalborg University, Denmark, to fulfill the requirements for obtaining the PhD degree. The PhD program was commenced on August 1, 2010 and carried out at the Department of Mechanical and Manufacturing Engineering, Aalborg University, under the Mechanical Engineering Doctoral Program. The project was partially financed by the Danish Council for Strategic Research, under the Danish Agency for Science, Technology and Innovation. The financing was granted through the Danish innovation consortium "*Expanding the Weld Compatibility of Plastics*". The consortium consisted of: Coloplast A/S, Novo Nordisk A/S, Danish Technological Institute, FORCE Technology, University of Copenhagen, and Aalborg University [polymerwelding.com, 2013].

Reading Guide

The report consists of a body with chapters numbered 1 to 15. Figures and tables are consecutively numbered in order of chapter numbers. Book, website, and article sources are referred to in the text by the author-date method of style, also known as the Harvard-method of referencing. The full references are presented in the bibliography on page 143. All internal cross-references are written in red, while citations are blue.

The body of the report is structured according to the AIMRAD-method (Abstract, Introduction, Methods, Results, And Discussion), thus it is written as a scientific report addressed to collaborators within the consortium and others interested in weldability of plastics. The AIMRAD structure is divided into 5 parts:

I Introduction: The thesis is introduced with three chapters. Chapter 1 presents the project background, while industrial and scientific challenges and perspectives are discussed in chapter 2. The introduction concludes in a problem statement in chapter 3.

II Review of Polymer Welding: Three chapters on the background theory of welding technology and polymer physics. If these subjects are well-known to the reader, chapters 4 and 5 may be skipped. Finally, chapter 6 is a thorough survey of literature of the overall subject: Polymer welding.

III Materials and Methods: Based upon the knowledge provided in part II, three main hypotheses are formed and presented in chapter 7. In the chapters 8 and 9, the materials and methods employed to test the hypotheses are presented.

IV Results and Discussion: The three hypotheses each constitute a peer-reviewed journal paper presented in chapters 10, 11, and 12, while an overall discussion is provided in chapter 13.

V Concluding Remarks: The overall conclusions and possible future perspectives are presented in chapters 14 and 15, respectively.

Furthermore, a CD with the following content is enclosed:

Thesis: An electronic edition of the report in pdf-format, where references are marked as hyperlinks making quick navigation throughout the report possible.

Papers: The publications from chapters 10, 11, and 12 in case the font size in the printed version is too small.

Matlab functions and scripts: Routines and functions used in various examples throughout the report are attached.

Materials: All materials utilized are presented in detail, including data sheets, DSC, and rheometry results.

Welding and mechanical testing: Raw data from the laser welding experiments conducted at Coloplast and related mechanical testing results.

EXPAND program: The developed software from chapter 13 is attached in a compiled version (EXPAND.exe) as well as the C# source code.

Acknowledgments

In connection with this work, I wish to express my sincere gratitude to several people. I want to emphasize a few who have contributed with ideas and inspiration. Thanks to:

- My supervisor, Professor, PhD, Jesper de Claville Christiansen, for providing me with the opportunity to conduct this work, and for his guidance, advice, and patience during the project period.
- My colleagues and co-workers in the research group of Material Science and Engineering, particularly thanks to: Associate Professor, PhD, Erik Appel Jensen; Post doc, PhD, Catalina-Gabriela Sanporean; PhD, Rasmus Klitkou; and the assistant engineers in the department.
- The Danish Council for Strategic Research under the project "Expanding the Weld Compatibility of Plastics" for financial support. Also, thanks to all the partners within the consortium – none mentioned, none forgotten – for good collaboration and knowledge sharing.
- Professor, PhD, Ronald G. Larson, Chemical Engineering, University of Michigan, Ann Arbor, USA, for hosting me as a Visiting Scholar for 8 months. Also thanks to the remainder of the group, especially: PhD student, MSc, Priyanka Desai, and Post doc, PhD, Indranil Saha Dalal. Moreover, I would like to thank all the wonderful and inspiring people I met in Ann Arbor for a memorable experience.
- Finally, thanks to my friends, family, and girlfriend for their support and for coping with me throughout the project period.

NOMENCLATURE

Throughout the thesis, conventional calculus and linear algebra notations are used, and SI units and IUPAC nomenclature are preferred. Below, only important and non-trivial nomenclature and abbreviations relevant for general understanding are presented.

Abbreviations

ABS	Acrylonitrile butadiene styrene
ADCB	Asymmetric double cantilever beam
CB	Carbon black
CDT	Corona discharge treatment
CFD	Computational fluid mechanics
COC	Cyclic olefin copolymer
DCB	Double cantilever beam
DOP	Degree of polymerization
DMA	Dynamic mechanical analysis
DSC	Differential scanning calorimetry
DTI	Danish Technological Institute
EVA	Ethylene vinyl acetate
FH	Flory-Huggins
hhPP	Head-to-head polypropylene
HDPE	High density polyethylene
iPP	Isotactic polypropylene
IPC	Impact propylene copolymer
IR	Infra red
LCT	Lower critical temperature
LDPE	Low density polyethylene
LLDPE	Linear low density polyethylene
LTW	Laser transmission welding
NR	Neutron reflection
m-	Metallocene
MC	Monte carlo
MD	Molecular dynamics
MFI	Melt flow index
PA	Polyamide (Nylon)
PBT	Poly(butylene terephthalate)
PC	Polycarbonate
PDI	Polydispersity index
PE	Polyethylene
PEO	Polyethylene oxide
PET	Poly(ethylene terephthalate)
PLA	Polylactic acid
PMMA	Poly(methyl methacrylate) (Plexiglas)

POM	Polyoxymethylene
PP	Polypropylene
PS	Polystyrene
PTFE	Polytetrafluoroethylene (Teflon)
PVC	Polyvinyl chloride
PVDC	Polyvinylidene chloride
SAN	Styrene-acrylonitrile
SANS	Small angle neutron scattering
SAXS	Small angle X-ray scattering
SEM	Scanning electron microscope
SIMS	Secondary ion mass spectrometry
TEM	Transmission electron microscopy
TGA	Thermal gravimetric analysis
TTLW	Through transmission laser welding
UCT	Upper critical temperature
UHMW	Ultra high molecular weight
w%	Weight percent
WBL	Weak boundary layer
z-	Ziegler-Natta

Greek symbols

α [m^2/s]	Thermal diffusivity (eq. 4.8 on page 35)
α [mm^{-1}]	Absorption constant (eq. 4.7 on page 31)
γ [J/m^2]	Surface tension/energy (sec. 6.2 on page 59)
δ [$MPa^{1/2}$]	Solubility parameter, Hildebrand or Hansen (sec. 6.3.1 on page 63)
Δ [mm]	Razor thickness (eqs. 6.37 and 6.39 on page 79)
ϵ	True strain
ζ [kg/s]	Monomeric friction coefficient (sec. 5.3 on page 44)
η_0 [Pa· s]	Zero shear viscosity (eq. 5.35 on page 48)
κ	Absorption coefficient (eq. 4.7 on page 31)
λ [W/(m· K)]	Thermal conductivity (eq. 4.8 on page 35)
λ_{laser} [nm]	Laser wavelength (eq. 4.7 on page 31)
ν	Poisson's ratio
ρ [kg/m^2]	Density (tab. 5.1 on page 54)
σ_U [MPa]	Ultimate stress (eq. 3.9 on page 16)
τ_0 [s]	Rouse relaxation time for a single Kuhn segment (eq. 5.29 on page 46)
τ_e [s]	Equilibration time (eq. 5.28 on page 46)
τ_R	Longest Rouse relaxation time for whole chain (eq. 5.27 on page 46)
τ_{rep} [s]	Reptation time (eq. 5.31 on page 47)
φ	Volume fraction (eq. 6.13 on page 64)
φ_c	Critical concentration (eq. 6.17 on page 66)
χ	Flory-Huggins interaction parameter (sec. 6.3.1 on page 63)
χ_c	Critical interaction parameter (eq. 6.18 on page 66)

Latin symbols

a [nm]	Tube diameter (eq. 5.17 on page 43)
a [mm]	Crack length (eqs. 6.37 to 6.40 on page 79)
a [mm]	Optical inter-penetration depth (eq. 4.4 on page 30)
A	Absorbance
b [nm]	Statistical segment length (eq. 5.10 on page 41)
b_n [nm]	Effective random walk step (eq. 5.9 on page 41)
b_K [nm]	Kuhn segment length (eq. 5.11 on page 42)
c [w%]	Concentration (eq. 4.2 on page 30)
c [J/(kg·K)]	Specific heat capacity (eq. 4.8 on page 35)
C_∞	Characteristic ratio (eq. 5.4 on page 40)
d_beam [mm]	Laser beam waist (fig. 4.6 on page 31)
D_m [m^2/s]	Mutual diffusion coefficient (eqs. 5.49 and 5.50 on page 52)
D_s [m^2/s]	Self-diffusion coefficient (eq. 5.46 on page 51)
E [MPa]	Elastic modulus or Young's modulus (eqs. 6.37 and 6.39 on page 79)
$E_\mathrm{a,dec}$ [kJ/mol]	Activation energy of decomposition (sec. 6.1.2 on page 59)
$E_\mathrm{a,diff}$ [kJ/mol]	Activation energy of diffusion (eqs. 5.40 and 5.41 on page 50)
E_line [J/mm]	Laser line energy, $E_\mathrm{line} = P_\mathrm{laser}/v\mathrm{laser}$
ΔG_mix [J]	Gibbs free energy of mixing (eq. 6.13 on page 64)
G_Ic [J/m^2]	Critical energy release rate (eqs. 6.37 and 6.39 on page 79)
G_N^0 [MPa]	Plateau modulus (eq. 5.16 on page 43)
h [mm]	Cantilever thickness (eqs. 6.37 to 6.40 on page 79)
ΔH_mix [J]	Enthalpy of mixing (eq. 6.13 on page 64)
j	Number of backbone bonds per monomer, $j = n/N$ (eq. 5.6 on page 41)
k_B [J/K]	Boltzmann's constant, $k_\mathrm{B} = 1.381 \cdot 10^{-23}$ J/K
K_c	Critical stress intensity factor (eq. 6.29 on page 75)
K_g	Geometric constant, $K_\mathrm{g} = 0.816$ (eq. 5.7 on page 41)
l [Å]	Average backbone bond length, (tab. 5.1 on page 54)
$l(t)$ [nm]	Minor chain length (eq. 5.52 on page 52)
L [nm]	Contour length (eq. 5.7 on page 41)
L_e [nm]	Contour length between entanglements (tab. 5.1 on page 54)
n	Number of backbone bonds (eq. 5.4 on page 40)
n	Refractive index (eq. 4.1 on page 28)
N	Degree of polymerization, M/M_0
N	Number of bonds (eq. 5.1 on page 39)
N_K	Number of Kuhn segment, M/M_K (eq. 5.12 on page 42)
N_e	Number of entanglement in one polymer chain, $N_\mathrm{e} = M/M_\mathrm{e}^\mathrm{G}$
$N_\mathrm{K,e}$	Number of Kuhn segments between entanglements (tab. 5.1 on page 54)
N_A [mol^{-1}]	Avogadro's number, $N_\mathrm{A} = 6.022 \cdot 10^{23}$ mol^{-1}
M [g/mol]	Molecular weight, used when monodispersity is assumed
M_0 [g/mol]	Molecular weight of monomer (tab. 5.1 on page 54)
M_K [g/mol]	Molecular weight of Kuhn segment (tab. 5.1 on page 54)

M_e^G [g/mol]	Molecular weight between entanglements, Graessley's definition (eq. 5.16 on page 43)
M_c [g/mol]	Critical molecular weight (eq. 5.19 on page 44)
M_n [g/mol]	Number average molar mass
M_w [g/mol]	Weight average molar mass
p	Number of bridges (eq. 6.28 on page 71)
p [Å]	Packing length (eq. 5.18 on page 44)
P_{laser} [W]	Laser output power
$\vec{r}_i$	Individual bond vector (eq. 5.1 on page 39)
R [J/(mol · K)]	Gas constant, $R = 8.314$ J/(mol · K)
R	Reflectivity (eq. 4.1 on page 28)
$\vec{R}$ [nm]	End-to-end vector (eq. 5.1 on page 39)
$\langle \vec{R}^2 \rangle$ [nm^2]	Root mean square end-to-end vector (eq. 5.2 on page 39)
$\langle \vec{R}^2 \rangle_0$ [nm^2]	Actual RMS end-to-end vector (eq. 5.4 on page 40)
R_g [nm]	Radius of gyration (eq. 5.6 on page 41)
$R_{g,e}$ [nm]	Radius of gyration of entangled segment (tab. 5.1 on page 54)
S	Scattering
S [J/m^2]	Spreading coefficient (eq. 6.3 on page 60)
ΔS_{mix} [J/K]	Entropy of mixing (eq. 6.13 on page 64)
t [s]	Time
t_{molten} [s]	Time in molten state during welding
T	Transmittance
T [K] or [°C]	Temperature
T_d [°C]	Decompostion temperature (sec. 6.1.2 on page 59)
T_f [°C]	Flowing temperature (tab. 5.1 on page 54)
T_g [°C]	Glass transition temperature (fig. 9.10 on page 95)
T_m [°C]	Melting temperature (fig. 9.9 on page 95)
T_c [°C]	Crystallization temperature (fig. 9.10 on page 95)
v_{laser} [mm/s]	Translational weld speed
V_m [cm^3/mol]	Molar volume (sec. 6.3.1 on page 63)
w [nm]	Inter-penetration depth (eq. 6.23 on page 68)
w_∞ [nm]	Equilibrium inter-penetration depth (sec. 6.3.3 on page 68)
W_A [J/m^2]	Work of adhesion (eq. 6.2.2 on page 61)
X [nm]	Inter-diffusion depth, $X_\infty = 0.81 R_g$ (eq. 3.5 on page 14)
$y_{1/e}$ [mm]	Beam waist in y direction (eq. 4.14 on page 37)
Z	Number of entanglements, M/M_K (eq. 5.17 on page 43)
$z_{1/e}$ [mm]	Beam waist in z direction, equal to a (eq. 4.14 on page 37)

EXECUTIVE SUMMARY

Polymer welds and polymer interfaces are ubiquitous. Polymer welds are not only present in structural elements of consumer products, but are also found in, e.g., paints, injection molded parts, and self-healing materials. This thesis is an attempt to understand the strength development at these polymer weld interfaces. Another purpose is to understand the weld compatibility of plastics. This means to provide an explanatory model of the weld chart presented in table 1.2 on page 5. The hope is to exploit the attained knowledge and understanding in order to expand and improve the weldability of plastics in general.

A comprehensive literature survey suggests that the main mechanism responsible for strength in polymer weld interfaces is *diffusion and entanglements*. This mechanism only comes to pass if the two polymer surfaces intended for welding are sufficiently *melted*, leading to *wetting*, which again allows *diffusion and entanglements* in case the two polymers are sufficiently *compatible*, as illustrated in figure 6.1 on page 58. Additionally, maximum strength is achieved when the polymer-polymer inter-penetration depth exceeds one radius of gyration (R_g), which occurs after one reptation time (τ_{rep}).

Therefore, based on the survey of literature, the reptation time is determined for HDPE, PP, PS, and POM. For the selected materials, see table 8.1 on page 87, at relatively high temperatures, i.e., above 200 °C, the reptation time is in the millisecond range, which is much shorter than the usual processing time of, e.g., laser welding [Juhl et al., 2013a,b]. Thus, when welding at relatively high temperatures, the dynamics of diffusion can be neglected.

Regarding the weld compatibility of polymers, the following hypothesis is proposed: The equilibrium inter-penetration depth (w_∞), the green area in figure 6.1, should be as wide as possible, while the largest mesh size (a_{max}) of the two welded polymers should be small to ensure entanglements. This means that a large w_∞ / a_{max} ratio should lead to weldability. w_∞ is estimated using Helfand's theory:

$$w_\infty = 2\sqrt{\frac{b_1^2 + b_2^2}{12\chi_{12}}}$$

$$\chi_{12} = \frac{V_m\left[(\delta_{D1} - \delta_{D2})^2 + \frac{1}{4}(\delta_{P1} - \delta_{P2})^2 + \frac{1}{4}(\delta_{H1} - \delta_{H2})^2\right]}{RT},$$

where the interaction parameter (χ_{12}) is given in terms of Hansen solubility parameters presented in the table below.

Polymer	**HDPE**	**PP**	**PMMA**	**PS**	**PBT**	**PC**
δ_D [MPa$^{1/2}$]	11.9	17.2	18.8	18.2	20.3	19.9
δ_P [MPa$^{1/2}$]	5.5	3.1	12.8	9.0	5.3	10.7
δ_H [MPa$^{1/2}$]	3.8	2.2	4.2	2.7	6.1	2.0

The temperature of relevance in the model is the highest crystallization or glass transition temperature (T_c) of the two welded polymers. This was chosen since the polymer melt at a cooler temperature than this is frozen in, therefore prohibiting molecular inter-diffusion. Other data relevant for the w_∞ / a_{max} calculation is presented on the next page.

	PP	PMMA	PS	PBT	PC	a [nm]	b [Å]	T_c [°C]	V_m [cm^3/mol]
HDPE	0.89	0	0	0	0	3.6	5.64	119.2	32.9
PP		0.16	0.13	0	0	6.9	5.25	118.3	49.1
PMMA			1.04	0.05	1.12	7.0	6.24	111.0	86.5
PS				0	0.99	8.5	6.89	100.4	98.0
PBT					1.06	3.5	5.70	201.6	143.5
PC						3.8	10.7	140.2	174.4

In addition, the weldability is experimentally investigated for the six polymers. Transmission laser welding (TLW), see figure 4.2 on page 26, is selected as the joining process and 0.4 w% carbon black is utilized as an absorber. In the left part of the table above, the relative weld strength is presented. The relative weld strength is defined as the weld strength of the dissimilar polymer combination divided by the strength of the weakest of the two welded polymers. In the figure below this is plotted against the w_∞/a_{max} ratio.

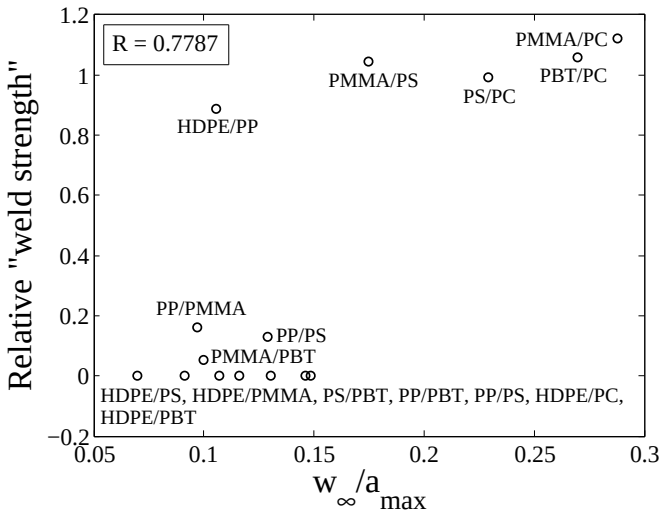

It is clear that w_∞/a_{max} correlates with the relative weld strength and that weldability is obtained when $w_\infty/a_{max} > 0.15$ with only HDPE/PP not fulfilling this threshold [Juhl et al., 2013]. Based on this model, the program EXPAND is developed. The program can predict weldability based on the above mentioned material properties. From a technological point of view, this approach to polymer weldability may ease the material selection process and inspire design engineers to combine polymers not yet considered. Also, from a scientific viewpoint, the findings are interesting for novel research areas, e.g., smart materials and self-healing materials.

In conclusion, the understanding of polymer welding and especially polymer laser welding is increased. The knowledge of polymer weldability is also expanded, i.e., it is now possible to predict the weldability of two polymers based on their chemical and physical properties, instead of a trivial trial-and-error approach.

SAMMENFATNING

Plast-svejsninger og polymer-grænseflader findes overalt. Plast-svejsninger findes ikke kun i strukturelle dele af større produkter, men findes også i f.eks. malinger, sprøjtestøbte emner og selv-helende materialer. Formålet med denne afhandling er netop at forstå mekanismerne bag styrkeudviklingen i polymer-svejseflader. Et andet formål er at opnå forståelse af plastmaterialers svejsekompatibilitet, hvilket indebærer at foreslå en forklaringsmodel bag svejseskemaet fra tabel 1.2. Håbet er at udnytte den opnåede viden og forståelse til at udvide og forbedre svejsbarheden af plast generelt.

Et omfattende litteraturstudie antyder, at *diffusion og sammenfiltring* har hovedansvaret for den mekaniske styrke over to polymer-grænseflader. Dette er dog kun muligt, hvis de to polymer-overflader, som ønskes svejst, er tilstrækkeligt *smeltede*, hvilket fører til *vædning*. Alt dette tillader *diffusion og sammenfiltring*, såfremt de to polymerer er tilstrækkeligt kompatible, som illustreret på figur 6.1. Derudover er maksimal styrke opnået, når polymererne har inter-diffunderet en dybde svarende til en gyrationsradius (R_g), hvilket sker efter én reptationstid (τ_{rep}).

Grundet konklusionerne af litteraturstudiet er det besluttet at bestemme reptationstiden for HDPE, PP, PS og POM. For de valgte materialer, se tabel 8.1, ved relativt høje temperaturer, dvs. over 200 °C, er reptationstiden i millisekund-området, hvilket er meget kortere end den normale procestid af f.eks. lasersvejsning [Juhl et al., 2013a,b]. Når der svejses ved relativt høje temperaturer, kan diffusionsdynamikken derfor negligeres.

Mht. svejsbarheden af plast er følgende hypotese foreslået: Ligevægts-inter-penetrationsdybden (w_∞), det grønne område på figur 6.1, skal være så bredt som muligt, mens den største net-størrelse (a_{max}) af de to svejste polymerer skal være så lille som muligt for at sikre sammenfiltringer. Dette betyder, at et stort w_∞/a_{max}-forhold burde medføre svejsbarhed. w_∞ estimeres vha. Helfands teori:

$$w_\infty = 2\sqrt{\frac{b_1^2 + b_2^2}{12\chi_{12}}}$$

$$\chi_{12} = \frac{V_m\left[(\delta_{D1} - \delta_{D2})^2 + \frac{1}{4}(\delta_{P1} - \delta_{P2})^2 + \frac{1}{4}(\delta_{H1} - \delta_{H2})^2\right]}{RT},$$

hvor interaktionsparameteren (χ_{12}) er bestemt vha. Hansens opløselighedsparametre, som er vist i tabellen nedenfor.

Polymer	**HDPE**	**PP**	**PMMA**	**PS**	**PBT**	**PC**
δ_D [MPa$^{1/2}$]	11.9	17.2	18.8	18.2	20.3	19.9
δ_P [MPa$^{1/2}$]	5.5	3.1	12.8	9.0	5.3	10.7
δ_H [MPa$^{1/2}$]	3.8	2.2	4.2	2.7	6.1	2.0

Den relevante temperatur i modellen er den højeste krystallisations- eller glastransitionstemperatur (T_c) af de to svejste polymerer. Dette er valgt, da polymersmelten ved denne temperatur indefryser, hvilket forhindrer molekylær interdiffusion. Data til beregning af w_∞/a_{max}-forholdet er præsenteret på næste side.

	PP	PMMA	PS	PBT	PC	a [nm]	b [Å]	T_c [°C]	V_m [cm^3/mol]
HDPE	0.89	0	0	0	0	3.6	5.64	119.2	32.9
PP		0.16	0.13	0	0	6.9	5.25	118.3	49.1
PMMA			1.04	0.05	1.12	7.0	6.24	111.0	86.5
PS				0	0.99	8.5	6.89	100.4	98.0
PBT					1.06	3.5	5.70	201.6	143.5
PC						3.8	10.7	140.2	174.4

Derudover er svejsbarheden eksperimentelt undersøgt for de seks polymerer. Transmissionslasersvejsning, se figur 4.2, er udvalgt som sammenføjningsprocessen og 0.4 % carbon black er benyttet som absorber. I den ovenstående tabels venstre side ses den relative svejsestyrke. Den relative svejsestyrke er defineret som styrken af den uens kombination divideret med styrken af det svageste af de to modermaterialer svejst med sig selv. Nedenfor er den relative svejsestyrke plottet som funktion af $w_\infty/a_{\max}$-forholdet.

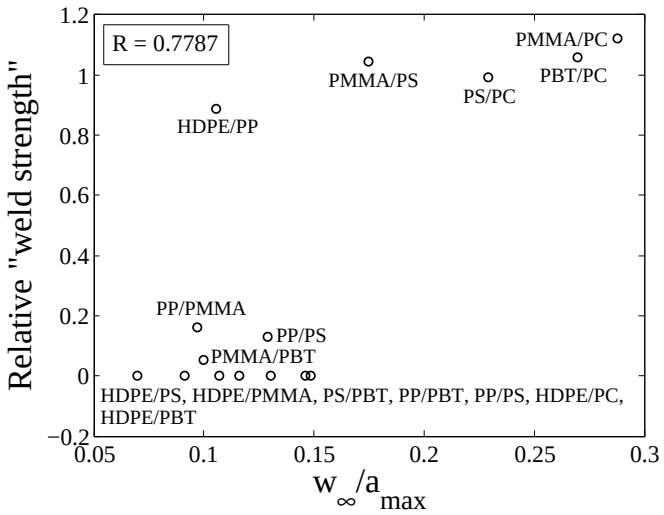

Det står klart, at $w_\infty/a_{\max}$ korrelerer med den relative svejsestyrke og at svejsbarhed opnås, når $w_\infty/a_{\max} > 0.15$, hvor kun HDPE/PP ikke opfylder denne tærskelværdi [Juhl et al., 2013]. På denne baggrund er programmet EXPAND udviklet. Programmet kan forudsige svejsbarhed baseret på de førnævnte materialeegenskaber. Denne tilgang kan fra en teknologisk synsvinkel lette materialevalgsprocessen samt inspirere designere til nye plastkombinationer. Ydermere kan resultaterne fra et videnskabeligt perspektiv være interessante for nye forskningsområder, såsom smart materials og selv-helende materialer.

Det kan konkluderes, at forståelsen af plastsvejsning og især lasersvejsning af plast er forbedret. Generelt er indsigten i plasts svejsbarhed forøget, hvilket betyder, at det nu er muligt at forudsige svejsbarheden af to polymerer på baggrund af deres kemiske og fysiske egenskaber fremfor en triviel trial-and-error tilgang.

CONTENTS

PART I

INTRODUCTION

CHAPTER 1

PROJECT BACKGROUND

Polymer interfaces and polymer welds are ubiquitous. Polymer welds are found in large polymeric piping systems with diameters of several meters to micro or even nano-sized biomedical devices [Rotheiser, 2009; Zhou, 2008]. In principle, the heat welding process is a joining technique where workpieces are heated above their melting or softening point, joint, then cooled, and (if done correctly) a strong joint occurs. This is illustrated in figure 6.1 on page 58. The welding principle, however, does not only apply to joining of two structural elements in a product; welding is also important in order to understand each of the following subjects:

Paints: When solvent evaporates, latex particles coalesce and the polymer chains must inter-diffuse a distance of a radius of gyration to secure a fully healed paint [Wool, 2005].

Injection molding: In complex mold geometries, weld lines occur when the polymer melt front is split and then reunites later in the filling process. Weld lines in injection molding are minimized by computer-aided mold design and optimizing melt or tool temperatures [Chien et al., 2004; Debondue et al., 2004; Yokomizo et al., 2013]. Also co-extrusion and co-injection molding of dissimilar polymers are of interest [Jiang et al., 2009; Zhang et al., 2012b].

Self-healing materials: The concept of self-healing materials is essentially an internal welding in the material bulk or interface [Wool, 2001, 2008].

Polymer blends: When toughening brittle polymers like nylon, PS or epoxy resins with elastomers, internal welding and entanglements is necessary for achieving optimum properties [Swallowe, 1999].

Sintering: Sintering of polymer particles is also a welding process, e.g., 3D printers operating with thermoplastics. In this process particles coalesce forming a solid body. This technology is utilized by the Danish company Blueprinter [blueprinter.dk, 2013].

In a broader context, this project is an attempt to understand the mechanisms for development of strength in a welded joint. Intuitively, the material influence is crucial for the weld strength development. For instance, if polyethylene and polypropylene are welded together, problems with weld quality occurs; this is due to differences in chemical affinity, i.e., the two polymers phase separate in the weld interface, which results in lack of molecular entanglements [Wool, 1995].

This does not mean that dissimilar polymers cannot be welded. Various examples in literature show that dissimilar polymers are weldable, e.g., PE/PP [Chaffin et al., 2000; Zhang et al., 2011], PA/PEO [Cole et al., 2003], PLA/POM [Zhang et al., 2011], and PET/PBT [plasticsengineering.org, 2011]. Note that these pairs of weldable polymers possess chemical similarities, especially PE/PP and PET/PBT.

Nowadays, when design engineers select polymer materials for new products containing weld lines, constraints are put on the joining parts to polymers that are weldable. A popular tool for this selection process is *polymer weldability charts*. These charts are dedicated to specific processes, e.g., ultrasonic welding (see figure 1.1) or laser welding (see figure 1.2).

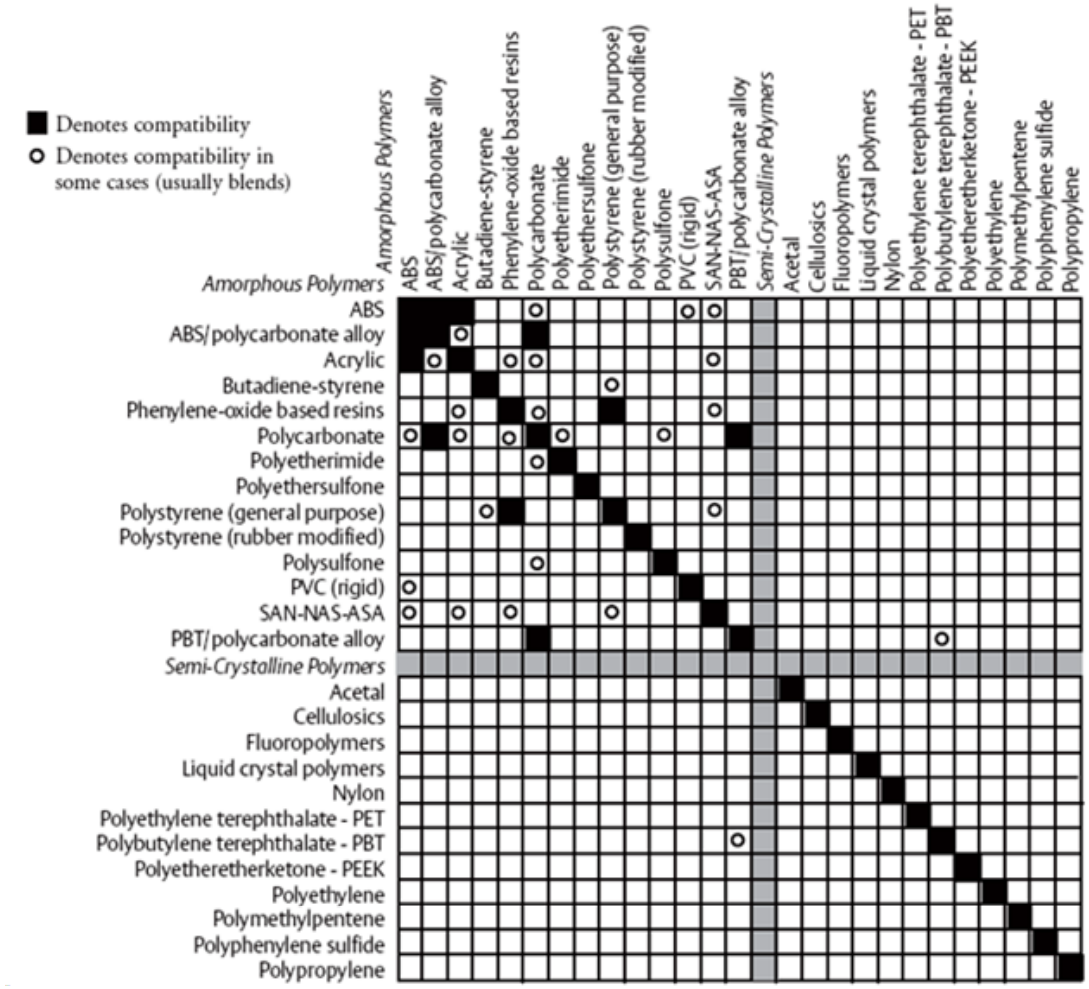

Figure 1.1: Weld compatibility matrix for ultrasonic welding [Branson, 2008]. Amorphous polymers possess better weldability compared to semi-crystalline polymers. Note the symmetry and that all polymers are self-weldable.

Weld charts are based on experience within companies and research institutions and the predicted strength is only a qualitative evaluation and does not rely on a standard methodology. The charts do not take part design, process parameters, or material variations into

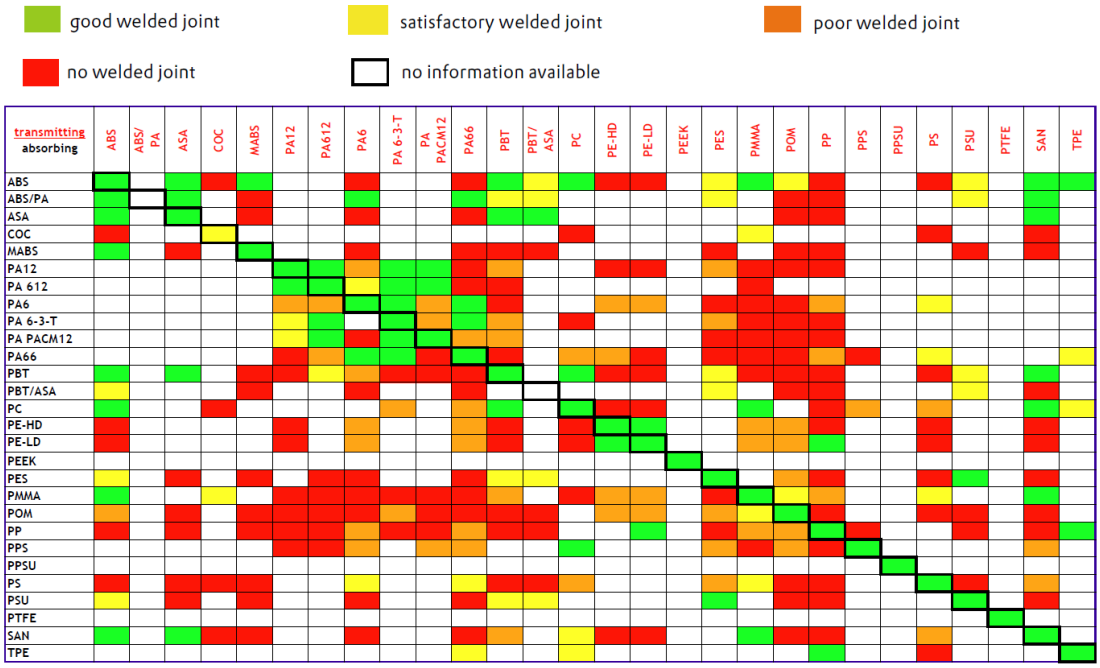

Figure 1.2: Laser weld chart [laserplasticwelding.com, 2012]. Note that all polymers are fully weldable to themselves, except for COC (cyclic olefin copolymer). The chart is also non-symmetric, for instance absorbing PMMA to transparent PC results in "no welded joint", while the reverse combination aPC/tPMMA results in a "good welded joint". The strength is a quantitative evaluation based experience within companies and research institutions.

account. Another disadvantage is the large amount of work necessary when a new material is developed, since this material needs to be test welded to all existing materials from the charts. And obviously, not all materials are present, e.g., a common material as PVC is not present in the laser chart [lpkfusa.com, 2012]. Moreover, a vague rule of thumb for weldability prediction is that "Generally, the polymer must be in the same plastic family and have both similar resin properties and melting temperatures" [lpkfusa.com, 2012].

Therefore, what is really needed in a world where polymers constitute an increasing part of products within electronics, telecommunication, and medical devices, and where new materials enter the market more frequently, is a general understanding of polymer weldability, and a more scientific approach for understanding weldability of dissimilar polymers. Moreover, this understanding may be utilized to expand the weldability even further, i.e., having more green areas in the weld chart in figure 1.2. These considerations have led to the following initiating problem.

"What is decisive for strength development in polymer weld interfaces, and can this knowledge be exploited to expand the weldability of plastics?"

CHAPTER 2

INDUSTRIAL CASES

The two industrial partners in the innovation consortium, Coloplast and Novo Nordisk, both face challenges and seek new opportunities in relation to welding processes, which is also why the two companies participate in this project. Throughout the project period various aspects of these challenges and opportunities have been discussed within the consortium, and these discussions constitute the foundation of this chapter, where specific industrial cases are presented. The Coloplast case is primarily based on discussions with Gunhild Rude Nielsen and Kim Bager, while the Novo Nordisk case is based on information from Torben Ruby.

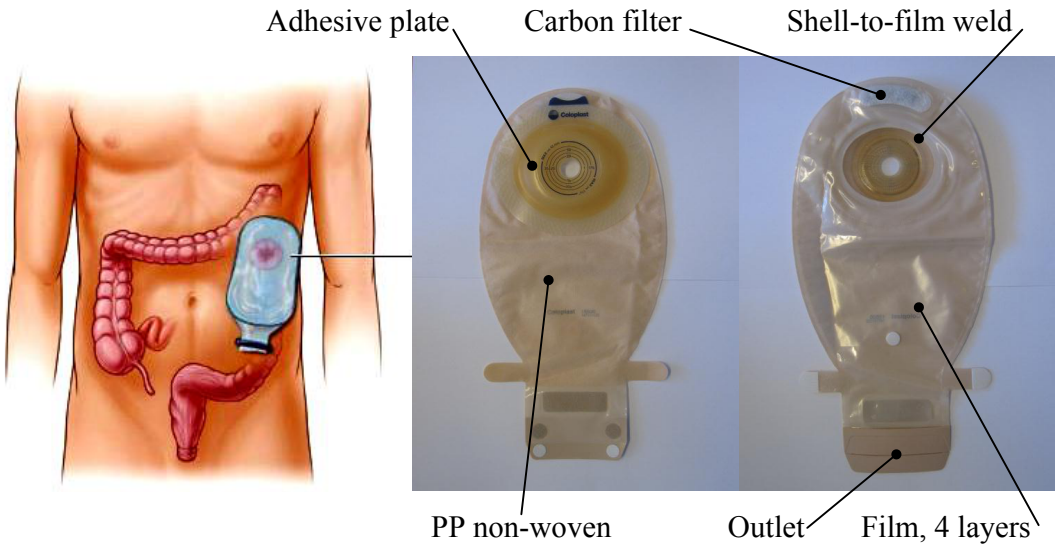

Figure 2.1: The ostomy pouch bag – probably Coloplast's most famous product. Here the product SenSura® Convex Light Wide Outlet. Basically, the product is a number of blow molded films welded together and also welded to an injection molded shell. On top of the shell, an adhesive plate is mounted which is the part sticking to the user's ostomy.

2.1 Coloplast A/S

Coloplast is a global company, which develops, manufactures, and markets medical devices and services related to ostomy, urology, continence, and wound care. One major product group involves ostomy bags, where a product example is presented in figure 2.1. In this section only important product details are presented. Ostomy bag products exists in various sizes and include several varieties for different users and markets around the world.

Manufacturing of medical devices is difficult due to high requirements to quality from users and political regulation. In the Coloplast products a majority of the challenges originates from joining processes, such as welding. The various joints in the SenSura® Convex Light Wide Outlet product is illustrated in figure 2.2.

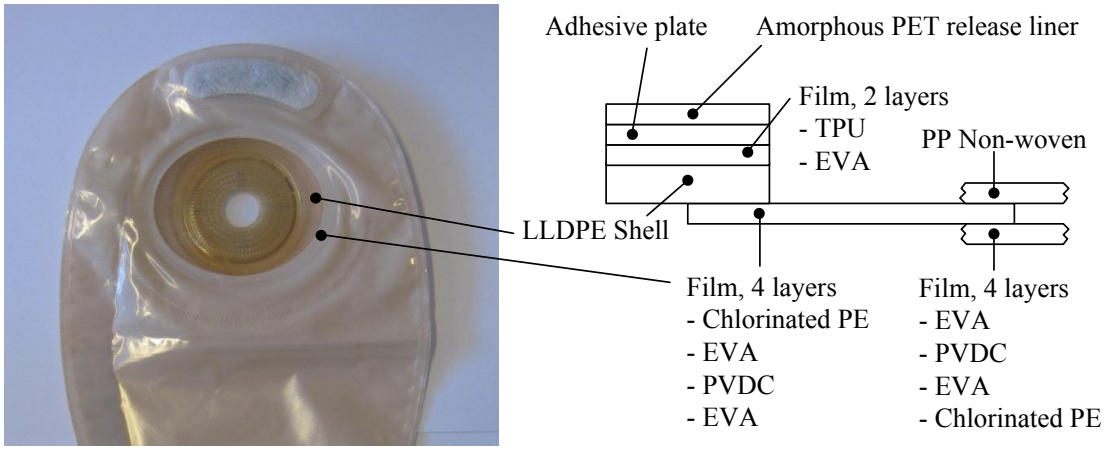

Figure 2.2: The SenSura® Convex Light Wide Outlet. A sketch shows the various joints and materials.

When manufacturing ostomy bags, the majority of welding processes serves to join plastic films, achieving a hermetic product without leakage. The plastic films used are often multiple layer films – figure 2.2 shows a 4-layer film including chlorinated PE, EVA, and PVDC – where the inner layers possess the barrier properties, while the outer layers possess good weldability. The number of welded films within a bag varies around the contour of the bag, but obviously at least two layers are needed to form a bag capable of containing liquids.

As seen in the figure most joining processes are film/film welds, which are performed using heated tool processes. Besides film/film welds, shell/film welds also exist, i.e., chlorinated PE welded to LLDPE. In production this joint turns out to be difficult, and in the following a specific case from Coloplast's SenSura® product is presented.

2.1.1 Shells-to-Film Joining

The convex shells are injection molded and are available in various sizes. The multilayered films are welded to these shells using heated tools. The shell colors vary between transparent, white, and brown; of which the white and brown versions are presented in figure 2.3 along with a 4-layer film.

In Coloplast's production it is experienced that heat welding of especially the white and brown rings results in inferior quality and mechanical strength compared to the transparent

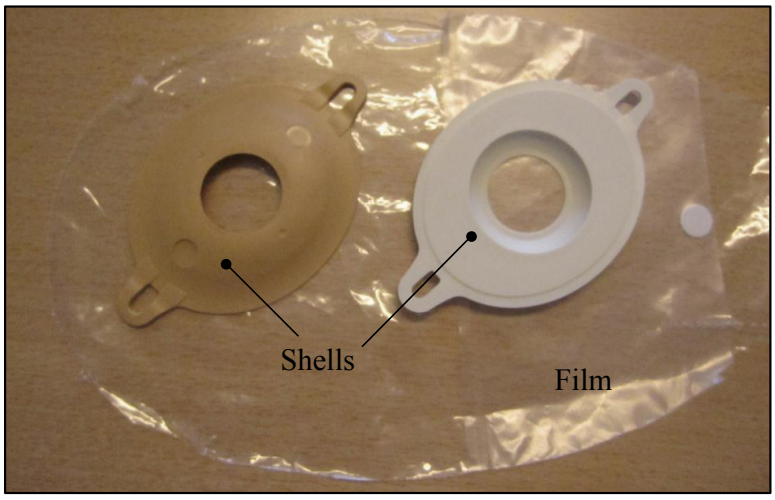

Figure 2.3: Two injection molded shells in white and brown and the blow molded 4-layer film.

shells. Also the variance in quality is significant for the white and brown shells – the weld quality varies from mechanical strength similar to the transparent shells to not weldable at all. These variations can happen by changing a material batch. In collaboration with their suppliers, polymer specialists at Coloplast have suggested that this problem might be due to color additives in the white and brown shells. Furthermore, it is identified that the melt flow index (MFI) can vary up to 12 g/10 min from batch to batch, while thermal and mechanical properties are unaltered.

Another challenge occurs when exchanging materials in production. This can either be caused by suppliers closing down production of a specific plastics grade, or substituting a polymer to obtain a competitive advantage, e.g., changing to a cheaper polymer or a polymer with improved physical properties. When materials are substituted, it is often experienced that the weld strength is deteriorated, even though a lot of effort is put into selecting materials, which "on paper" show similar chemical properties compared to the original materials.

2.1.2 Conclusions

Based on Coloplast's experience, small changes in the polymer quality or addition of additives seem to substantially alter the weldabilty. Furthermore, it is not clear if this issue is due to processing, materials, or both. These challenges are Coloplast's motivation for joining the innovation consortium. First of all, the challenge constitute an **understanding** part, i.e., why can small changes to material quality or processing result in dramatically deteriorated weld strength? And moreover, if the weldability of plastics can be **expanded**, some of the layers in the product in figure 2.2 are unnecessary. The final product might therefore be cheaper due to reduction of material costs.

2.2 Novo Nordisk A/S

Novo Nordisk is a global company, which develops, manufactures, and markets pharmaceuticals, medical devices, and services primarily related to diabetes. The largest and most famous product group is the Novo Nordisk Insulin Pens and Needles, illustrated in figure 2.4 with NovoPen® 3. The NovoPens are complex high-end injection devices, containing many

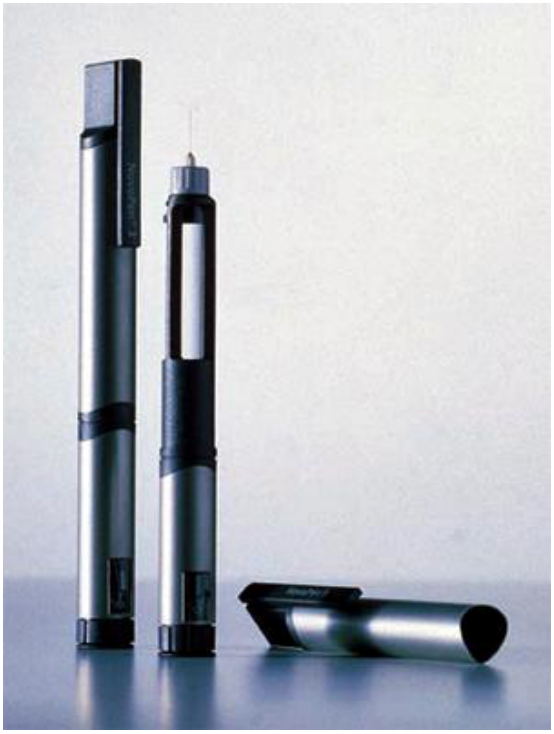

Figure 2.4: The NovoPen® 3.

massive requirements to technology and quality. Among the novel technologies interesting for Novo Nordisk is polymer laser welding due to advantages that will be mentioned later in section 4.2.1 on page 27. In the following the background, challenges, and considerations for Novo Nordisk to enter this project are described.

2.2.1 Considerations Regarding Laser Welding

Even though polymer laser welding is a relatively new technology, Novo Nordisk is already harnessing its advantages in manufacturing. For instance in the production of the **novo***fine*® Autocover®, see figure 2.5, which is a sterile needle and cover intended for single use. The needle has an automatic safety lock reducing the risk of unintended use, but also to secure single usage. This is illustrated in figure 2.5 where the used needle-head has a red mark. **novo***fine*® Autocover® is laser welded in two points – the white outer cylinder is laser spot welded to the inner transparent cylinder, both in polypropylene. The laser system utilized is based on a series of 980 nm diode lasers.

Nowadays, the overall requirements to medical devices are massive. In general for medical devices, mechanical reliability, hygiene, and barrier properties are important. Moreover

Figure 2.5: The **novo***fine*® Autocover® before (left) and after (right) use [novonordisk.com, 2013].

in the Novo Nordisk case, the devices often contain electronics and pharmaceuticals making their manufacture very sensitive. Another important aspect is the production volume, which for Novo Nordisk is estimated between hundreds of thousands and millions depending on product family. Future products will also contain an increasing number of features and complexity, resulting in more mechanical parts contained in the same volume, which again makes demand on miniaturization.

To realize these high demands and new features, and simultaneously maintain quality, new advanced manufacturing technologies are required. One of the technologies complying with the challenges is laser welding, which is described in section 4.2 on page 26.

2.2.2 Perspectives

From the challenges facing Novo Nordisk, it seems obvious to investigate and harness the possibilities of polymer laser welding. Laser welding in polymers is a relatively new technology, and the process and its limitations are not well understood. Therefore, a deeper **understanding** of the interplay between process parameters, material choice, and mechanical design is wanted. This may lead to better informed decisions when considering production equipment, selecting materials, and in general designing devices.

This project is also interesting from a materials science point of view. If the weldability of plastics could be **expanded**, the necessity of complex injection molding tools can be eliminated. Specifically, it is desired to weld polyoxymethylene (POM) to polypropylene (PP), such that the device shell (POM) could be welded directly to the needle from the **novo***fine*® Autocover® product.

CHAPTER 3

PROJECT DESCRIPTION

When dealing with welding and self-diffusion in polymeric systems, it seems obvious to harness the contemporary knowledge within Molecular Dynamics (MD). However, it turns out that polymeric systems consisting of highly entangled molecules, which diffuses relatively long distances compared to the size of single atoms, are too large for ordinary computers to handle [Mark, 2007]. Although, a few articles concerning novel coarse-grained simulations of polymer interfaces using super-computers have been published [Ge et al., 2013; Pierce et al., 2011]. Thus, other approaches for investigation of polymer dynamics must be considered. These approaches mainly include experimental studies and analytical models.

Chapters on polymer physics of former PhD dissertations [Fink, 2001; Podlech, 2007; Vingaard, 2009] within the field of polymer surfaces tend to be a short reproduction of Wool's book from 1995 [Wool, 1995]. When dealing with *Wool's classic theory*, one should keep in mind that it is not one theory, but a series of theories developed in the 80s and 90s [Willett and Wool, 1993] and later compiled in his book from 1995. This thesis will try to expand and ascertain the limitations in Wool's existing theories. The limitations in Wool's theories are presented in section 3.1.3 on page 17.

In order to understand these original theories, it is recommended to read chapter 5 on page 39 about polymer physics. Chapter 5 acts as a theoretical background for the Wool theories, but also as a background for chapter 6 and the thesis in general.

3.1 Wool's Classic Theory

The most famous contribution in the understanding of polymer weld strength development is Richard Wool's book *Polymer Interfaces – Structure and Strength* from 1995 [Wool, 1995]. The focus of the book is strength development from inter-diffusion and is especially focused on inter-penetration of *similar* (often called symmetric) amorphous melts. Wool has studied the welding process, considering the phenomenon of crack healing at a polymer-polymer interface in terms of static and dynamic properties of random coil chains. The models present various scaling relationships between the molecular weight and time and macroscopic properties, such as the critical energy release rate (G_{Ic}) or the ultimate stress (σ_U).

Wool's basic idea of strength development at a polymer-polymer interface is sketched in figure 3.1, which is a highly reproduced figure within the field [Zhang and Rong, 2011]. The conspicuous part of this theory is that full strength is obtained when the polymers are inter-diffused 81 % of the radius of gyration (R_g), and that further inter-penetation will not lead

to a further increase in strength – neither ultimate stress (σ_U) nor critical energy release rate (G_{Ic}). Moreover, this inter-penetration depth is obtained at the reptation time (τ_{rep}), i.e., full strength is obtained when inter-diffusion has proceeded for a time period τ_{rep}, after which the strength no longer increases.

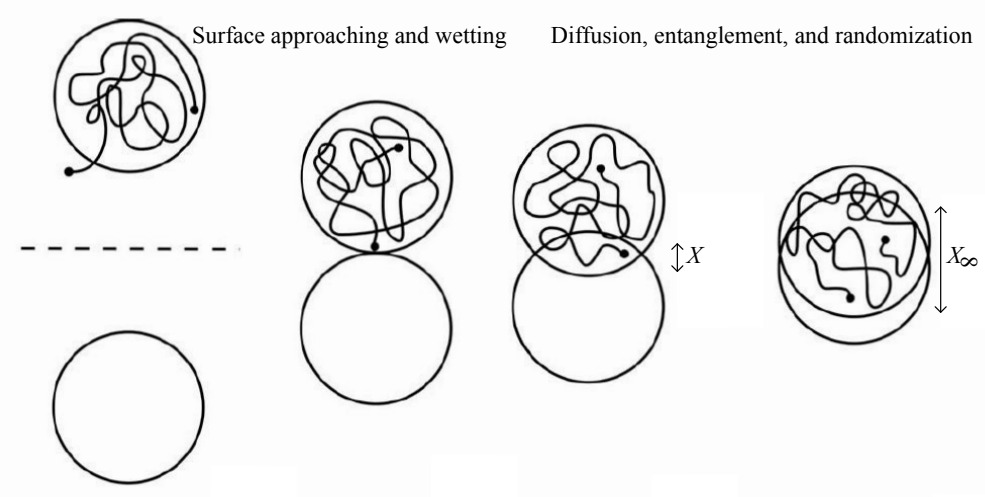

Figure 3.1: Inter-diffusion at an interface. X is the overlap distance (in this thesis w is the preferred notation), and X_∞(=0.81 R_g) denotes the equilibrium inter-penetratration depth, i.e., the depth where full strength is obtained [Wool, 1995].

Additionally, Wool [1995] has developed a concept concerning *percolation threshold* in interfaces; however, these ideas are controversial and do not comply with other parts of the established polymer physics theory [Larson, 2012]. These aspects are therefore not dealt with in this summary of Wool's classic theory.

3.1.1 Inter-diffusion

According to Wool [1995], the inter-diffusion depth ($X(t)$) must be divided into different time scales, τ_0, τ_e, τ_R, and τ_{rep}, within which the mechanisms of molecular motion varies.

for $t < \tau_0$	$X(t) \propto t^{1/2}$	Single segment Fickian diffusion	(3.1)
for $\tau_0 < t < \tau_e$	$X(t) \propto t^{0.36}$	$X(\tau_e) = 0.8 R_{g,e}$	(3.2)
for $\tau_e < t < \tau_R$	$X(t) \propto t^{1/4}$	$X(\tau_R) = 0.8 R_{g,e} \cdot Z^{1/4}$	(3.3)
for $\tau_R << t < \tau_{rep}$	$X(t) \propto t^{1/4}$	$X(\tau_{rep}) = \frac{3}{4}\sqrt{\frac{3\pi}{8}} R_g = 0.81 R_g = X_\infty$	(3.4)
for $t > \tau_{rep}$	$X(t) \propto t^{1/2}$	Single molecule Fickian diffusion	(3.5)

The time and length scales are all explained in chapter 5. Wool's results from above are not in full agreement with the Doi-Edwards tube model where the diffusion-exponents are 1/2, 1/4, 1/8, 1/4, and 1/2, respectively, for the five above-mentioned time domains [Doi and Edwards, 1986]. A plausible explanation for this is the complicated nature of relaxation at interfaces where Rouse and reptation mechanisms work simultaneously. Moreover, note that the fourth time domain only applies close to τ_{rep}, because the expression in the full $\tau_R <$

$t < \tau_{rep}$ time domain is complicated with four different terms [Wool, 1995], which by the way is incorrect, since the units do not match each other, and the resulting concentration profile is not physically meaningful when plotted.

The five time domains have been validated experimentally in the famous *ripple experiment*. In this experiment two types of deuterated polystyrene was prepared; one labeled H-D-D-H and one labeled D-H-H-D, where H and D represent blocks of polystyrene labeled with hydrogen and deuterium, respectively. Evaluating the concentration profile at the interface using Secondary Ion Mass Spectrometry (SIMS), a discontinuity at the interface is detected leading to the very important conclusion: *Yes, polymers move like snakes at the interface*, i.e., reptation is the dominating mechanism for inter-diffusion [Agrawal et al., 1996; Wool, 1995].

Monte Carlo (MC) simulations have also been carried out to confirm the time scaling at the interface. The simulations also confirm that interfaces are fully healed when the weld time equals τ_{rep} [Haire and Windle, 2001]. This is supported by novel large-scale MD simulations[1], although they show a more blurry picture of the scalings, since the crossover areas are smoothed. However, scaling exponents of 1/2 and 1/4 are easily seen, while an exponent of 0.18 is detected in the pre-reptation regime [Pierce et al., 2011]. All conclusions from above are collected in table 3.1. From the table it can be concluded that polymer mo-

Time regime	Bulk[a]	Interface (theory)[b]	Interface (MC)[c]	Interface (MD)[d]
$t < \tau_0$	1/2	1/2	N/A	N/A
$\tau_0 < t < \tau_e$	1/4	0.36	N/A	N/A
$\tau_e < t < \tau_R$	1/8	1/4	N/A	1/4
$\tau_R << t < \tau_{rep}$	1/4	1/4	1/4	0.18
$t > \tau_{rep}$	1/2	1/2	1/2	1/2

Table 3.1: Motion scalings of polymers in the bulk and at the interface from theory and MD simulations assuming a symmetric interface. The number refer to the exponent a in $X \propto t^a$, where $X(t) = \sqrt{\langle (R(t) - R(0))^2 \rangle}$, also known as the root mean square displacement with time. Note the difference from the bulk. [a] refer to [Doi and Edwards, 1986], [b] refer to [Wool, 1995], [c] refer to [Haire and Windle, 2001], [d] refer to [Pierce et al., 2011].

tion at interfaces differs from motion in the bulk. Pierce et al. [2011] appoint this difference to motion of ends, which play a much larger role at the interface compared to the bulk. This also explains the fact that branched polymers are weldable even though their self-diffusion coefficient is very low. Moreover, it must be noted that these exponents are slightly dependent on molecular weight. Even nowadays these models seem to be valid to a certain extent [Zhang et al., 2012a].

[1] The biggest simulated system consisted of 4800 chains of length 500 monomers, i.e., a total of 2.4 million monomers. Using 10^7 time steps, the system run time was 4.0 million processing hours at the New Mexico Computing Application Center (NMCAC)!

3.1.2 Strength Development

Although Wool's theories are relatively old, the idea that full strength is developed when molten surfaces have been in contact for one reptation time or longer is still accepted [Zhang and Rong, 2011]. This means that strength development over time only makes sense for $t < \tau_{rep}$. Important results for strength development are [Wool, 1995]:

$$X(t) = X_\infty \left(\frac{t}{\tau_{rep}}\right)^{1/4} \quad \text{for } \tau_R << t < \tau_{rep} \tag{3.6}$$

$$G_{Ic}(t) = G_{Ic,\infty} \left(\frac{t}{\tau_{rep}}\right)^{1/2} \quad \text{for all } \tau_R << t < \tau_{rep} \tag{3.7}$$

$$G_{Ic}(X) = G_{Ic,\infty} \left(\frac{X}{X_\infty}\right)^{2} \quad \text{for all } t \tag{3.8}$$

$$\sigma_U(t) = \sigma_{U,\infty} \left(\frac{t}{\tau_{rep}}\right)^{1/4} \quad \text{for } \tau_R << t < \tau_{rep} \tag{3.9}$$

$$\sigma_U(X) = \sigma_{U,\infty} \left(\frac{X}{X_\infty}\right) \quad \text{for all } t \tag{3.10}$$

Again, note that the relations involving t only yield when t is close to the reptation time, because when $t << \tau_{rep}$ Rouse dynamics is predominant as described in section 5.3 on page 44. Equation 3.8 has turned out to be difficult to confirm experimentally. A study has shown that a proportionality of X^1 has the same statistical significance [Schnell et al., 1998]. In addition, the influence of molecular weight is more debatable, and different relations have been suggested [Zhang and Rong, 2011]:

$$G_{Ic} \propto t^{1/2} M^{-3/2} \tag{3.11}$$

$$G_{Ic} \propto t^{1/2} M^{-1} \tag{3.12}$$

$$G_{Ic} \propto t^{1/2} M^{-1/2} \tag{3.13}$$

Although many of these models have not yet been applied in practice, they are kept in mind because of their predictability and guidability [Zhang and Rong, 2011]. In figure 3.2 the conclusions of the Wool theory is presented graphically.

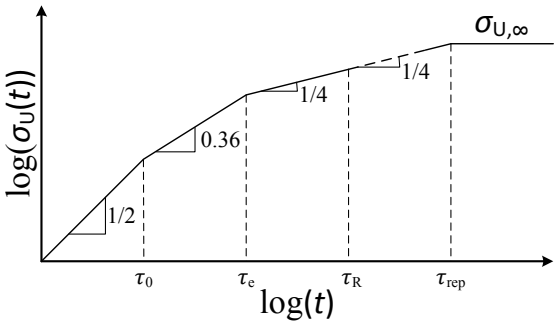

Figure 3.2: Ultimate strength of a polymer-polymer interface versus the time of interpenetration. The graph is based on table 3.1 and equation 3.10.

3.1.3 Limitations of the Wool Theory

Wool's classic theory turns out to work well for amorphous polymers welded in a very controllable fashion for times shorter than the reptation time. In particular, the theory works out well for polystyrene. The advantage of amorphous polymers is that the random coil model applies in any state – molten or solid [Kausch and Tirrell, 1989].

To model the inter-diffusion analytically, various model simplifications are applied. For instance, constant temperature is assumed which is far from reality in industrial weld applications. This assumption means that only heating tool presses can be used for experimental investigation, and that subsequent quenching is necessary in order to avoid inter-diffusion in the cooling phase.

Basically, the simplified model does not include the polymer melting and polymer crystallization, which are essential for semi-crystalline polymers. As described above, Wool's theory predicts that the polymers have to inter-diffuse $0.81R_g$, however, challenges exist with this theory:

1. Why are (nearly) all polymers capable of being laser welded to themselves with full strength, as seen in figure 1.2 on page 5? This is surprising since the laser welding process only keeps material molten for a few seconds [Klein, 2011], and the reptation time of, e.g., PS with a molecular weight of 245,000 g/mol is reported to be 1860 minutes at 118 °C [Wool, 1995]. Two explanations are possible:

   a) The reptation time is highly temperature dependent and will drop quickly as the temperature rises well above the glass transition

   b) The required inter-penetration depth of $X_\infty = 0.81R_g$ is not valid, and smaller inter-penetration depths should also provide full strength.

2. Not only the inter-penetration depth must be decisive for weld strength. The number of the density of entanglements in the interface must also influence the final strength. Moreover, the crystallization of polymers at interfaces must play a central role in strength development for semi-crystalline polymers.

All things considered, Wool's classic theories are still valid and have never been proven wrong; however, they have never been verified at very high temperature, where the reptation time plausibly is relatively low.

3.2 Problem Delimitation

In order to answer the initiating problem, it is necessary to consider what is meant by *strength development in polymer weld interfaces*. In this project *strength* refers to mechanical strength of a welded joint between two polymers. Full strength is achieved when the weld joint is no longer the weakest link in mechanical tests, i.e., a tensile tested weld line will fracture outside the welded joint [Grewell et al., 2003]. Fracture and strength of polymer interfaces are further discussed in section 6.6 on page 74. The initiating problem also deals with *expanded weldability*, facilitating the welding of dissimilar plastics, which nowadays are non-weldable.

The challenges in this project can be broken down to three parts. These include a processing part (welding – see chapter 4), a material part (polymers – see chapter 5), and a

design part. As indicated in figures 1.1 and 1.2, polymer weldability depends on the selected process, the specific materials, and joint design. Obviously, neither all materials nor welding processes can be investigated; therefore, the research project is limited with respect to materials, processes, and design.

Material composition:

Matrix material: In order to investigate the expanding part of this project, it is important to select materials from the chart in figure 1.2 that include amorphous, semi-crystalline, polar, and non-polar polymers, and that range in weldability from "good welded joint" to "no welded joint". Furthermore, in order to keep it simple homopolymers are preferred over blended compounds. With these requirements the selected materials are high density polyethylene (HDPE), polypropylene (PP), poly(methyl methacrylate) (PMMA), polystyrene (PS), poly(butylene terephthalate) (PBT), and polycarbonate (PC); see table 8.1 on page 87 for further specifications. Throughout part II the polymers from table 8.1 constitute the basis for a number of concrete examples.

Absorber: As discussed in section 4.2.2 on page 30, various absorbers exist on the market. However, the most widespread and cheapest is carbon black. Moreover, carbon black have been reported to expand the weldability of plastics compared to other absorbers [Acherjee et al., 2012a]. The absorber amount was fixed at 0.4 w%, which was decided in collaboration with the consortium partners. Other groups have previosly reported successfull results with 0.2 w% [Acherjee et al., 2012a] and up to 2.0 w% [Klein, 2011].

Processing conditions:

Preparation technique: Incorporation of carbon black into the different polymer matrices by melt compounding has been preferred, even though in-situ polymerization often have been reported to result in an increased degree of exfoliation when dealing with polymer nanocomposites [Paul and Robeson, 2008]. Melt compounding is chosen over in-situ polymerization due to its attractiveness to industry. For manufacture of sheets for laser welding injection molding is an obvious choice, which also is well-known for all project partners. For further details on processing see section 9.1 on page 89.

Welding process: It is decided to focus the project on one welding technique, namely laser welding. Laser welding is chosen due to its novelty to modern manufacturing and its ability to expand polymer weldability compared to other welding techniques [Klein, 2011]. Also, laser welding is a natural choice, since the competences within the consortium partners lies within this technology. More information on specific parameters are given in section 9.2 on page 91.

Design considerations:

Test specimens: Mechanical testing is limited to two standard types as discussed in section 6.6.3 on page 77 in the literature survey. The selected specimen is presented in figures 9.2 and 9.3 on page 91 obvious for welding lap-joints. The specimens and equipment for processing all originates from Coloplast R&D.

3.3 Problem Statement

In the light of the content of part I – particularly the initiating problem from page 5 and the problem delimitation in the previous section, it has been possible to set up a list of concrete topics to be investigated. In chapter 7 on page 85 three hypotheses are formed to sharpen the problem statement. The problem statement is presented below:

In the light of the contents of this chapter and especially the initiating problem and the problem delimitation, it has been possible to set up a list with five concrete topics to be investigated in this project, all of which are presented in the following:

1. **Understanding weldability of plastics:** A thorough survey of literature is conducted to understand and identify limitations in the welding process. This is done in chapter 6 on page 57 and is not limited to laser welding. For the laser welding process, it is desired to identify the process "bottleneck", i.e., what is the limiting factor when welding plastics with lasers.

2. **Laser welding of HDPE and PP:** HDPE and PP are often claimed to be weld incompatible [laserplasticwelding.com, 2012], but relatively new research has proven full strength weldability [Chaffin et al., 2000; Zhang et al., 2011]. Also, from an industrial point of view it is desired to weld these two polymers. This is summarized in chapter 10 on page 101.

3. **Development of methods for mechanical testing:** In accordance with the work package of AAU [polymerwelding.com, 2013], new methods for testing mechanical strength will be considered and developed. This is summarized in chapter 11 on page 109.

4. **Predicting and expanding the weldability of plastics:** Based on the 6 materials selected in the problem delimitation and knowledge from bullet points 1 and 2, it will be investigated if any correlation exists between the physical and chemical properties of polymers and the weld strength. It will also be investigated whether or not this knowledge can be harnessed to expand the weldability in general. This is summarized in chapter 12 on page 117.

5. **Development of software for predicting weldability of plastics:** The obtained knowledge from bullet points 1 and 4 will be implemented in a material selection software. This is documented in section 13.1 on page 125.

PART II

REVIEW OF POLYMER WELDING

CHAPTER 4

WELDING TECHNOLOGY

Besides mechanical joining and adhesive bonding, welding is one of the major joining techniques for plastic components. In general, welding in industry is defined as a joining process caused by coalescence of parts. Coalescence is often achieved from heating/melting of the parts. And simply put, polymer welding is the welding process involving coalescence of thermoplastics. As mentioned earlier, one major advantage of welding, compared to other joining techniques, is the possibility of making strong joints with mechanical, corrosion/degradation, and diffusion dependent properties that approach those of the parent material. Add to this that the joints can be hermetically sealed if the right welding method is utilized; this is for instance important for medical devices, as discussed in chapter 2 [Grewell et al., 2003; Rotheiser, 2009].

It is worth noting that plastic welding processes are limited to thermoplastics, since these are the only polymeric materials that can be softened and afterwards diffuse and solidify. Both semi-crystalline and amorphous thermoplastics can be welded. Semi-crystalline polymers must be in molten state to coalesce, while amorphous polymers must be above a certain softening point, found above the glass transition temperature [Klein, 2011]. In the following, both states are referred to as molten.

Design, *process*, and *material* are all important, but here the focus is on *process* and *material*. Design guidelines are explained elsewhere in literature [Klein, 2011; lpkfusa.com, 2012].

4.1 Classification of Welding Techniques

Polymer welding processes can be classified in terms of which heating technique is used in the heating phase of the process. Generally, welding processes can be divided into two major groups; *external* and *internal* heating, as illustrated in figure 4.1.

In the figure, *mechanical fastening* and *adhesion* are also shown as the two alternative joining techniques. These two techniques are favorable when working with thermosets [Rotheiser, 2009].

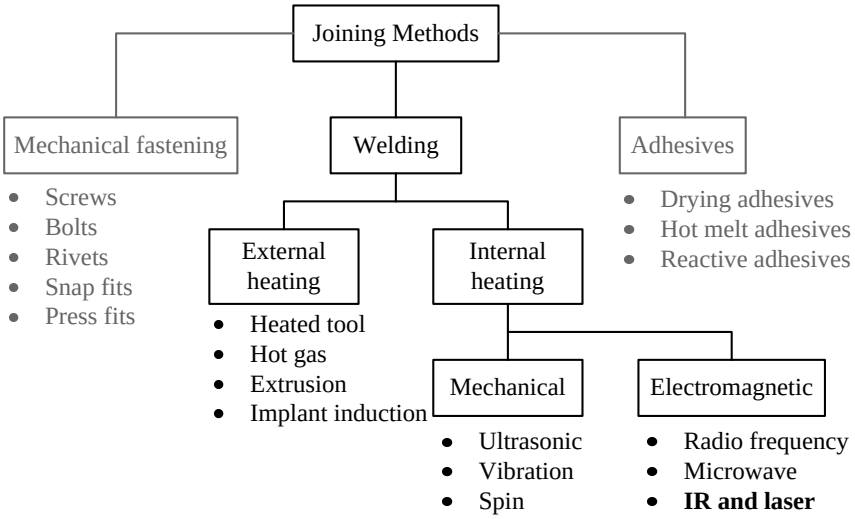

Figure 4.1: The three major techniques for joining of plastics. Welding is one of them, which is further sub-classified into different techniques based on the heat input [Grewell et al., 2003].

4.1.1 External Heating

Basically, external heating rely on convection/conduction of heat to the weld surface. External heating is also referred to as direct heating since the polymer surface is heated directly from a heat source. External heating methods include [Grewell et al., 2003]:

Heated tool: Heated tool or hot plate welding is one of the most popular polymer welding techniques due to its simplicity, reliability, and low cost. The technique works by pressing the two polymer surfaces against a hot tool. The tool is then removed and the molten polymers are pressed against each other, forming a strong joint after solidification. This method is especially used for welding pipes.

Hot gas: A hot gas is used to heat up the two surfaces and melt a filler rod in between them. This method is the polymer equivalent of TIG-welding of metals. The method is often done manually and is therefore preferred for manufacturing of prototypes.

Extrusion: Molten plastic is extruded directly between the two polymers, melting them and creating a joint. This method is equivalent to MIG/MAG-welding of metals. Extrusion welding is faster than the similar hot gas welding; thus, it is often used in serial production.

Resistive implant: In resistive implant welding an alternating current is passed through an electrically conductive implant placed between the two parts being joined. The Ohmic resistance in the electrodes heats the implant and melts together the implant and the polymer. Therefore, the implant is a part of the weld seam afterwards, and one requirement is weldability between implant and plastics part. This method is often used when welding thermoplastic composites.

4.1.2 Internal Heating

Internal heating or indirect heating relies on transferring, e.g., mechanical or electromagnetic energy into heat.

Mechanical

Internal mechanical heating relies on transferring mechanical energy into heat energy. This is done through surface friction and intermolecular friction. The mechanical processes include [Grewell et al., 2003]:

Ultrasonic: Surfaces are joined using ultrasonic (10–70 kHz) vibrations on the parts, which are wanted to be welded. The cyclical deformation of the workpieces heats up and melts the surfaces. Ultrasonic welding is limited by requirements of the polymer's acoustic properties. The method is fast and very suitable for mass production.

Vibration: Vibration welding is also known as friction welding and relies on conversion of mechanical friction into heat energy. This method uses larger amplitudes, but lower frequencies than ultrasonic, and opposed to ultrasonic welding, where longitudinal waves generally are used, transverse vibrations are typically used here. Therefore, vibration welding is suitable for welding of larger parts. The method is particularly widespread in the automotive industry, where big parts cannot be injection molded in one single piece.

Spin: Spin welding is also a friction welding method. One part is fixed, while the other part is rotated fast against the first part. The method has the same advantages as ultrasonic welding, although rotational symmetry is required. On the other hand, the investment cost is lower.

Electromagnetic

Internal electromagnetic heating relies on the absorption and conversion of electromagnetic radiation into heat. These processes include [Grewell et al., 2003]:

Radio Frequency: RF welding is also known as dielectric welding and the method relies on energy conversion from electromagnetic to heat energy due to dielectric hysteresis in thermoplastics. Therefore, the thermoplastics require a dipole moment, which is why polyolefins cannot be welded this way, however, PVCs, nylons, and polyesters can.

Microwave: The polymer surfaces are welded together with microwaves ranging from 300 MHz to 300 GHz. Some polymers are transparent to these wavelengths, while others absorb them. The technique is very new and few examples are found in matured manufacturing.

IR and Lasers: In IR and laser welding an additive, capable of absorbing the utilized laser wavelength, is added to one of the polymers to be joined. In the absorbing additive heat develops and melts the materials, which after cooling are joined. The process has been used since the 1990s and has proved to be a very promising future process. Since this thesis focuses on laser welding, more specifically laser transmission welding; this method is further described in the next section.

4.2 Laser Transmission Welding

Laser transmission welding (LTW) or through transmission laser welding (TTLW) is the most common technique when referring to polymer laser welding. The basic concept of LTW is depicted in figure 4.2. Also the homepage laserplasticwelding.com [2013] is worth a visit. The method is in particular used in the telecommunication, automotive, and medical industries. According to novel literature, the technique is very promising as it is possible to weld soft-to-soft materials and soft-to-hard materials, which is not possible with conventional welding methods, so already here the *expanding* part of the project is fulfilled [Klein, 2011].

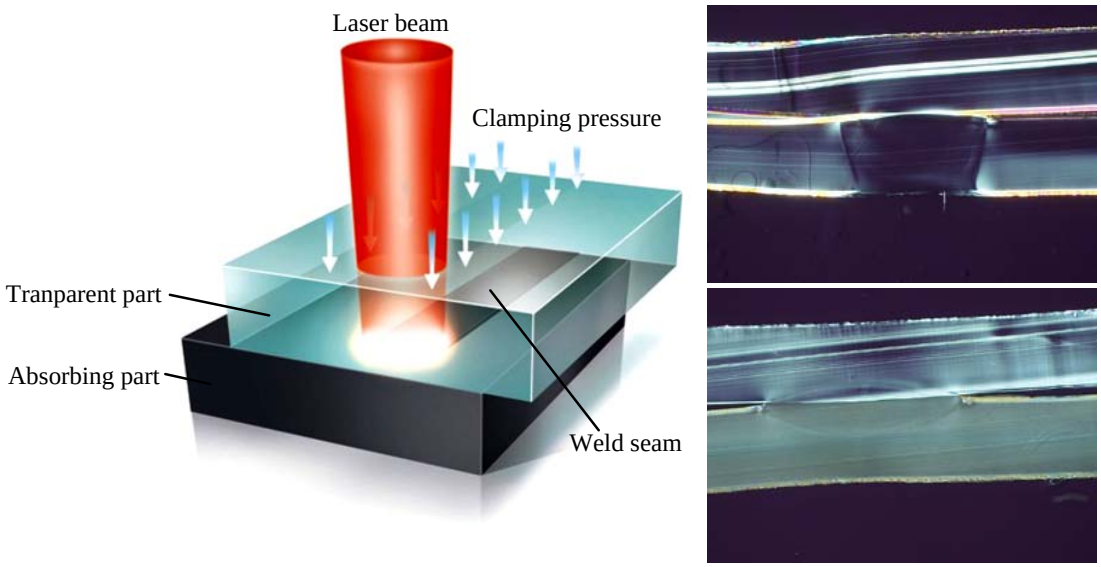

Figure 4.2: Left: Principle sketch of a transmission laser welded lap-joint. Right: Low quality lap-joint with a clearly visible weld seam (top) and a high quality weld seam (bottom) [lpkf.com, 2012].

The basic idea is that a part transparent to the incident laser wavelength is placed on top of a part absorbing the wavelength (usually because of light absorbing particles added to the polymer) – resulting in a so-called lap-joint. The laser beam will heat up and melt the absorbing part which will wet, heat up, and melt the transparent part. When both materials are molten and wetting has occurred, the polymer molecules are able to inter-diffuse and form entanglements [Klein, 2011; Wool, 1995].

Parameters often varied in the process include laser power (P_{laser}), translational weld speed (v_{laser}), and clamping pressure. It turns out, however, that the process window for the clamping pressure is large, meaning that variations in clamping pressure does not significantly affect the weld quality [dsm.com, 2011; lpkfusa.com, 2012]. Moreover, when laser systems are set up, the laser beam can be manipulated in many ways in order to secure an optimum beam pattern for melting.

Typically, the laser energy input technique is **contour welding**, which means that the laser beam follows a predefined path. In contour welding the laser beam only moves a single time over the path to form the joint. Other laser energy input techniques include [dsm.com,

2011; Klein, 2011]:

Simultanious welding: In simultaneous welding the entire weld seam is formed at the same time. This is done using specially designed optical systems to form the laser beam into a pattern of the desired weld seam. Note that there is no movement of laser pattern or part.

Quasi-simultaneous welding: Quasi-simultaneous welding combines contour and simultaneous welding. A single, focused laser beam is guided by a mirror, tracing the weld path multiple times at very high speeds. Thereby, the weld seam is heated and formed simultanouesly.

Mask welding: In mask welding the weld seam is shaped by a contact perforation mask. A laser beam (typically with a pattern like in simultaneous welding) is scanned over a patterned mask, determining the shape of the weld seam.

These four basic modes of laser welding are presented graphically in figure 4.3. Moreover, other innovative and dedicated techniques exist, such as TWIST, Globo, and Hybrid welding [lpkfusa.com, 2012].

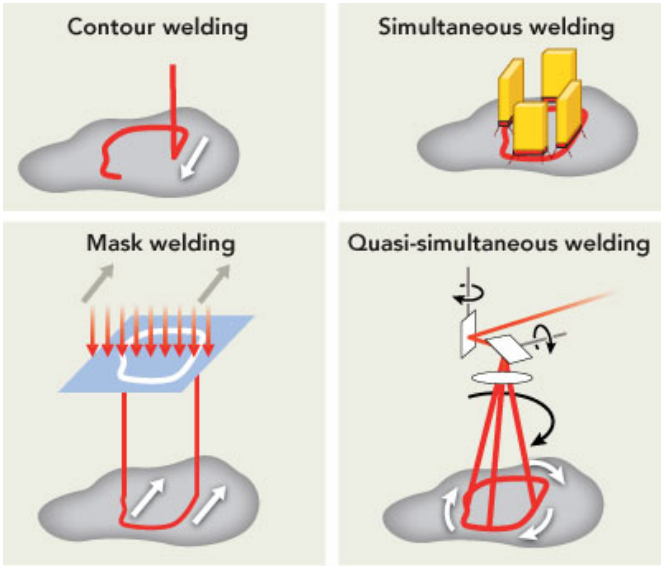

Figure 4.3: The four basic modes of laser transmission welding (LTW) [industrial lasers.com, 2012].

4.2.1 Advantages

The LTW process has various advantages. First of all, it is increasingly attractive to the industry due to a continually decreasing investment and maintenance cost. Diode lasers in particular are now affordable compared to other welding technologies due to relatively high effect compared to laser price, while maintaining an acceptable beam quality. However, the process can still not compete with heated tool welding in established manufacturing.

The quality is unique compared to other welding methods. This means that strong, tough, non-contaminated, and aesthetically perfect welds are achievable. The process can also be monitored to document quality. Moreover, sub-millimeter welds in size and precision (miniaturization) are feasible, making LTW perfect for medical devices and microfluidics.

Regarding automation and implementation in modern, flexible, and reconfigurable manufacturing systems, LTW is advantageous over competitive welding technologies. Lasers are easily integrated in robotics systems, making them easy to (re-)program. This also renders possible the welding of 3D and complex shapes with curvature and large height changes.

Lastly and very important for this project, the weldability of plastics is expanded; permitting high strength welds between dissimilar materials [dsm.com, 2011; Klein, 2011; laser-plasticwelding.com, 2012].

4.2.2 Laser Welding Physics

In this section the physics of the welding process will be described in further detail. In figure 4.4 it is illustrated what happens to the incident laser light. Basically, light can be transmitted (T), absorbed (A), reflected (surface reflection (R) or internal reflection (R_i)), or scattered (S). Transmission and absorption is discussed in the following sections.

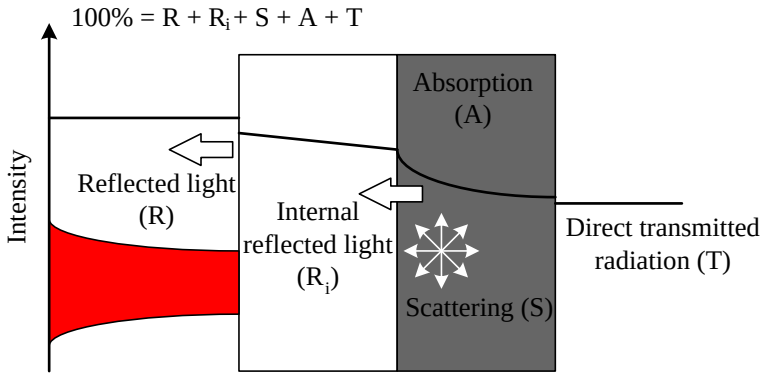

Figure 4.4: Illustration of the loss of laser intensity through a lap joint [Klein, 2011]. Electromagnetic energy can be dissipated as reflection (surface or internal), scattering, absorption, or transmitted.

Surface reflection occurs when electromagnetic radiation strikes the interface between two materials with a difference in refractive index. The reflectivity (R) is given in terms of the Fresnel equations, which for a perpendicular angle of incidence reduces to [Klein, 2011]:

$$R = \frac{(n_1 - n_2)^2}{(n_1 + n_2)^2}, \tag{4.1}$$

where n_i is the refractive index of material i. If the difference in refractive index is zero, no radiation will be reflected, while an air/iPP ($n_{air} = 1$, $n_{iPP} = 1.49$) interface will reflect 4 % of the incident radiation.

Scattering is caused by the inhomogeneous structure of the material, e.g., spherulites or particles. Scattering of the transmitted beam will reduce the laser beam intensity at the interface, which not necessarily is a bad thing. In some process designs only 5 % of the incident radiation reaches the interface. Scattering in the transparent part is often preferred

when the melting temperature is higher than the absorbing part, since the scattering process tends to increase the temperature. Thereby, the melting temperature difference to overcome is decreased [Klein, 2011].

Scattering in the absorbing part is often desirable, since light scattering might result in a short beam penetration depth, leading to a higher interface temperature. In figure 4.2 the high quality weld was performed with TiO_2 as a scattering additive, while the low quality weld was created without use of TiO_2. Furthermore, scatterers are much cheaper than organic near infra-red (NIR) absorbers, hence, these are preferred if there is no requirement for the optical clarity of the product. Another common additive that also has scatter effects is carbon black.

Laser Transparent Top Layer

Most thermoplastic resins are transparent to laser light in their pristine form, i.e., without additives or fillers. When using lasers for industrial welding in the LTW process, the laser wavelengths of interest are 808-980 nm. Due to the different wavelengths, laser transparency in this area does not imply transparency for visible light. Polyethylene, for instance, is white translucent in its pristine state, but transparent for the laser wavelengths under consideration.

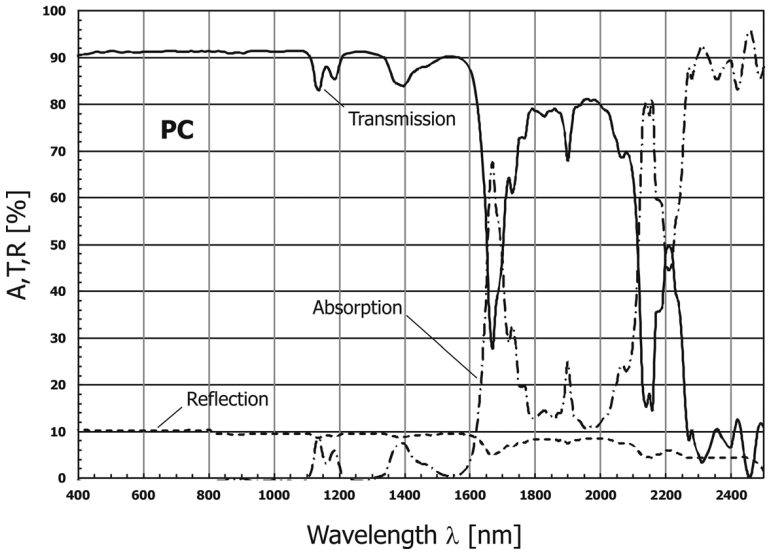

Figure 4.5: Transmission, absorption, and reflection of PC at wavelengths between 400 and 2500 nm. Note that PC is transparent for wavelengths between 808 and 980 nm, which are the wavelengths of interest for NIR lasers [Klein, 2011].

Several factors influence the laser transmission. These include additives (such as UV stabilizers, colorants, heat stabilizers) and fillers (such as glass fiber, carbon fiber, blowing agents). Moreover, polymer crystallinity affects light transmission since these can scatter light, which defocuses the laser beam, resulting in lower intensity at the interface. The material thickness of the transparent part is also relevant since the intensity at the weld interface decreases exponentially with thickness. Therefore, the transparent part is not recommended to be thicker than 3-5 mm [Klein, 2011].

Laser Absorbing Bottom Layer

The bottom layer needs to absorb the laser wavelength, so the electro-magnetic energy from the laser can be converted into heat energy, which will heat up and melt the material. To make the transparent pristine plastic absorbent, it is necessary to add fillers, which will absorb the laser wavelength. The most common additive for this purpose is carbon black, and a common amount is 0.2-0.4 w%. The *absorption constant* (α) in a material is directly proportional to the amount of carbon black, which for polycarbonate for instance is [Acherjee et al., 2012a,b]:

$$\alpha = 82 \frac{1}{\text{mm} \cdot \text{w\%}} \cdot c, \tag{4.2}$$

where α is the absorption constant in mm^{-1}, and c is the weight percent (w%) of carbon black in a PC or iPP matrix [Klein, 2011]. Using the assumption of linear absorption the reduction in radiation intensity can be described by Lambert's absorption rule [Klein, 2011]:

$$I_T(z) = I_0 \cdot \text{e}^{-\alpha \cdot z}, \tag{4.3}$$

where z is the penetration depth, and I_0 is the beam intensity at the material surface ($z = 0$). The *optical inter-penetration depth* ($z = a$) is defined as the depth where the initial intensity has decreased to 1/e, i.e:

$$\frac{1}{\text{e}} = \frac{I_T(a)}{I_0} = \text{e}^{-\alpha \cdot a} \Rightarrow a = \frac{1}{\alpha}, \tag{4.4}$$

Example 4.1
What is the absorption constant (α) and the optical inter-penetration depth (a) of an iPP with 0.4 w% carbon black?

From equation 4.2 α is calculated to:

$$\alpha = 82 \frac{1}{\text{mm} \cdot \text{w\%}} \cdot 0.4\text{w\%} = 33\text{mm}^{-1}. \tag{4.5}$$

a is determined from equation 4.4:

$$a = \frac{1}{33\text{mm}^{-1}} = 30\mu\text{m}. \tag{4.6}$$

Therefore, by adding 0.4 w% carbon black, practically all radiation energy from the laser is absorbed in the interface between the transmissive and absorbent part. However, note the difference between optical and thermal penetration depth.

The limitation of carbon black is obviously that the final product appears optically black for the human eye, which is not always desirable. Therefore, commercial laser absorbers have been developed, which are transparent to radiation in the visible spectrum, 380-740 nm, but absorbent to a specific laser wavelength between 808 and 980 nm. Commercially available absorbers include; Clearweld and Lumogen – with Lumogen it is possible to engineer the laser absorbent part in a variety of colors [Klein, 2011].

The molten depth ratio (t_{TL}/t_{AL}), see figure 4.6, is also affected by the CB amount. A large amount results in a symmetric weld seam, while a low amount results in a small molten phase in the transparent material. The type of absorption changes from volume to surface absorption [Acherjee et al., 2012a].

The absorption constant (α) does also depend on laser wavelength as [Klein, 2011]:

$$\alpha = \frac{4\pi\kappa}{\lambda}, \tag{4.7}$$

where κ is the absorption *coefficient* and λ is the incident wavelength. Note that κ is also a function of temperature and wavelength.

Influence of Laser Process Parameters

The welding quality obviously depends on the process parameters [dsm.com, 2011; Klein, 2011]. Hadriche et al. [2010] have investigated process parameters with a DoE approach, while Acherjee et al. [2012b] performed a DoE approach on a finite element simulation. When dealing with the influence of process parameters, it is important to establish some clearly defined measures of the weld seam; these are illustrated in figure 4.6.

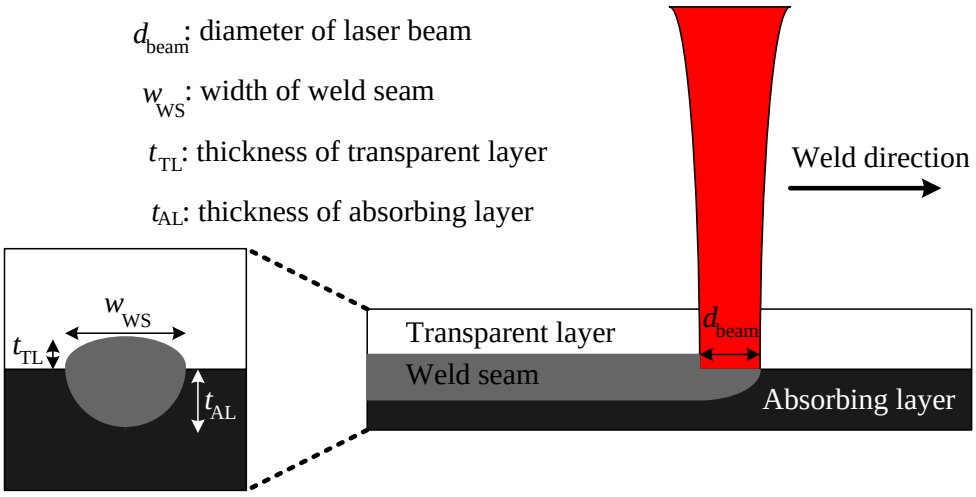

Figure 4.6: Sketch illustrating the various dimensions in a laser welded joint. The situation is not as black and white as sketched, as a heat affected zone (HAZ) is present around the weld seam. This zone is often stronger than the weld itself due to polymer re-crystallization [Pocius, 2002].

The influence of some variable input parameters are summarized below:

Laser power, P_{laser}: The laser power is obviously important – more power results in more heat and thereby a higher temperature and more melting [Acherjee et al., 2012b]. This turns out to be important for the molecular mobility as explained in section 5.4 on page 47. On the other hand, too much power will degrade the absorbing polymer, see section 6.1.2 on page 59. Another parameter related to the power is the intensity distribution, i.e., the mode structure of the Gaussian intensity. The intensity distribution

turns out to be very complex and a lot of effort is put into optimizing this intensity pattern.

Laser wavelength, λ_{laser}: The typical wavelength for laser welding in polymers are 808-980 nm, which belongs to the near infrared (NIR) spectrum, ranging from 750–1400 nm. The wavelength depends on the type of laser active media, e.g., diode lasers (λ = 800 – 2000 nm), Nd:YAG lasers (1064 nm), fiber lasers (1030-1620 nm), and CO_2 lasers (10.6 μm). The laser wavelength also strongly influences the properties for beam propagation, and of course the wavelength is important when dealing with the absorbance of the polymer. Moreover, the wavelength determines the degree of scattering; the Rayleigh scattering is proportional to λ^{-4}, i.e., longer wavelengths result in less scattering.

Laser beam diameter, d_{beam}: Increasing the laser beam diameter will cause the peak temperature to decrease. Also the seam width increases with increasing d_{beam}, although this is only true to a certain extent; for relatively large beam diameters the width remains constant [plasticsengineering.org, 2011]. Since the energy density decreases with increasing d_{beam}, the melt depth decreases and also the melt depth in the transparent part decreases [Acherjee et al., 2012b].

Laser weld speed, v_{laser}: Together with laser power, the laser weld speed determines the heat input in the weld interface [Acherjee et al., 2012b]. In modeling, a high welding speed is often preferred, because of the high-speed approximation, see section 4.3.2 on page 35. Moreover, the laser weld speed is of great importance when evaluating process cycle times and thereby manufacturing economics.

Line energy, E_{line}: The line energy is not an independent variable, but nevertheless a central parameter for the welding process. This property is defined as the ratio between laser power and laser weld speed, i.e., $E_{\text{line}} = P_{\text{laser}} / v_{\text{laser}}$. For high weld speeds, the line energy alone determines the weld quality; thus, E_{line} is often stated in literature. It is important to note that too low line energy results in no melting, while a too high line energy results in material decomposition. Hence, an optimum line energy exists in any given laser welding process.

Clamping pressure: Clamping pressure is important for securing intimate contact between transparent and absorbing part. If the clamping pressure is too low, intimate contact is not achieved. On the other hand, if the pressure is too high, the molten material distributes over a large area, which is not desirable. It turns out, however, that as the major part of the pressure is supported by unaffected material, the process window for the clamping pressure is large, meaning that variations in clamping pressure does not significantly affect the weld quality.

Surface Preparation

Experience from laser welding shows that the surface preparation prior to welding is central for achievement of strong joints. Surface preparation is mostly used for manual welding processes, since the materials are more likely to be contaminated than in automated processes, but do also appear in automated processes, such as laser welding. Cleaning can be

done using a solvent or simply by machining the contaminated area away. Most contamination in automated processes comes from mold release agent, which usually is avoided by applying a thermosetting release layer to the mold surface [Grewell et al., 2003].

Another reason for treating surfaces prior to welding is due to removal of the weak boundary layer, see section 6.5.1 on page 73, but also for uniformizing surfaces during production, resulting in more robust manufacturing. Another effect of surface preparation might be improved topography and roughness.

Methods often utilized for surface treatment in automated manufacturing include [wiley.com, 2011]:

Corona Discharge Treatment (CDT): This surface preparation method is typically used for polyolefins and polyesters. Basically, the solid polymer surface is bombarded with ionized air at atmospheric pressure. The blue glow from the ionized air is called the corona. The ion-bombardment leads to surface oxidation, i.e., creation of carbonyls. The oxidized surfaces are very reactive and are able to covalently bond to other oxidized surfaces. Due to the very reactive nature of the oxidized surface, the welding process should be performed immediately after the CDT.

Flame treatment: The surface is exposed to a flame for 0.01–0.1 s. Besides oxidation, this also induces amide surface groups, which increases the bondability further compared to CDT.

Plasma treatment: A plasma gas bombards the polymer surface with effects similar to CDT. However, this method needs to be operated under low pressure.

Acid etching: For polyolefins chromic acid is used to remove parts of the polymer surface, primarily to increase roughness. Moreover, various polar groups are introduced to the surface. Acid etching is used especially when dealing with adhesive technology and not only welding.

Surface grafting: Grafting the workpiece surface with foreign monomers or polymers is sometimes done to be able to weld incompatible polymers. This is also referred to as adhesion-promoting systems [Hopmann and Weber, 2013]. The technique has also recently been refined, making it possible to graft a metal surface with polymer brushes to which a compatible polymer can be laser welded. This technique facilitates strong welds between metals and plastics [bedreinnovation.dk, 2013; Chernyy et al., 2013].

4.3 Modeling of Laser Transmission Welding

Process modeling of polymer laser welding, more specifically the LTW process, is very interesting from an industrial viewpoint. The available models vary from analytical models, such as the Rosenthal approximation, to very complex finite element models [Acherjee et al., 2012a; Van de Ven, 2006]. The aim for this thesis is not to propose a new complex model for heat development in the LTW process; however, a simple model will be presented in order to give an idea of the maximum temperature in a weld seam and the molten time, i.e., the time in which the interface is molten and polymer diffusion is possible.

As an alternative to models, thermo-couples are often suggested for predicting temperature profiles. However, it is often reported that these direct measurements of temperature

do not provide a representative picture of the temperature profile. Also pyrometers have been reported problematic [Van de Ven, 2006].

In this section some of the results from the advanced finite element models are presented before the relatively simple Rosenthal model. This is done in order to verify the Rosenthal model. Furthermore, this section is useful to keep in mind when reading section 6.1 on page 57.

4.3.1 Temperature Development with Advanced Models

The term *temperature development* refers to the temperature profile over time at a fixed point in the welding seam (typically the center of the seam). One characteristic of the laser welding process is that the maximum temperature can become very high, i.e., near the polymer decomposition temperature. Finite difference modeling of an iPP/iPP lap-joint with $P_{\text{laser}} = 100$ W and $v_{\text{laser}} = 70$ mm/s has estimated a peak temperature of more than 250 °C, and a molten-time of approximately 0.1 s, see figure 4.7 [Hadriche et al., 2010].

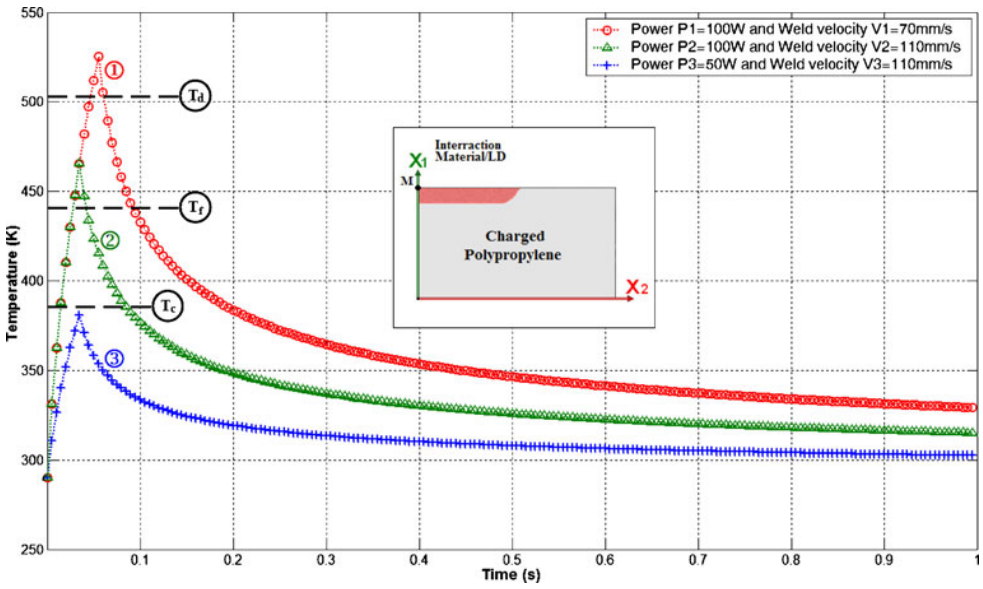

Figure 4.7: Temperature profiles measured in Kelvin at the point M for three different line energies. Note the short processing time and the relatively high temperature [Hadriche et al., 2010].

Other finite element models have been suggested; Mayboudi et al. [2010] modeled the temperature profile in a T-joint of PA6 using $P_{\text{laser}} = 60$ W and $v_{\text{laser}} = 10$ mm/s resulting in a maximum temperature of 333 °C and a molten-time in the range of seconds.

A more analytical approach to determine the temperature profile in the weld seam is suggested by von Bulow et al. [2009]. They modeled a PEO/PEO lap-joint and took reflection and scattering into account, and with $P_{\text{laser}} = 107$ W and $v_{\text{laser}} = 200$ mm/s a maximum temperature of 250 °C was reported. This was also in correspondence with experiments.

Furthermore, Ilie et al. [2007] verified models taking Mie scattering into account using an experimental setup with $P_{\text{laser}} = 0.39$ W and $v_{\text{laser}} = 8$ mm/s, resulting in a very slow

temperature build-up of 65 s reaching a maximum of 58 °C. It should be noted that this was not enough to reach glass transition point of the weld material (PMMA), which also explains why the theory matches experiments nearly perfectly.

More extreme temperatures have also been suggested. In a self-developed finite-element code, Van de Ven [2006] computes a maximum temperature of more than 500 °C in a PVC/-PVC lap-joint with $P_{\text{laser}} = 10$ W and $v_{\text{laser}} = 50$ mm/s. The FEM model takes the temperature dependence of thermal and optical parameters into account – the most sophisticated model seen. Moreover, an important conclusion is that the highest temperature is reached at a distance inside the absorbing material (1.25 mm in this case). This relatively high temperature is supported by Acherjee et al. [2012b], who suggest a peak temperature in PC of 450 °C with $P_{\text{laser}} = 12$ W, $v_{\text{laser}} = 25$ mm/s, $d_{\text{beam}} = 1.5$ mm, and a carbon black content of 0.15 w%. Lastly, Zoubeir and Elhem [2011] have proven a temperature peak at 694 °C and a molten time of several seconds (> 4 s) with $P_{\text{laser}} = 100$ W and $v_{\text{laser}} = 110$ mm/s.

4.3.2 The Rosenthal Approximation

The advanced FE models are able to take the temperature dependence of specific heat capacity, density and thermal conductivity into account, and some models even incorporate the variation with pressure [Van de Ven, 2006]. In this section a simple analytical solution to laser welding with a moving heat source is presented. This solution is also known as the Rosenthal approximation, as it was originally presented by D. Rosenthal in the early 1940s for the welding of metals. The following is based on a lecture and discussion with Jens Klæstrup Kristensen [Klæstrup, 2011]. When applied to transmission laser welding of plastics, some of the simplifications to the model are:

- All energy is absorbed in the surface of the absorbing material.
- The heat conduction across the interface from the absorbing to the transmissive part is assumed perfect, i.e., without contact resistance, but alternatively a difference between the absorbing and transmitting part can be accounted for by introducing an adjusting parameter.
- The complex phase transition from the solid to the molten state of the polymer is ignored. Likewise, the temperature dependence on physical parameters, such as λ, ρ, and c, are neglected. For instance, Van de Ven [2006] reports that the absorbance (A) changes rapidly with temperature, e.g., for pure PVC, A changes from approximately 0 (only transmission) to nearly 0.9, when the temperature reaches 200 °C.
- The heat source is point-shaped, and the welded specimen is infinite in width, length, and thickness, as illustrated in figure 4.8. Likewise, another solution exist for a line-shaped heat source and for very thin specimens.

Fourier's second law for heat conduction states:

$$\frac{\partial T}{\partial t} = \alpha \nabla^2 T, \tag{4.8}$$

where α is the thermal diffusivity ($\alpha \equiv \frac{\lambda}{\rho c}$), T is the temperature, t the time, λ the material's thermal conductivity, ρ the density, and c the specific heat capacity. Equation 4.8 can also

be written as:

$$\frac{\partial^2 T}{\partial x^2} + \frac{\partial^2 T}{\partial y^2} + \frac{\partial^2 T}{\partial z^2} = \frac{1}{\alpha}\frac{\partial T}{\partial t}, \tag{4.9}$$

where x, y, and z are the coordinates in the fixed coordinate system as presented in figure 4.8.

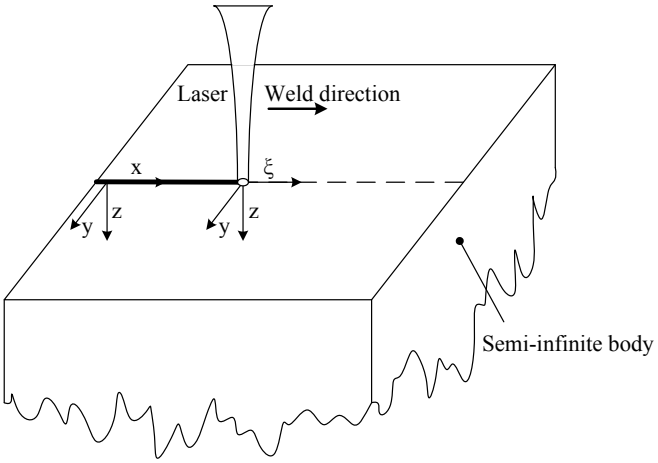

Figure 4.8: The fixed (x,y,z) coordinate system and the moving (ξ,y,z) coordinate system used for the Rosenthal approximation [Klæstrup, 2011].

The heat source is moving at a constant speed, v_{laser}, along the x-axis. A new moving coordinate system (ξ,y,z) is now introduced with the heat source at the origin, i.e., $\xi = x - v_{\text{laser}}t$. As a quasi stationary situation is reached, equation 4.9 transforms into:

$$\frac{\partial^2 T}{\partial \xi^2} + \frac{\partial^2 T}{\partial y^2} + \frac{\partial^2 T}{\partial z^2} = \frac{v_{\text{laser}}}{\alpha}\frac{\partial T}{\partial \xi}, \tag{4.10}$$

The solution to equation 4.10 for a semi-infinite body becomes:

$$T(R,x) = \frac{q}{2\pi\lambda R}\exp\left[\frac{-v_{\text{laser}}\xi}{2\alpha} - \frac{v_{\text{laser}}R}{2\alpha}\right], \tag{4.11}$$

where $R = \sqrt{\xi^2 + y^2 + z^2}$ is the 3D distance from the heat source to the point in question, while q is the heat power, i.e., the laser power. For welding of plastics, the high speed solution is very relevant, since compared to metals the welding speed is high and the thermal conductivity low; this combined makes heat conduction along the x-axis negligible[1]. By keeping q/v_{laser} constant and using the time (t) as a parameter instead of ξ, equation 4.11 reduces to:

$$T(y,z,t) = \frac{q}{2\pi\lambda v t}\exp\left[\frac{-(y^2+z^2)}{4\alpha t}\right], \tag{4.12}$$

[1] A rough estimation reveals that the high-speed approximation is valid at a distance less than 0.1 mm from the heat source when welding faster than 10 mm/s [Klæstrup, 2011].

The Fast Moving Gaussian Distributed Heat Source on a Semi-Infinite Body

Instead of having a point-shaped heat input, a Gaussian distributed heat input can be used, as proposed by Rykalin in the 1950s. With this modification, equation 4.12 becomes:

$$T(y,z,t) = \frac{q}{2\pi\lambda v} \cdot \frac{\exp\left(\frac{-z^2}{4\alpha(t_z+t)}\right)}{\sqrt{t_z+t}} \cdot \frac{\exp\left(\frac{-y^2}{4\alpha(t_y+t)}\right)}{\sqrt{t_y+t}}, \tag{4.13}$$

where t_y and t_z are measures of the width of the Gaussian distribution in the y and z directions. t_y and t_z are calculated through $y_{1/e}$ and $z_{1/e}$, which are the distances in both directions, where the intensity is lowered to 1/e of the initial value. The relations are:

$$t_y = \frac{y_{1/e}^2}{4\alpha} \qquad t_z = \frac{z_{1/e}^2}{4\alpha}. \tag{4.14}$$

In equation 4.4 on page 30, the optical inter-penetration depth (a) is equal to $z_{1/e}$. At the surface (at $z = 0$), equation 4.13 becomes:

$$T(y,0,t) = \frac{q}{2\pi\lambda v} \cdot \frac{\exp\left(\frac{-y^2}{4\alpha(t_y+t)}\right)}{\sqrt{t_y+t}\sqrt{t_z+t}}, \tag{4.15}$$

Example 4.2
What is the temperature in the weld seam of a iPP/iPP lap-joint with a carbon black content of 0.4 w% (i.e., $z_{1/e} = 30\ \mu m$, see example 4.1) at various distances from the center weld line? The weld is performed with a 100 W laser with $y_{1/e} = 0.25$ mm and $v_{laser} = 110$ mm/s.

A theoretical temperature profile for the weld seam can be calculated from equation 4.15. The physical input parameters, such as λ, ρ, and c, are listed in table 5.1 on page 54. Using the Matlab program `laserweld`, the temperature profile is plotted in figure 4.9

By comparing the different curves in figure 4.7, it can be seen that the temperature decreases strongly as a function of the distance from the weld line center. Note that this plot has the same laser speed and laser power as the curve no. 2 in figure 4.7, where the maximum temperature reached 195 °C. This temperature is approximately reached when $y = 0.65$ mm. However, a major difference between figure 4.7 and figure 4.9 is the time in a molten state, which for the Rosenthal approximation is more than one second while the time in the finite difference model from figure 4.7 is less than 1/10 of a second.

Moreover, if the distance to the weld line center is kept constant ($y = 0.65$ mm), the model can be used to obtain an estimate of the importance of the welding speed by plotting for various speeds. This is illustrated in figure 4.10. This reveals how narrow the process window actually is, e.g., 75 mm/s results in a very hot weld seam, while a speed more than 150 mm/s results in a temperature below the melting point.

In conclusion, the analytical Rosenthal approximation can predict the temperature development of a polymer laser welding process. The results are consistent with earlier finite difference models. However, the predictions are limiting by the input parameters, which in this model do not vary with temperature and pressure. On the other hand side, the purpose of this thesis is not to accurately determine the temperature in a weld seam. The point is that the temperature gets very high – close to the decomposition temperature.

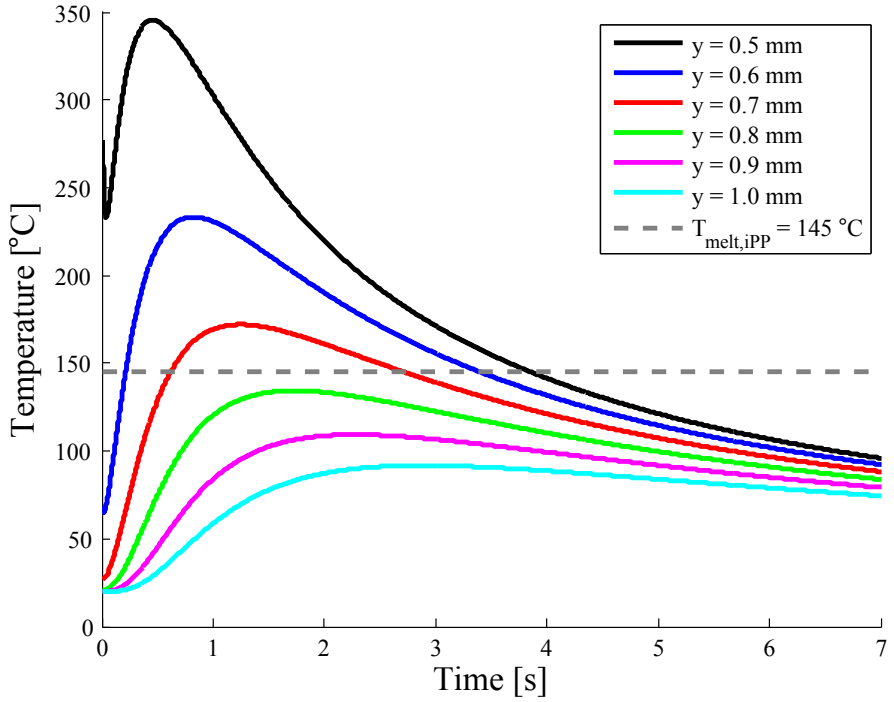

Figure 4.9: The temperature profile at different distances from the weld line. The plot assumptions are seen in example 4.2.

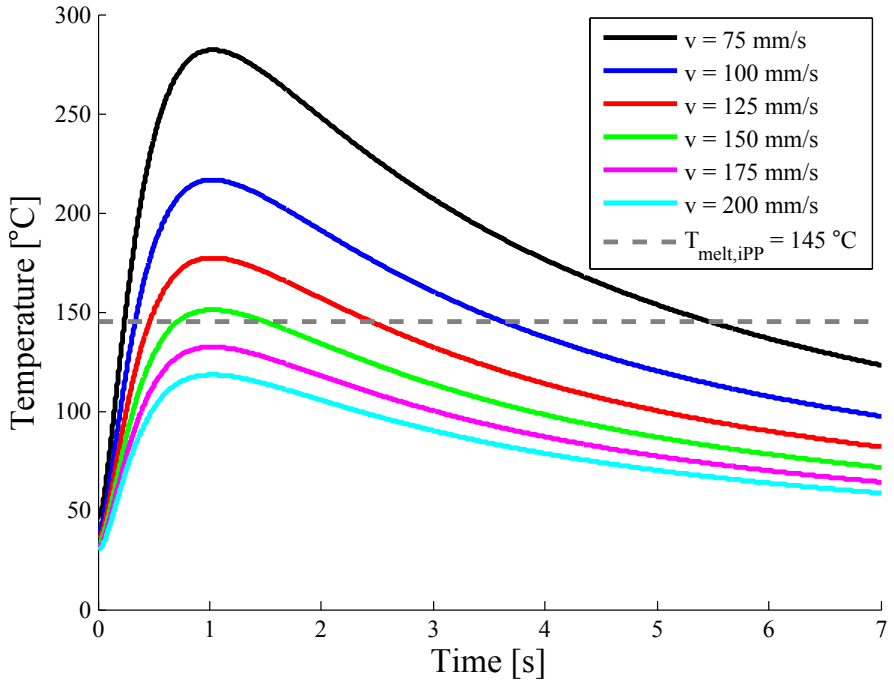

Figure 4.10: Temperature profiles for y fixed at 0.65 mm with parameters set as discussed in example 4.2.

CHAPTER 5

POLYMER PHYSICS

The word polymer is Greek and translates to *many parts*, i.e., a chemical substance consisting of many (10^2 to 10^9) identical parts called monomers taking the form (A–A–A–…–A–A). For these very large molecules the spatial appearance is difficult to predict, and therefore statistical tools are necessary to predict physical properties like size, shape, and mobility [Doi, 1996].

In this chapter the general accepted theories of polymer physics are presented, while more recent research is presented in chapter 6. The chapter deals with several new material constants, which might be new to the reader. In section 5.6 on page 55 these constants are summarized in two tables.

5.1 Molecular Chain Conformation

A polymer molecule has many internal degrees of freedom, for instance the rotational freedom about each C–C bond in a polyethylene molecule, and does therefore occupy different spatial configurations. On the atomic level the bond angle in the C–C–C configuration is 109.46°, and the molecular configuration is therefore not random. However at longer scales, all bond directions have the same probability, i.e., no correlation between different bonds exist; thus, the polymer chain configuration can be considered a random walk. In figure 5.1 a random walk of a polymer chain is presented and important quantities denoted. An important quantity in random walk theory is the end-to-end vector, $\vec{R}$, defined as the sum of individual bond vectors, i.e:

$$\vec{R} = \sum_{i=1}^{N} \vec{r}_i . \tag{5.1}$$

Clearly, the average value $\langle \vec{R} \rangle$ of $\vec{R}$ is zero, since the $\vec{r}_i$'s are independent and thereby the probability distribution function is symmetric around zero. Instead, the average of the square of $\vec{R}$, $\langle \vec{R}^2 \rangle$, is therefore considered:

$$\langle \vec{R}^2 \rangle = \sum_{n=1}^{N} \sum_{m=1}^{N} \langle \vec{r}_n \cdot \vec{r}_m \rangle . \tag{5.2}$$

Again, when $n \neq m$ no correlation between bond directions exist, i.e., $\langle \vec{r}_n \cdot \vec{r}_m \rangle = \langle \vec{r}_n \rangle \langle \vec{r}_m \rangle = 0$; thus,

$$\langle \vec{R}^2 \rangle = \sum_{n=1}^{N} \langle \vec{r}_n^2 \rangle = Nb^2, \tag{5.3}$$

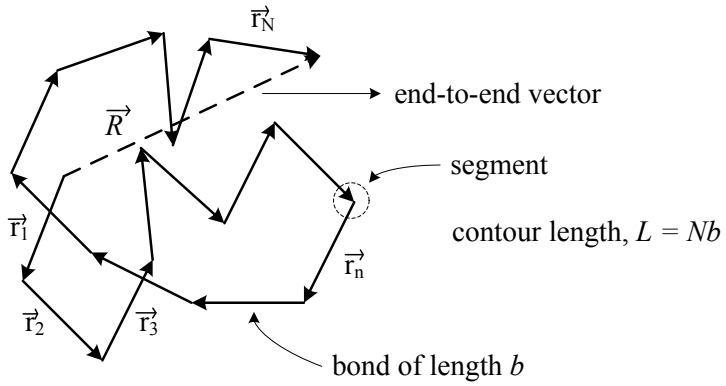

Figure 5.1: The random walk model of a polymer consisting of N links of length b. Note that b is not the length of a C–C bond, but instead the length of a number of bonds ensure the random walk assumption, see section 5.1.2 on the next page.

i.e., polymer size scales with $N^{1/2}$; hence, also $M^{1/2}$ [Doi, 1996; Pethrick, 2010]. Polymers for which the root-mean-square end-to-end distance scales with $M^{1/2}$ are said to be in the theta-state. In the melt state polymers also exhibit an $M^{1/2}$ scaling [Dealy and Larson, 2006].

5.1.1 Real Polymer Chains

In real polymer chains the bonds will not be free to adopt an arbitrary angle in space; the bonds are *valence constrained*, i.e., bond angles are restricted due to valence electrons and other chemical bonds. For instance, a carbon atom in a polyethylene molecule is covalently bonded to two hydrogen atoms and two other carbon atoms, where the C–C–C bond angle is 109.46° [Pethrick, 2010].

Furthermore, each monomer segment does not exhibit rotational freedom around the azimuthal angle of the polymer backbone. For PE the CH_2-segments are distributed in *gauche* and *trans* structures along the backbone in order to minimize potential energy [Doi, 1996].

Long-range interaction of segments can also cause the polymer chain to spatially increase. This is often referred to as the *excluded volume effect*, i.e., segments cannot occupy areas already occupied by another segment. In one-dimensional models, this restriction is crucial, whereas in three dimensions the consequence is minor [Doi, 1996].

In polymer melts, all three above-mentioned mechanisms imply that the actual $\langle \vec{R}^2 \rangle$ must be larger than the results from the random walk model. The ratio between the actual square end-to-end vector, $\langle \vec{R}^2 \rangle_0$, and the theoretical value obtained from the random walk model is denoted C_∞ and is defined as:

$$C_\infty \equiv \frac{\langle \vec{R}^2 \rangle_0}{nl^2}, \tag{5.4}$$

where n is the number of covalent bonds in the backbone and l is the bond length. C_∞ can be interpreted as a measure of the chain flexibility. The ∞-symbol indicates that the number of chains is very large, resulting in C_∞ converging towards a material constant [Fetters et al., 2007].

Radius of Gyration

The end-to-end vector can only be represented for linear polymer chains. For architecturally complex, e.g., branched polymers, the radius of gyration is more convenient. The square of radius of gyration is given as [Doi, 1996].

$$R_g^2 = \frac{1}{N}\sum_{n=1}^{N}\left\langle\left(\vec{R}-\vec{R_G}\right)^2\right\rangle, \tag{5.5}$$

where R_G is the center of gravity. For linear polymers, with molecular weight M, monomer molecular weight M_0, and j backbone bonds pr. monomer, the radius of gyration is given as:

$$\langle R_g\rangle = \sqrt{\frac{C_\infty l^2 j}{6M_0}M}, \tag{5.6}$$

again, note the $M^{1/2}$ scaling. Physically, the radius of gyration of a given object can be interpreted as an equivalent sphere with all mass gathered in the sphere shell and same moment of inertia as the object.

5.1.2 Polymer Chain Dimensions

The polymer backbone for polyolefins are zig-zagged, which means that the length of a fully extended polymer – the contour length (L) – is given as [Fetters et al., 2007]:

$$L = l\cdot n\cdot\sin(\theta/2) = l\cdot n\cdot K_g. \tag{5.7}$$

K_g is called the geometric constant and is equal to 0.816 for $\theta = 109.46°$. Equation 5.4 can be rewritten using terms from polymer physics:

$$\langle R^2\rangle_0 = C_\infty n l^2 = C_\infty j N l^2 = C_\infty j\frac{M}{M_0}l^2, \tag{5.8}$$

where j is the number of backbone bonds pr. monomer, M is the molecular weight, M_0 is the monomer molecular weight. Regarding the step length of polymers, three definitions exist [Dealy and Larson, 2006]:

Effective random walk step (b_n): Defined from the number of backbone bonds:

$$b_n \equiv \sqrt{\frac{\langle R^2\rangle_0}{n}}, \tag{5.9}$$

Statistical segment length (b): Defined from the degree of polymerization:

$$b \equiv \sqrt{\frac{\langle R^2\rangle_0}{N}}. \tag{5.10}$$

Consequently, $b = b_n\sqrt{j}$.

Kuhn segment length (b_K): Defined from the extended contour length:

$$b_K \equiv \frac{\langle R^2 \rangle_0}{L} = \frac{C_\infty n l^2}{n l K_g} = \frac{C_\infty}{K_g} l. \tag{5.11}$$

This means that the number of Kuhn links (N_K) is given as:

$$N_K = \frac{K_g^2}{C_\infty} n. \tag{5.12}$$

In literature both b and b_K are frequently used, and it is important to note carefully which definition is used [Dealy and Larson, 2006; Fetters et al., 2007].

Example 5.1
What is the radius of gyration of the three polymers (mHDPE, mPP, and PS) from table 8.1 on page 87?

Utilizing data from table 5.1 on page 54 and equation 5.6, radius of gyration is determined to:

$$R_{g,\text{mHDPE}} = \sqrt{\frac{7.38 \cdot 2 \cdot 128{,}000 \text{g/mol}}{6 \cdot 28.05 \text{g/mol}}} \cdot 0.154\text{nm} \qquad = 16.3\text{nm} \tag{5.13}$$

$$R_{g,\text{mPP}} = \sqrt{\frac{6.15 \cdot 2 \cdot 237{,}000 \text{g/mol}}{6 \cdot 42.08 \text{g/mol}}} \cdot 0.154\text{nm} \qquad = 16.5\text{nm} \tag{5.14}$$

$$R_{g,\text{PS}} = \sqrt{\frac{14.2 \cdot 2 \cdot 192{,}000 \text{g/mol}}{6 \cdot 104.14 \text{g/mol}}} \cdot 0.154\text{nm} \qquad = 14.4\text{nm} \tag{5.15}$$

Note that the root-mean-square of the end-to-end vector is $\sqrt{6}$ times larger.

5.2 Entanglements

When single polymer chains move around in a polymer melt, they experience movement restrictions as their length exceed a certain threshold. These restrictions are called *entanglements*, and in an entangled melt the polymer movement is blocked perpendicular to its contour, while the ends are free to move. This picture of a single polymer in an entangled melt is called *the tube model*, which is illustrated in figure 5.2. Entanglements are not really understood – some regard them as "knots", while other just see them as a virtual explanation for entangled polymer melts [Graham, 2002].

5.2.1 Tube and Entanglement Dimensions

As indicated in figure 5.2b there is a certain length between each entanglement comparable to the mesh size, and equivalent to this length is the molecular weight between entanglements, M_e. This molecular weight can be defined in different ways, and it is important to

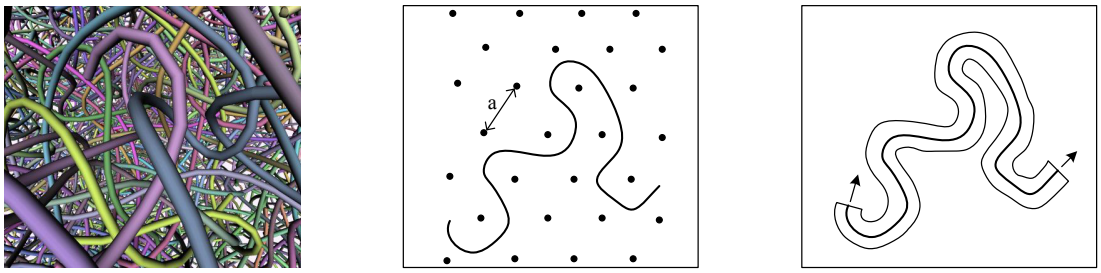

(a) (b) (c)

Figure 5.2: The concept of polymer entanglements: (a) An entangled system of polymers – a multi-body problem. (b) A transverse section of one polymer – other polymers are cut and form obstacles in a mesh structure. (c) Instead of a mesh, the obstacles can be pictured as a tube in which the polymer can move back and forth.

realize which one is used. In this thesis, Graessley's definition is preferred [Graessley, 1980; Larson et al., 2003]:

$$M_e^G \equiv \frac{4}{5}\frac{\rho RT}{G_N^0}, \tag{5.16}$$

where ρ is the density of the polymer melt, and G_N^0 is the plateau modulus. This definition should only apply to highly entangled systems, since G_N^0 is slightly dependent on the degree of entanglement. If the $4/5$ factor is omitted, the molecular weight between entanglements (M_e^F) are known as Fetters' definition [Graham, 2002; Larson et al., 2003].

$\langle R^2 \rangle_0$ could be simplified as a random walk of N_K links with length b_K. Similarly, it can be given as a random walk with Z links of length a; $Z \equiv M_w/M_e^G$ being the number of entangled segments and a being the segment length. In literature, a is referred to as the *tube diameter*[1], and can be estimated as:

$$N_K b_K^2 = Z a^2 \Rightarrow a = b_K\sqrt{\frac{N_K}{Z}} = b_K\sqrt{N_{K,e}}, \tag{5.17}$$

where $N_{K,e}$ is the number of Kuhn links between entanglements.

[1] This name is misleading, since a does not denote a diameter, but is a measure of the mesh size.

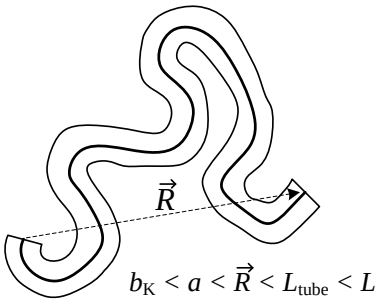

Figure 5.3: The various dimensions of the tube model. b_K is the Kuhn length, a is the tube diameter, $\vec{R}$ is the end-to-end vector, L_{tube} is the contour length of the tube, and L is the polymer contour length [Larson et al., 2003].

5.2.2 Critical Molecular Weight, M_c

The critical molecular weight (M_c) denotes the transition in zero shear viscosity (η_0) as function of polymer molecular weight as the exponent change from ~1 to ~3.4. Empirically, a relation between M_e^G and M_c is determined through the packing length (p). The packing length is defined as the ratio between the occupied volume of a chain and $\langle R^2 \rangle_0$ [Fetters et al., 2007]:

$$p \equiv \frac{M}{\langle R^2 \rangle_0 \rho N_A} = \frac{M_K}{b_K^2 \rho N_A}, \tag{5.18}$$

by which M_c is estimated to:

$$M_c = M_e^G \left[\frac{6.60\text{Å}}{p} \right]^{0.534}, \tag{5.19}$$

The ratio M_c/M_e^G is reported to range from 0.93 to 5.0 [Fetters et al., 2007] and not 2.0 for all polymers as suggested by Wool [1995]. For HDPE, iPP, and PS the ratio is 5.0, 2.0, and 2.4, respectively, see table 5.1 on page 54.

5.3 Rouse Dynamics

As discussed in section 5.1, the random walk model or bead-rod model is valid for describing static properties of a polymer molecule. Therefore, a *bead-spring model* should be evident for describing the dynamics of a polymer molecule. The bead-spring model was originally proposed by Rouse [1953] and is still being modified in modern theories [Likhtmann, 2011].

Basically, the polymer chain is modelled as $N+1$ beads connected by N springs with a spring constant $k = 3k_B T/b_K^2$, which is shown in rubber elasticity theory. Each bead feels a drag force from the surrounding solvent proportional to their relative velocity, i.e., $\vec{F}_n = -\zeta_0 \partial \vec{R}_n / \partial t$, where ζ_0 is called the monomeric friction coefficient [Doi, 1996]. This simple version of the bead-spring model neglects important features, and the following assumptions are made:

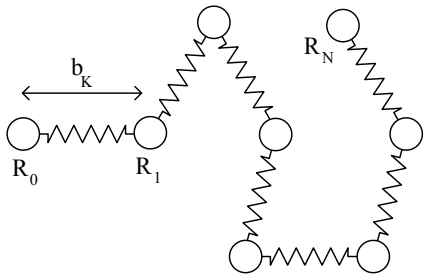

Figure 5.4: The bead spring model. Numbers (n and N) and lengths (b_K) refer to Kuhn segments.

No hydrodynamic interactions: Beads moving in the solvent will not affect movement of other beads. In reality if one bead moves, the surrounding solvent will also move, influencing the movement of other beads.

No topological constraints: Beads are not prohibited from passing through each other and take up the same location in space.

No inertial forces: No forces from the acceleration term ($m\partial^2\vec{R}_n/\partial t^2$), i.e., no second derivative part in the equations of motion.

This seemingly unphysical model turns out to be very useful, especially for polymer melts [Dealy and Larson, 2006; Doi, 1996]. This is further discussed in section 5.3.2 on page 47.

5.3.1 Equations of Motion

The bead positions are labeled $\vec{R}_0, \vec{R}_1, \ldots, \vec{R}_N$, and the force due to the nth spring is calculated using $\vec{r}_0 = \vec{R}_n - \vec{R}_{n-1}$. All things considered, the beads experience forces from drag, springs, and random Brownian collisions. A free body force analysis on the nth bead gives following set of equations of motion:

$$\zeta\frac{\partial\vec{R}_n}{\partial t} = \frac{3k_BT}{b_K^2}\left(\vec{R}_{n-1} - 2\vec{R}_n + \vec{R}_{n+1}\right) + \vec{f}_n(t), \tag{5.20}$$

where $\vec{f}_n(t)$ is the random Brownian force. To ensure that equation 5.20 is valid at the chain ends, following boundary conditions are introduced.

$$\vec{R}_{-1} = \vec{R}_0 \quad \wedge \quad \vec{R}_{N+1} = \vec{R}_N. \tag{5.21}$$

Equations 5.20 and 5.21 define a system which can be solved to give the trajectories of each bead. However, it turns out that it is more convenient to consider the continuous limit, which is easily[2] recognized as:

$$\zeta\frac{\partial\vec{R}}{\partial t} = \frac{3k_BT}{b_K^2}\frac{\partial\vec{R}}{\partial n^2} + \vec{f}(n,t), \tag{5.22}$$

[2] $\vec{R}_{n-1} - 2\vec{R}_n + \vec{R}_{n+1}$ is the discrete version of the continuous $\frac{\partial\vec{R}}{\partial n^2}$, as known from finite difference [Doi and Edwards, 1986]

with boundary conditions

$$\frac{\partial \vec{R}}{\partial n} = 0 \quad \text{for} \quad n = 0, N. \tag{5.23}$$

Solutions

To solve the equations of motion in equation 5.22, it is convenient to develop a Fourier series to obtain a system of ordinary differential equations. The equation is diaganolized by the following transformation[3].

$$\vec{X}_{\mathrm{p}}(t) = \frac{1}{N}\int_0^N \vec{R}(n,t)\cos\left(\frac{p\pi n}{N}\right) dn, \tag{5.24}$$

where the inverse transform is given as.

$$\vec{R}(n,t) = \vec{X}_0 + 2\sum_{\mathrm{p}=1}^{\infty} \vec{X}_{\mathrm{p}}\cos\left(\frac{p\pi n}{N}\right). \tag{5.25}$$

Applying this transform to equation 5.22 gives,

$$\frac{\vec{X}_{\mathrm{p}}}{\partial t} = -\frac{3k_{\mathrm{B}}Tp^2\pi^2}{N^2 b_{\mathrm{K}}^2 \zeta}\vec{X}_{\mathrm{p}} + \vec{g}_{\mathrm{p}}(t), \tag{5.26}$$

where $\vec{X}_{\mathrm{p}}$ is the pth Fourier component of the random force $\vec{f}(n,t)$. The pre-factor on the right-hand-side of equation 5.26 is often written as p^2/τ_{R}, where τ_{R} is the longest Rouse time of relaxation, which is given as[4]:

$$\tau_{\mathrm{R}} = \frac{\zeta b_{\mathrm{K}}^2 N_{\mathrm{K}}^2}{3\pi^2 k_{\mathrm{B}}T} = \frac{\zeta b_{\mathrm{K}}^2 M^2}{3\pi^2 M_{\mathrm{K}}^2 k_{\mathrm{B}}T}. \tag{5.27}$$

Another important quantity is the equilibration time (τ_{e}), which is defined as the Rouse time for a polymer chain of length $M_{\mathrm{e}}^{\mathrm{G}}$ [Dealy and Larson, 2006]:

$$\tau_{\mathrm{e}} = \frac{\zeta a^2 M_{\mathrm{e}}^{\mathrm{G}}}{3\pi^2 k_{\mathrm{B}}T M_{\mathrm{K}}}. \tag{5.28}$$

Note the important relation that $\tau_{\mathrm{R}} = Z^2\tau_{\mathrm{e}}$. Finally, the Rouse relaxation time for a single Kuhn segment (τ_0) must be determined, which can be done by substituting M_{K} with M in equation 5.27; thus τ_0 is also a material constant.

$$\tau_0 = \frac{\zeta b_{\mathrm{K}}^2}{3\pi^2 k_{\mathrm{B}}T}. \tag{5.29}$$

[3] Mathematical details for this step are provided by Doi and Edwards [1986] and Likhtmann [2011].

[4] Note that N here switches to N_{K}.

5.3.2 Validity of the Rouse Model

As discussed above, seemingly drastic assumptions and simplifications have been made in deriving the Rouse model. For instance, the neglect of hydrodynamic interactions causes the model to fail for dilute solutions. This can be corrected for using the Zimm model; however, for concentrated solutions or melts the Rouse model is still valid [Doi, 1996]. For melts this means that the ζ-parameter can be considered a fitting parameter; the temperature dependence is also within ζ, which is given by the Volger-Fulcher equation [Dealy and Larson, 2006]:

$$\ln \zeta = A + \frac{B}{T - T_0}. \tag{5.30}$$

Note that for $T_0 = 0$, the expression simplifies to an Arrhenius model. The Volger-Fulcher relation is reasonable since ζ is proportional to η_0 [Dealy and Larson, 2006]. ζ-values are rarely reported in literature, and they often deviate a lot, e.g., for PE the ζ-value at 190 °C ranges from $4.74 \cdot 10^{-13}$ kg/s [van Meerveld, 2004] to $1.30 \cdot 10^{-12}$ kg/s [Vega et al., 2004].

Regarding PP, van Meerveld [2004] has compared various studies and reported ζ_{iPP} at 190 °C to range from $1.04 \cdot 10^{-12}$ kg/s to $1.86 \cdot 10^{-12}$ kg/s. The difference is explained by different definitions of M_e^G. Moreover, it is noticeable that the ζ-value of aPP is in the range of 10^{-10} kg/s [van Meerveld, 2004].

In the chapters 10 [Juhl et al., 2013a] and 11 [Juhl et al., 2013b] the temperature dependence of ζ is determined for mHDPE, mPP, and PS.

5.4 Reptation Dynamics

Reptation is another mode of relaxation for entangled polymers. The idea of reptation is to predict the disengagement time relying on the work of de Gennes [1971][5] who pictured an entangled polymer chain as a snake trapped inside a tube. Inside the tube, the polymer is allowed to move back and forth in order to experience new configurations; and when one end escapes the initial tube, it is freed from entanglements, see figure 5.5. Assuming a lattice model of reptation where the motion of center of mass is considered, the disengagement time or reptation time can be estimated to [Doi, 1996]:

$$\tau_{\text{rep}} = \frac{\zeta N_K^3 b_K^4}{\pi^2 k_B T a^2} \tag{5.31}$$

where N_K is number of Kuhn segments and b_K is the Kuhn segment length. Note that $\tau_{\text{rep}} \propto N_K^3 \propto M^3$; however, this is only true for $Z >> 1$, and for engineering polymers the exponent is more likely to be 3.4 ± 0.2.

[5] This paper has more than 2,400 citations, and de Gennes was awarded the Nobel Prize in physics in 1991 "*for discovering that methods developed for studying order phenomena in simple systems can be generalized to more complex forms of matter, in particular to liquid crystals and polymers*" [nobelprize.org, 2011].

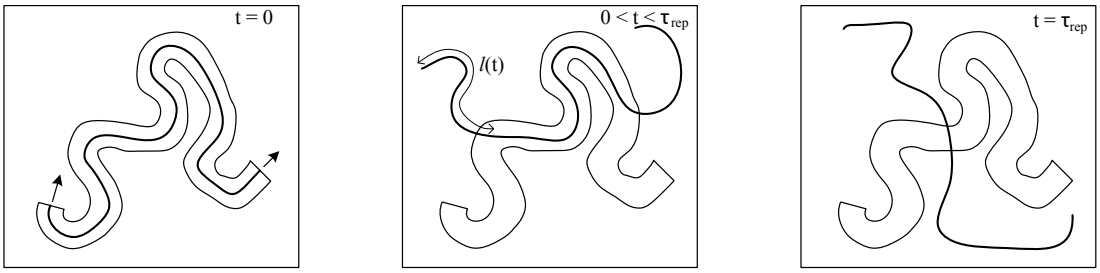

Figure 5.5: Relaxation of the minor chain inside the tube (a) Initially, the polymer is trapped inside its tube. (b) As time passes, the chain ends start to relax, and the minor chain length ($l(t)$) increases with $t^{1/2}$. (c) At the reptation time the polymer is fully relaxed and has escaped its tube.

Example 5.2

What is the reptation time for HDPE and iPP at 190 °C using the reptation model?

Data from table 5.1 on page 54 are put into equation 5.31, and values of ζ are determined:

$$\tau_{\text{rep,PE}} = \frac{3.40\cdot10^{-13}\text{kg/s}\cdot\left(\frac{128{,}000\text{g/mol}}{150.4\text{g/mol}}\right)^3\cdot(1.37\text{nm})^4}{\pi^2 k_\text{B}\cdot 463\text{K}\cdot(3.60\text{nm})^2} = 0.90\text{ms} \tag{5.32}$$

$$\tau_{\text{rep,iPP}} = \frac{1.60\cdot10^{-12}\text{kg/s}\cdot\left(\frac{237{,}000\text{g/mol}}{187.8\text{g/mol}}\right)^3\cdot(1.14\text{nm})^4}{\pi^2 k_\text{B}\cdot 463\text{K}\cdot(6.90\text{nm})^2} = 1.8\text{ms} \tag{5.33}$$

Compared to τ_{rep} from equations 5.44 and 5.45, deviations are quite large, especially for iPP. This is implemented in the EXPAND program.

Equation 5.31 is very convenient to couple to equations 5.27 and 5.28, giving:

$$\tau_{\text{rep}} = 3Z\tau_\text{R} = 3Z^3\tau_\text{e}. \tag{5.34}$$

The reptation model exists in a few variants. The most famous is the one presented in equation 5.31, where the reptation time is given as a function of the monomeric friction coefficient (ζ). Another version linking the reptation time to a macroscopic feature such as zero shear viscosity is [Doi, 1996; Doi and Edwards, 1986]:

$$\eta_0 = \frac{\pi^2 c k_\text{B} T}{20 N_\text{e}}\tau_{\text{rep}}, \tag{5.35}$$

where c is the number density of monomers, and thus equals $\rho N_\text{A}/M_0$. To determine the reptation time, it is also noticeable that it depends linearly on η_0, which varies with time. Therefore, equation 5.35 can be rewritten to:

$$\tau_{\text{rep}}(T) = \frac{20 N_\text{e} M_0}{\pi^2 k_\text{B} T\rho(T) N_\text{A}}\eta_0(T) = \frac{20 M_\text{e}^\text{G}}{\pi^2 RT\rho(T)}\eta_0(T), \tag{5.36}$$

where $M_e^G (= N_e M_0)$ is Graeslley's definition of molecular weight between entanglement, $R = k_B N_A$ is the gas constant, $\rho(T)$ is the temperature dependent melt density.

Combining equations 5.35 and 5.36, the macroscopic feature η_0 can be coupled to the microscopic features ζ and τ_{rep}. This knowledge is utilized in chapters 10 and 11.

5.4.1 Influence of Additives

Commercial plastics contain additives – small molecules, macromolecules, or particle fillers. In laser welding applications absorbers are needed; thus, it is necessary to evaluate how these will influence the reptation time. Addition of nano-particles, such as carbon black or TiO_2, will generally increase the reptation time, since the particles will block the reptation dynamics. On the other hand, if molecular absorbers, such as Lumogen®, are added the effect will be similar to adding short polymers, i.e., tube dilution will occur and the reptation time will decrease [Dealy and Larson, 2006].

5.5 Diffusion

In literature, the term polymer diffusion can be confusing due to various different definitions and diffusion mechanisms [Klein, 1990]. Examples of different phenomena are; conformational, rotational, one-dimensional, Rouse and Brownian diffusion [Doi, 1996]. In this thesis, two types of diffusion are considered [Kausch and Tirrell, 1989]:

Self-diffusion: Refers specifically to the case where a molecule moves in an environment of identical neighbors, e.g., a polymer melt.

Inter-diffusion: Refers to diffusion of polymer molecules among distinguishable molecules, e.g., diffusion of polymers across boundaries, surfaces, interfaces, etc.

5.5.1 Self-diffusion

The self-diffusion coefficient (D_s) is basically defined as,

$$D_s = \lim_{t \to \infty} \frac{\left\langle [R_G(t + t_0) - R_G(t_0)]^2 \right\rangle}{6t}, \tag{5.37}$$

where R_G is the center of mass. D_s is extremely sensitive to molecular weight, chain branching and chemical composition in general. The self-diffusion coefficient can be determined using pulsed field gradient nuclear magnetic resonance, infrared spectroscopy, neutron and small-angle X-ray scattering, and radioisotopic labeling [Kausch and Tirrell, 1989].

When dealing with self-diffusion in polymeric systems, it seems obvious to harness the contemporary knowledge within Molecular Dynamics (MD). However, it turns out that polymeric systems consisting of highly entangled molecules, which diffuses relatively long distances compared to single atoms, are too large for computers to handle [Mark, 2007]. Thus, other approaches for investigation of polymer dynamics must be considered, and one of the most accessible is rheometry.

A very central work, linking polymer physics and dynamics to rheology, is Doi and Edwards [1986]. Based on this work, consequences for self-diffusion can be derived, and two

ways of estimating the self-diffusion coefficient has been proposed [Graessley, 1980]:

$$D_s = \left(\frac{\rho RT}{270}\right)\left(\frac{M_c}{M}\right)^2\left(\frac{R_g^2}{M}\right)\left(\frac{1}{\eta_{0,M_c}}\right) \quad \text{[Pecorini and Seo, 1996]} \tag{5.38}$$

$$D_s = \left(\frac{G_N^0}{135}\right)\left(\frac{\rho RT}{G_N^0}\right)^2\left(\frac{M_e^F}{M^2}\right)\left(\frac{R_g^2}{M}\right)\left(\frac{1}{\eta_{0,M_c}}\right) \quad \text{[Jud et al., 1981]} \tag{5.39}$$

where G_N^0 is the plateau modulus, M_e^F is the molecular weight between entanglements (Fetters' definition), and M_c is the critical molecular weight. Note that Fetters' definition for entanglements has been used, however, if the two equations are compared, one will find that $M_e = 0.52M_c$, which is only true for some polymers, cf. equation 5.19 on page 44. From equations 5.38 and 5.39 the diffusion coefficient is proportional to M^{-2} which is in correspondence with Doi and Edwards [1986].

For simple linear molecules the self-diffusion coefficient (D_s) depends both on molecular weight and temperature. In general for polymers with $M > M_c$, D_s is proportional to $M^{-2}\cdot\exp(-E_a/RT)$, where E_a is the activation energy. Specifically, Lo and Narasimhan [2005] have determined the self-diffusion coefficient (D_s) for PE and iPP to[6]:

$$D_{s,PE}(M,T) = 3.54\cdot10^{-2}\frac{m^2g^2}{s\cdot mol^2}\cdot M^{-2}\cdot\exp\left(\frac{-22.3kJ/mol}{RT}\right) \tag{5.40}$$

$$D_{s,iPP}(M,T) = 4.26\cdot10^{-2}\frac{m^2g^2}{s\cdot mol^2}\cdot M^{-2}\cdot\exp\left(\frac{-39.0kJ/mol}{RT}\right) \tag{5.41}$$

Example 5.3

What is the diffusion coefficient of mHDPE and mPP from earlier examples at 200 °C? And how long will it take a polymer molecule to diffuse a radius of gyration?

From equations 5.40 and 5.41, self-diffusion coefficients are estimated to:

$$D_{s,PE}(M,T) = 3.54\cdot10^{-2}\frac{m^2}{s}\cdot128{,}000^{-2}\cdot\exp\left(\frac{-22.3kJ/mol}{R\cdot473K}\right) = 7.44\cdot10^{-15}\frac{m^2}{s} \tag{5.42}$$

$$D_{s,PP}(M,T) = 4.26\cdot10^{-2}\frac{m^2}{s}\cdot237{,}000^{-2}\cdot\exp\left(\frac{-39.0kJ/mol}{R\cdot473K}\right) = 3.74\cdot10^{-17}\frac{m^2}{s} \tag{5.43}$$

These can be compared to the radii of gyration from example 5.1, giving disengagement times of:

$$\tau_{rep,HDPE} = \frac{(16.3nm)^2}{7.44\cdot10^{-15}\frac{m^2}{s}} = 39ms \tag{5.44}$$

$$\tau_{rep,PP} = \frac{(16.6nm)^2}{3.74\cdot10^{-17}\frac{m^2}{s}} = 1.6s \tag{5.45}$$

[6] The two equations are based on extrapolation of data from Lo and Narasimhan [2005]. These equations are therefore just used for comparison with the reptation model. Note that these are based on Arrhenius kinetics, while the Volger-Fulcher kinetics is preferred for ζ in equation 5.30 on page 47

The reptation time of PP differs 3 orders of magnitude from the time estimated in example 5.2, which is explained from the extrapolations of equation 5.41. From the EXPAND program the self-diffusion coefficients are estimated to $7.25 \cdot 10^{-14} \frac{m^2}{s}$ and $4.38 \cdot 10^{-14} \frac{m^2}{s}$, respectively.

Self-diffusion due to Reptation

As discussed in section 5.4, reptation is the main relaxation mechanism for entangled polymers. In equation 5.31 the reptation time is given in terms of constants from polymer physics, and the corresponding self-diffusion coefficient is determined as [de Gennes, 1971; Doi, 1996]:

$$D_s = \frac{R^2}{3\pi^2 \tau_{rep}} = \frac{k_B T a^2}{3 N_K^2 \zeta b_K^2}. \tag{5.46}$$

As τ_{rep} is proportional to M^3, D_s is proportional to M^{-2}; and as the real exponent for the τ_{rep} is more likely 3.4, the exponent for D_s is approximately -2.3 [Doi, 1996].

5.5.2 Inter-diffusion

The characteristic diffusion coefficient for inter-diffusion is the *mutual diffusion* coefficient (D_m). Inter-diffusion is sometimes also referred to as cooperative or collective diffusion [Kausch and Tirrell, 1989]. In Fick's first law when mixing two different substances, the attending diffusion coefficient is D_m,

$$\vec{J}_i = -D_m \nabla c_i. \tag{5.47}$$

Fick's first law, equation 5.47, states that the flux of component i ($\vec{J}_i$) opposes the concentration gradient (∇c_i). The mutual diffusion coefficient can be determined from the interfacial concentration profile, which typically is determined by secondary ion mass spectrometry (SIMS) or neutron reflection (NR) [Wool, 1995]. The concentration profile can afterwards be compared to Fick's Second Law of diffusion, equation 5.48, and D_m can be estimated.

$$\frac{\partial c}{\partial t} = D_m \frac{\partial^2 c}{\partial x^2}. \tag{5.48}$$

Fick's second law is shown in one dimension, since the inter-penetration at a flat interface is only one-dimensional.

Mutual Diffusion Coefficient

For asymmetric interfaces, i.e., the welding of dissimilar polymers, the compatibility of the two materials affects the inter-diffusion. The mutual diffusion coefficient (D_m) reveals information on the mutual diffusion kinetics. Thus, D_m depends on the self-diffusion coefficients D_1, D_2, and the interaction parameter χ, see section 6.3 on page 63. If the interface consist of a slow polymer, i.e., low D_s, and a fast polymer, i.e., high D_s, the mutual diffusion of these can be dominated by the slow or the fast polymer – named slow mode theory or fast

mode theory, respectively [Lo and Narasimhan, 2005; Zhang et al., 2012b]. The slow mode theory states [Akcasu et al., 1995; Brochard et al., 1983]:

$$D_{\mathrm{m,slow}} = \left(\frac{N_1 D_1 N_2 D_2}{N_1 D_1 \phi_1 + N_2 D_2 \phi_2}\right) \cdot \left(\frac{\phi_2}{N_1} + \frac{\phi_1}{N_2} - 2\phi_1\phi_2\chi_{12}\right), \tag{5.49}$$

while the fast mode theory states [Akcasu et al., 1995; Binder, 1983]:

$$D_{\mathrm{m,fast}} = \left(N_1 D_1 \phi_2 + N_2 D_2 \phi_1\right) \cdot \left(\frac{\phi_2}{N_1} + \frac{\phi_1}{N_2} - 2\phi_1\phi_2\chi_{12}\right). \tag{5.50}$$

The fast mode theory is in best correspondence with experimental data [Kawaguchi et al., 2011; Zhang et al., 2012b]. Note that $D_\mathrm{m} = D_\mathrm{s}$ for symmetric interfaces.

Simple Fickian Diffusion

In simple Fickian diffusion, the mass transfer across the interface is described from Fick's second law of diffusion presented in equation 5.48. The equation is a partial differential equation of second order, and if the boundary is located at $x = 0$, as in figure 5.6 on the facing page, and initial conditions $n(x,0)$, the solution is:

$$C(x,t) = n(0)\mathrm{erfc}\left(\frac{x}{2\sqrt{D_\mathrm{m} t}}\right), \tag{5.51}$$

where $2\sqrt{D_\mathrm{m} t}$ is called the diffusion length and is a measure for the diffusion in the x-direction – note the $t^{1/2}$-dependence characteristic for Fickian diffusion. From Wool's theory the Fickian solution to the inter-diffusion problem only applies when $t > \tau_\mathrm{rep}$.

Diffusion from Reptation

When $t < \tau_\mathrm{rep}$, Fickian diffusion does not apply as discussed in section 3.1 on page 13. Therefore, for time scales less than the reptation time, the reptative motion must be taken into account. Such model is proposed by Zhang and Wool [1989] and is based on minor chain diffusion of single polymers. The minor chain is the part of the polymer which has escaped the initial tube through reptation, see figure 5.5 on page 48.

The minor chain length ($l(t)$) develops as the square root of time, since the reptation motion can be related to Fickian diffusion of the whole chain in one dimension. Moreover, $l(t)$ has the constriction that $l(\tau_\mathrm{rep}) = L/2$, where L is the polymer contour length. With this in mind $l(t)$ is suggested as [Wool, 1995]:

$$l(t) = \frac{L}{2}\sqrt{\frac{t}{\tau_\mathrm{rep}}}. \tag{5.52}$$

By evaluating the reptation motion across an interface, Zhang and Wool [1989] suggest following expression for the interfacial concentration profile:

$$C(x,t) = \frac{\rho}{M_0}\left[\left(\frac{l(t)}{L} + \frac{x^2}{b_\mathrm{K} L}\right)\mathrm{erfc}\left(\frac{x}{\sqrt{2l(t)b_\mathrm{K}}}\right) - \frac{x}{L}\sqrt{\frac{2l(t)}{\pi b_\mathrm{K}}}\exp\left(\frac{-x^2}{2l(t)b_\mathrm{K}}\right)\right], \text{for} \, t \geq 0. \tag{5.53}$$

Example 5.4
Plot the concentration profile at different fractions of τ_{rep} of a mHDPE/mHDPE interface welded at 190 °C. What is the diffusion length at τ_{rep} compared to interface dimensions?

Equation 5.53 is implemented in Matlab in `Concentration_reptation.m` and equation 5.51 in `Concentration_Fick.m`. Input parameters for the plots come from tables 5.1 and 5.2. The plots are presented in figure 5.6.

The diffusion length at the reptation time is,

$$l_D = 2\sqrt{5.98 \cdot 10^{-14} \frac{m^2}{s} \cdot 9.02 \cdot 10^{-4} s} = 14.7nm = 0.90 R_g. \tag{5.54}$$

Therefore, during the reptation time, i.e., less than 1 ms, the inter-penetration distance is big enough to secure full developed strength.

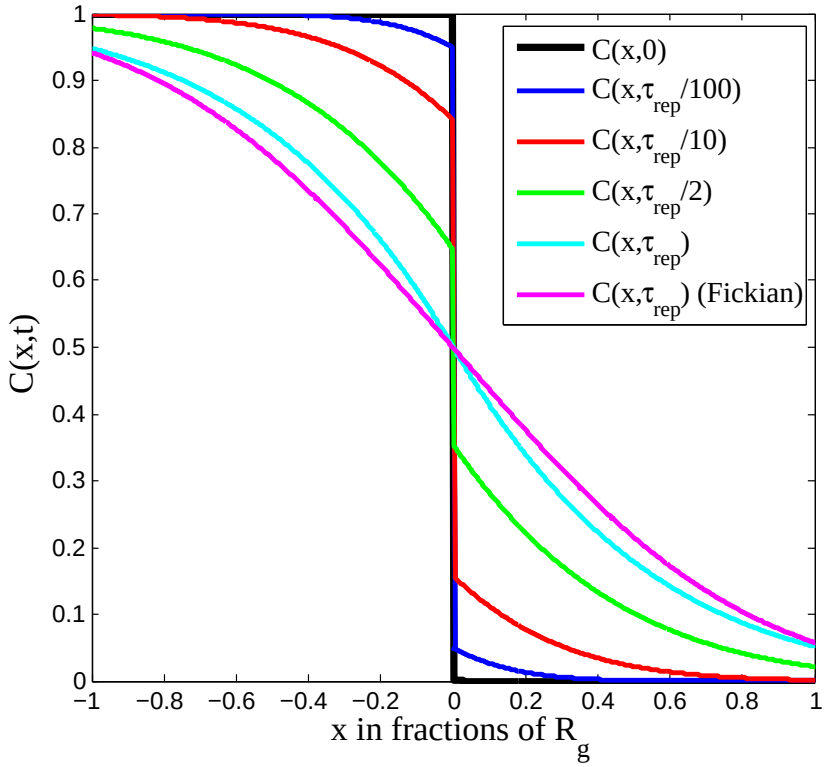

Figure 5.6: Plot of equations 5.53 and 5.51. Note the discontinuity at the interface at the times lower than τ_{rep}, which is in correspondence with the ripple experiment [Agrawal et al., 1996]. The radius of gyration is equal to 16.3 nm.

Polymer	HDPE (140 °C)	iPP (190 °C)	PS (170 °C)
l [Å] [a]	1.54	1.54	1.54
b_K [Å] [a]	13.7	11.4	26.9
$b = l\sqrt{C_\infty j}$ [Å] [b]	5.64	5.25	6.89
a [Å] [a]	36.0	69.0	85.2
C_∞ [a]	7.38	6.15	14.2
C_∞ [b]	6.7	5.8	10
j [b]	2	2	2
ζ [kg/s]	$4.74{\cdot}10^{-13}$ [e]	$1.04{\cdot}10^{-12}$ [e]	$7.89\cdot10^{-5}$ [b]
	$13.0{\cdot}10^{-13}$ [f]	$1.86{\cdot}10^{-12}$ [e]	$6.37{\cdot}10^{-5}$ [h]
	$9.32{\cdot}10^{-13}$ [i]	$1.60{\cdot}10^{-12}$ [i]	$2.13{\cdot}10^{-7}$ [i]
τ_e [s] (eq. 5.28)	$3.97{\cdot}10^{-10}$	$8.32{\cdot}10^{-9}$	$7.04{\cdot}10^{-4}$
M_0 [g/mol] [a]	28.05	42.08	104.14
M_K [g/mol] [a]	150.4	187.8	1,655
M_e^G [g/mol] [a]	832	3,880	13,280
M_c [g/mol] [b]	4,200	7,600	32,000
$N_{K,e} = a^2/b_K^2$ [a]	6.91	36.6	10.0
G_N^0 [MPa] [a]	2.6	0.43	0.19
$L_e = \frac{C_\infty M_e j l^2}{M_0 b_K}$ [nm] [b,c] $= N_{K,e} b_K$	9.44	41.6	26.9
$R_{g,e} = \sqrt{\frac{C_\infty M_e j}{6M_0}}\, l$ [nm] [a,b]	1.32	2.12	3.78
T_g [°C] [j]	-95	-19	97
T_f/T_m [°C] [j]	130–146	160–208	160
T_d [°C] [j]	360–390	336–366	318–348
E_a [kJ/mol] (diff.) [d]	25	44	59
E_a [kJ/mol] (dec.) [d]	264	243	230
δ [MPa$^{1/2}$] [d]	16.0	17.0	19.1
V_m [cm^3/mol] [d]	32.9	49.1	98.0
γ [mJ/m^2] [d]	28.7	22.6	43
ρ [kg/m^3] [a]	785	766	969
n [d]	1.535	1.490	1.591
λ [g] [W/m·K]	0.52	0.12	0.13
$c_{p,sol}$ [J/kg·K]	1550	1630	1210
$c_{p,liq}$ [J/kg·K]	2260	2140	1720
G_c [kJ/m^2] [k]	6–7	8	2
K_c [MPa$\sqrt{\text{m}}$] [k]	2	3	2

Table 5.1: Physio-molecular properties of polymers. [a] refers to [Fetters et al., 2007], [b] refers to [Wool, 1995], [c] refers to [Dealy and Larson, 2006], [d] refers to [van Krevelen and te Nijenhuis, 2009], [e] refers to [van Meerveld, 2004], [f] refers to [Vega et al., 2004], [g] refers to [Mark, 2007], [h] refers to [Majeste et al., 1998], [i] refers to own experiments, see chapter 10 on page 101, [j] refers to [Klein, 2011], [k] refers to [Ashby and Jones, 2012]. According to Fetters et al. [2007], the ratio M_c/M_e can range from 0.93 to 3.5.

5.6 Summary

Material specific constants from this chapter is gathered in table 5.1. It is important to keep in mind that for physical data of polymers, especially C_∞ and M_e^G, quantities often vary 15 % depending on the source of literature [Halary et al., 2011].

Properties of the specific grades used in this project m6091 (HDPE) from Total Petrochemicals, Metocene HM562S (PP) from Total Petrochemicals, and Polystyrene MFCD0008-4450 (PS) from Sigma-Aldrich are presented in table 5.2; see chapter 8 on page 87 for further specifications.

Polymer	HDPE (140 °C)	PP (190 °C)	PS (170 °C)
M_w [kg/mol]	128	237	192
$N = M_w/M_K$	851	1260	116
$Z = M_w/M_e^G$	154	61.1	14.5
τ_0 [s] (eq. 5.29)	$1.04{\cdot}10^{-11}$	$1.10{\cdot}10^{-11}$	$8.50{\cdot}10^{-6}$
τ_e [s] (eq. 5.28)	$3.95{\cdot}10^{-10}$	$8.27{\cdot}10^{-9}$	$6.81{\cdot}10^{-4}$
τ_R [s] (eq. 5.27)	$7.50{\cdot}10^{-6}$	$1.75{\cdot}10^{-5}$	$1.14{\cdot}10^{-1}$
τ_{rep} [s] (eq. 5.31)	$2.78{\cdot}10^{-3}$	$1.81{\cdot}10^{-3}$	3.99
D_s [m^2/s] (eq. 5.46)	$1.94{\cdot}10^{-14}$	$3.08{\cdot}10^{-14}$	$7.11{\cdot}10^{-18}$
R_g [nm] (eq. 5.6)	16.3	16.6	14.4
L [nm] (eq. 5.7)	287	354	116

Table 5.2: Material specific properties of the polymers presented in table 8.1.

CHAPTER 6

STATE-OF-THE-ART LITERATURE

In order to understand strength development in weld interfaces, it is necessary to consider the physics of a welding process as listed in the problem statement bullet point 1 on page 19. The essence of the conclusions of this literature survey is presented in figure 6.1, where a principle sketch of the thermal welding process is illustrated, while a TEM image of a PE/PP interface is presented in figure 6.2. Basically, the objective of thermal welding is to melt two polymer interfaces, bring them together, wait for them to cool down, and if done correctly a strong joint appears. In more detail, from the initial solid state to a high strength welded joint, five central criteria for strength development are found – *melting*, *wetting*, *compatibility*, *diffusion and entanglement*, and *(co-)crystallization*.

As mentioned in section 3.1 on page 13, no good theory exists to describe the strength development in semi-crystalline weld seams, and the present theories only deal with long-term welding, i.e., weld lines are created over several minutes to hours. This chapter deals with weld strength establishment in general and not just laser welding. Thus, the chapter functions as an encyclopedia of polymer welding, and its conclusions are harnessed in chapter 7 on page 85, where hypotheses are formed.

6.1 Heat Development and Melting

What Wool [1995] weakly describes, is the heating and melting stage of the welding process – it is assumed that the weld pieces are molten to an initial temperature, which is held constant throughout the experiment. This simple assumption is not valid for any industrial process, where the temperature can vary a lot [Rotheiser, 2009]. Regarding heating and melting, three aspects are important to consider; *temperature development*, *melting kinetics*, and *polymer decomposition*.

Specifically for laser welding, the temperature development, initial heating phase, and final cooling stage are described in section 4.3 on page 33, where references to literature are also found. Melting kinetics and polymer decomposition are described in the following.

6.1.1 Melting Kinetics

Melting of polymers is not simple. It is in fact a complicated process going on for a range of temperatures. Another problem during melting appears from the entanglement distribution in the melt. When a semi-crystalline polymer melts, entanglements will be concentrated in the formerly amorphous areas of the solid polymer, while the entanglement

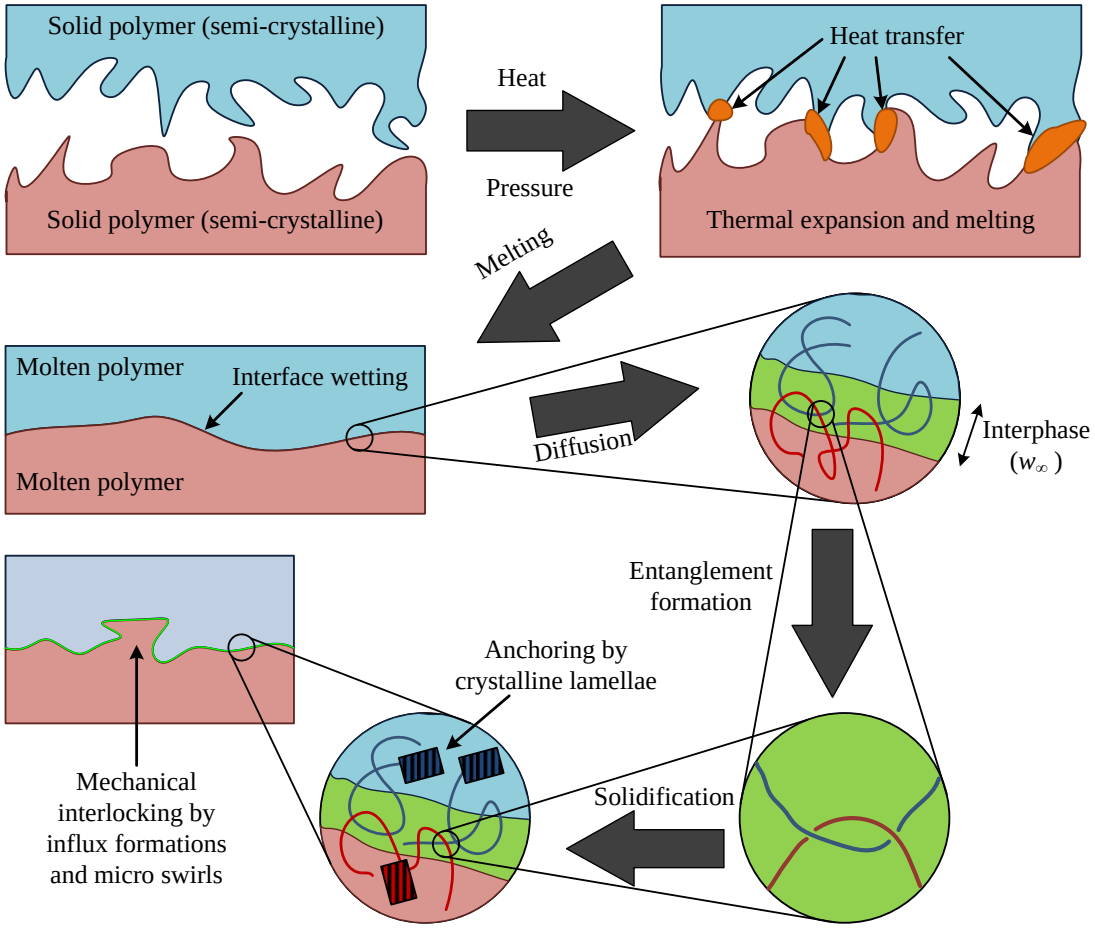

Figure 6.1: A principle sketch of a thermal welding of two semi-crystalline materials [Juhl, 2013]. Note the difference between interface and interphase, which is suggested by Pizzi and Mittal [2003].

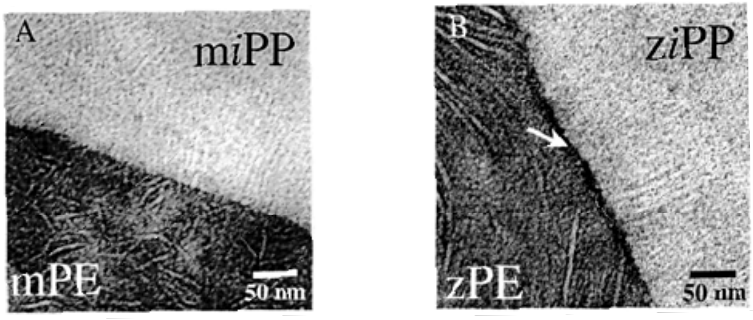

(a) **(b)**

Figure 6.2: TEM image from the interfacial region of (a) metallocene and (b) Ziegler-Natta catalyzed PE and iPP [Chaffin et al., 2000].

density of the crystalline part is very low. This means that the chains in the former crystalline areas are locked, resulting in limited polymer mobility due to blocking of the reptation mechanism. The time it takes these unevenly distributed entanglements (a heterogeneous melt) to become evenly distributed (homogeneous melt) is named the *tube renewal time*[1], which for nascent UHMW-PE powders ($M_w = 3.6 \cdot 10^6$ g/mol) is reported to be several hours [Rastogi et al., 2006].

6.1.2 Polymer Decomposition

Basically, decomposition means that the primary bonds in the polymer backbone break and material characteristics, such as mechanical or optical properties, change. The decomposition temperature (T_d) is usually measured from TGA with a heating rate of 3 K/min. T_d is then determined from the onset of weight loss. Another characteristic temperature is the half decomposition temperature $T_{d,1/2}$, which is defined as the temperature where half of the sample is decomposed. Typically, $T_{d,1/2}$ is 4–12 % larger than T_d [van Krevelen and te Nijenhuis, 2009].

If the heating rate is increased, T_d will also increase, i.e., for laser welding the decomposition temperature will be higher than table values claim. For instance, it is observed that it is possible to exceed the decomposition temperature when laser welding PA6. The maximum temperature in a PA6/PA6 weld seam is reported to 370 °C, which is 45 °C above the usual decomposition temperature [Bachmann and Russek, 2003; Van de Ven, 2006].

This is one of the major advantages of laser welding: very high temperatures resulting in very low reptation time making inter-diffusion possible, but the material will not decompose, because the heating rate is fast, and the material is only heated for a few seconds, see section 4.2 on page 26.

Additionally, a key issue is the activation energy for decomposition ($E_{a,dec}$) compared to the activation energy for diffusion ($E_{a,diff}$). For instance, $E_{a,dec}$ for HDPE is 264 kJ/mol, while $E_{a,diff}$ is 25 kJ/mol. This means that the effect of decomposition increases faster with increasing temperature. Therefore intuitively, the negative effect of decomposition will dominate the diffusion at large temperatures [Larson, 2012]. This trend is general for HDPE, iPP, and PS as seen in table 5.1 on page 54.

Interestingly, Beyler and Hirschler [2002] have reported cross-linking in polyethylene without additives to occur at 202 °C, while the decomposition will start at 292 °C. This means cross-linking could be controlled if the temperature could be controlled. Moreover, strength development of PET/PBT welds has been explained from trans-esterification in the interface, which is a well-known reaction between PET and PBT [plasticsengineering.org, 2011]. In general, however, cross-linking as a mechanism in the welding process is still not understood, though some considerations on the topic exists [LinkedIn.com, 2013].

6.2 Wettability

The first step in the formation of an adhesive bond is the establishment of *intimate contact* or *adsorption* by wetting Pizzi and Mittal [2003]. Intimate contact is important since van der

[1] The tube renewal time is normally used for something else – namely the time in a uniform melt for the tube to disappear and re-appear [Dealy and Larson, 2006].

Waals forces diminish with the distance to the inverse seventh power [Wu, 2001]. Intimate contact is also important to ensure diffusion.

The degree of wetting is a force balance between adhesive and cohesive forces which is usually described through *surface tension* or *surface energy*, γ. Surface tension/energy is an expression of the intermolecular (cohesive) forces, thus the γ-value is severely correlated to the type of intermolecular forces. Materials held together with primary chemical bonds are designated *high energy surfaces*, such as steel (γ = 1.3 J/m^2) or diamond (γ = 4 J/m^2), while materials held together with secondary bonds, such as van der Waals forces, have *low energy surfaces*. The HDPE, PP, and PS presented in table 5.1 on page 54 all possess low energy surfaces [Casco Nobel, 1992].

6.2.1 Thermodynamics of Wetting

From a thermodynamical point of view, the surface energy can be determined using contact angle (θ) measurements. The contact angle is illustrated in figure 6.3. The ideal situation from an adhesion point of view is $\theta = 0°$ resulting in complete intimate contact.

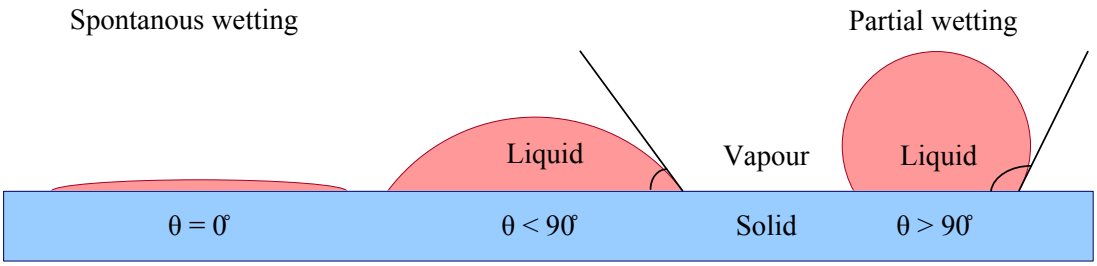

Figure 6.3: The concept of spontaneous and partial wetting [van Krevelen and te Nijenhuis, 2009].

Equilibrium contact angles of liquids on solids are usually discussed in terms of Young's equation [van Krevelen and te Nijenhuis, 2009]:

$$\gamma_{SV} = \gamma_{SL} + \gamma_{LV} \cos\theta, \tag{6.1}$$

where γ_{SV} is the surface energy between solid and vapor state and so on. For spontaneous spreading to occur, θ should equal zero, which leads the following inequality to be fulfilled for spontaneous wetting.

$$\gamma_{SV} \geq \gamma_{SL} + \gamma_{LV}. \tag{6.2}$$

Usually, γ_{SL} is small compared to γ_{LV} and γ_{SV}; thus, spontaneous wetting occurs if $\gamma_{SV} > \gamma_{SL}$, which is a fundamental rule within adhesive technology – the surface energy of the solid (the adherent) must be larger than the surface energy of the adhesive (glue) [Casco Nobel, 1992].

Equation 6.2 is often rewritten to;

$$S = \gamma_{SV} - \gamma_{SL} - \gamma_{LV} \geq 0, \quad \text{for spontanous wetting} \tag{6.3}$$

where S is the spreading coefficient, and a large positive value indicates that a liquid will spontaneously wet the solid surface. Conversely, $S < 0$ indicates only partial wetting, i.e., $\theta > 0°$ [wiley.com, 2011].

6.2.2 Work of Adhesion

A very important quantity when dealing with adhered joints is the work of adhesion, W_A, since it is directly proportional to the fracture energy, G_{Ic} [Wu, 2001]. The work of adhesion is defined between two substances – solid-solid, liquid-liquid, or solid-liquid systems. W_A is the work required to separate substance S_1 and S_2 creating unit areas of S_1 and S_2 surface at the expense of unit area of S_1S_2 interface, i.e [van Krevelen and te Nijenhuis, 2009]:

$$W_A = \gamma_{S_1} + \gamma_{S_2} - \gamma_{S_1S_2}. \tag{6.4}$$

$\gamma_{S_1S_2}$ is the interfacial surface energy between S_1 and S_2, which for substances without hydrogen-bonds is given as [van Krevelen and te Nijenhuis, 2009]:

$$\gamma_{S_1S_2} = \left(\gamma_{S_1}^{1/2} - \gamma_{S_2}^{1/2}\right)^2. \tag{6.5}$$

If equations 6.4 and 6.5 are combined following expression appears:

$$W_A = \gamma_{S_1} + \gamma_{S_2} - \left(\gamma_{S_1}^{1/2} - \gamma_{S_2}^{1/2}\right)^2 = 2\left(\gamma_{S_1}\gamma_{S_2}\right)^{1/2}. \tag{6.6}$$

Example 6.1
Does HDPE wet iPP at 200 °C, and what is the work of adhesion of the HDPE/iPP joint at room temperature?

The surface energies of HDPE and iPP at 200 °C are estimated from the Matlab function `gam`, giving $\gamma_{HDPE} = 25.3$ mJ/m^2 and $\gamma_{iPP} = 19.4$ mJ/m^2. The spreading coefficient, S, is thus estimated through equation 6.3, giving:

$$S = 19.4\text{mJ/m}^2 - 25.3\text{mJ/m}^2 - 0.4\text{mJ/m}^2 = -6.3\text{mJ/m}^2, \tag{6.7}$$

i.e. only partial wetting occurs. Vice versa, iPP is able to wet HDPE, which is an important result when considering the absorbent and transparent part in a laser weld, see section 4.2.2.

From equation 6.6 the work of adhesion at room temperature can be determined to:

$$W_A = (29.1 + 35.4 - 0.31)\text{mJ/m}^2 = 64.2\text{mJ/m}^2, \tag{6.8}$$

thus, the work required to separate a HDPE/iPP joint is only 64.2 mJ/m^2; however, the fracture energy is reported to be between 1 and 3 J/m^2, therefore other adhesion mechanisms play a larger role than the work of adhesion, but wetting is the fundamental for other mechanisms to take place [Packham, 2005; Pizzi and Mittal, 2003; wiley.com, 2011].

6.2.3 Other Considerations

The above-mentioned theory of wetting is only valid for non-contaminated smooth surfaces at equilibrium, which in reality rarely is the case. Therefore, following considerations must be taken into account:

Temperature: Since γ is proportional to the cohesive energy density, the surface temperature is important. The relationship between γ and T is given by the Guggenheim relation [van Krevelen and te Nijenhuis, 2009]:

$$\gamma(T) = \gamma_0 \left(1 - T/T_{cr}\right)^{11/9}, \tag{6.9}$$

where γ_0 and T_{cr} are fitting parameters. The expression means that γ_{PE} at room temperature is 35.4 mJ/m^2, while it at 200 °C decreases to 25.3 mJ/m^2. Equation 6.9 is implemented in the MATLAB function `gam`, which was utilized in example 6.1 on the preceding page.

Molecular mass: As the degree of polymerization decreases, the number of van der Waals forces likewise decreases leading to a lower cohesive energy density, which again results in a lower surface energy. The relationship is according to Wu [2001];

$$\gamma(M_n) = \gamma_\infty - k_e M_n^{-2/3}. \tag{6.10}$$

Note that $\partial\gamma/\partial M_n > 0$ which is in correspondence with the above-mentioned considerations. In practice for commercial plastics, $\Delta\gamma$ between low and high molecular weight resins is only within 2 mJ/m^2 [van Krevelen and te Nijenhuis, 2009].

Surface roughness: The surface topology is a central parameter regarding wetting and thereby weld quality. If the solid part is rough, the degree of wetting will be more pronounced than on a completely smooth surface. However in general, when dealing with welding the surface roughness does not have a significant role. But when considering adhesion of polymers, the roughness must be taken into account [Fink, 2001; Packham, 2005].

Time: The wetting time dependence is important to investigate when considering the weld strength development – will wetting occur instantly or will the degree of wetting develop over time? To answer this question following model has been suggested [Wool, 1995]:

$$G + \ln(1 - G) = -P t/\eta_0, \tag{6.11}$$

where $G = G(t)/G_\infty$ is the fractional peel energy, while P is the applied pressure and η_0 is the zero-shear viscosity.

Example 6.2

How long does it take a molten HDPE to wet a surface with a welding pressure of 5 bar ($5{\cdot}10^5$ Pa)?

From equation 6.11 the relative G can be plotted versus time, knowing the pressure and the zero-shear viscosity. This is shown in figure 6.4, where it is seen that 95 % strength is developed after 1.4 ms for the slowest case, i.e., T = 140 °C.

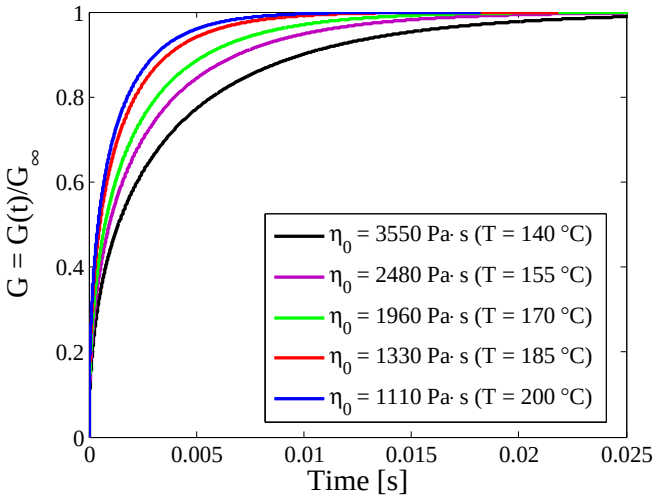

Figure 6.4: The wetting time at different temperatures, i.e., different η_0. Data is from the mHDPE utilized in chapter 10 on page 101 [Juhl et al., 2013a].

6.3 Compatibility

As indicated in figure 6.1 on page 58, an important criterion for mutual diffusion of polymers is polymer-polymer compatibility, i.e., the ability of two polymers to mix and be in one phase at thermodynamic equilibrium – the term *miscibility* is also used. A theoretical approach to this question is the Flory-Huggins (FH) theory of polymer-polymer mixtures [Bower, 2002; Flory, 1942; Wool, 1995]. Using FH theory, it is straightforward to show that two polymers with a high molecular weight ($M_w \approx 10^5$ g/mol) are incompatible, even though their solubility parameters (δ) are nearly identical [Oh and Bae, 2010].

Based on the FH theory, commercial plastics consisting of different polymers, such as PP and PE, should be immiscible – this does, however, not mean that they are not weldable. For instance, thermodynamical immiscible polymers such as iPP and HDPE have shown to be weld compatible [Chaffin et al., 2000], and one explanation is Helfand's theory, which correlates the interphase width (w_∞) with the FH interaction parameter (χ), see section 6.3.3 on page 68 [Lo and Narasimhan, 2005]. The fracture energy (G) of an asymmetric polymer interface is proportional to the square of w_∞ which again is proportional to the inverse χ-parameter [Godail and Packham, 2001]:

$$G \propto w_\infty^2 \propto 1/\chi \tag{6.12}$$

In this section the background of the Flory-Huggins theory and Helfand's theory is presented.

6.3.1 Flory-Huggins Theory

From experience it is known that it is very difficult – sometimes impossible – to create a uniform mixture of two different polymer types. The reason for this can be explained from the Flory-Huggins theory of polymer-polymer blends. If two polymers are mixed with respective degree of polymerization N_1 and N_2 and volume fractions φ_1 and φ_2 ($\varphi_1 + \varphi_2 = 1$), the

Gibbs free energy of mixing is given as [Doi, 1996; wiley.com, 2011]:

$$\frac{\Delta G_{\text{mix}}}{RT} = \underbrace{\chi_{12}\varphi_1\varphi_2}_{\text{enthalpy}} + \underbrace{\frac{\varphi_1}{N_1}\ln\varphi_1 + \frac{\varphi_2}{N_2}\ln\varphi_2}_{\text{entropy}}, \tag{6.13}$$

where χ_{12} is a non-dimensional parameter called the interaction parameter or just the χ-parameter. Doi [1996] uses a definition of χ based on statistical mechanics, while Hiemenz and Lodge [2007] prefer a thermodynamical definition:

$$\chi_{12} = \frac{V_{\text{m}}(\delta_1 - \delta_2)^2}{RT}, \tag{6.14}$$

where V_{m} is the molar volume, and δ_1 and δ_2 are the Hildebrand solubility parameters of polymer 1 and 2. When two polymers have different molar volumes a geometric mean is suggested for an effective molar volume, i.e., $V_{\text{m}} = \sqrt{V_{\text{m},1} \cdot V_{\text{m},2}}$ [Hansen, 2000]. It must, however, be noted that V_{m} and δ vary slightly with temperature and molecular weight. Moreover, the polymer composition greatly influences the χ-parameter, e.g., deuterated and hydrogenated PE have slightly different δ-values [Mortensen, 2009]. Also, note that this approach does only take weak van der Waals forces into account and in general the method only gives a qualitative picture of the χ-value; thus, it is suggested to add 0.34 (named β) to equation 6.14 [Hiemenz and Lodge, 2007].

Hansen Solubility Parameters

Instead of having one number describing the solubility parameter, such as Hildebrand δ, an alternative is to define the solubility as a set of parameters, describing the material's cohesive forces from three values; δ_{D}, δ_{P}, and δ_{H}. δ_{D} origins from dispersive cohesive forces, δ_{P} from polar cohesive forces, while δ_{H} are from cohesive hydrogen bonds. These are the Hansen solubility parameters (HSP).

These three parameters can be treated as a coordinate point in three dimensions. This is also called the Hansen space. If the spatial distance in the Hansen space is within the interaction radius (R_0) which is another material parameter, the materials are miscible; although, this is only valid for small molecules. For polymers the entropic gain of mixing is small, hence, the Flory-Huggins theory must also be taken into account. Therefore, the the HSP is used for better prediction of the interaction parameter as [Hansen, 2000]:

$$\chi_{12} = \frac{V_{\text{m}}\left[(\delta_{\text{D1}} - \delta_{\text{D2}})^2 + \frac{1}{4}(\delta_{\text{P1}} - \delta_{\text{P2}})^2 + \frac{1}{4}(\delta_{\text{H1}} - \delta_{\text{H2}})^2\right]}{RT}. \tag{6.15}$$

V_{m}, R, and T are similar to equation 6.14. The value of '4' is an empirical value found useful when establishing spherical plots in the Hansen space. However, it has also been derived theoretically [Hansen, 2000].

χ-values from Scattering

Another approach for determining the χ-parameter is using Small Angle X-ray Scattering (SAXS) or Small Angle Neutron Scattering (SANS) on polymer blends. Using SAXS, Lo et al. [2004] have determined the χ-value of a iPP (M_{n} = 47.5 kg/mol, PDI = 3.2) and a mLLDPE

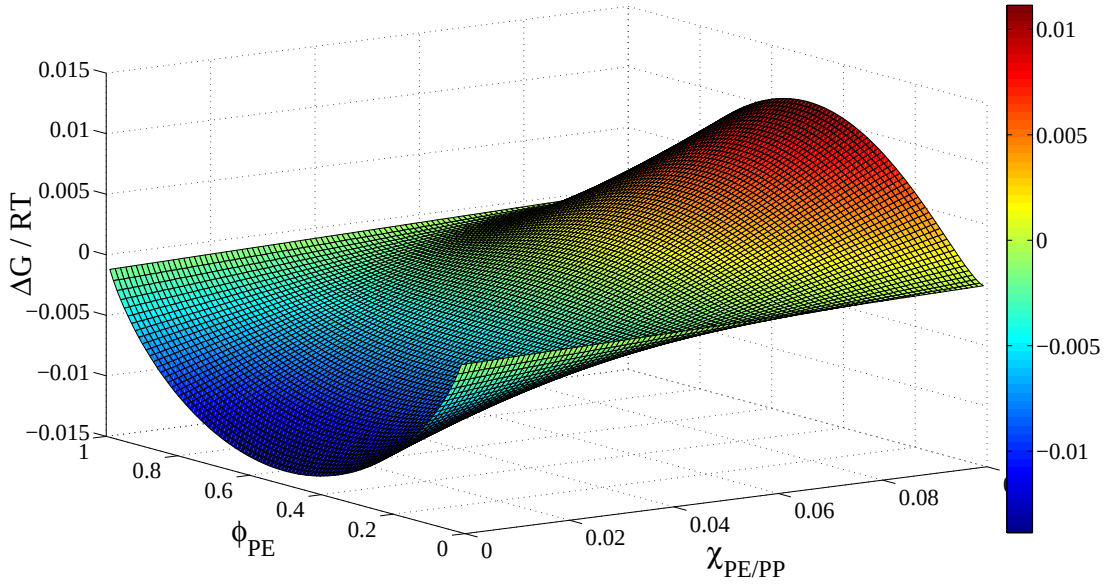

Figure 6.5: Surface plot of the Flory-Huggins model (eq. 6.16) representing $\Delta G/RT$ versus χ and φ. N is fixed to 50.

(M_n = 32.4 g/mol, PDI = 3.1) to be $\chi(T) = -0.0367 + 16.01/T$, and through FH theory they concluded that the upper critical temperature for phase separation was 143 °C.

Using SANS, Jeon et al. [1998] have determined the χ-parameter of head-to-head PP and HDPE to be $\chi(T) = -0.0276 + 17.56/T$ (hhPP deuterated) or $\chi(T) = -0.0311 + 17.60/T$ (PE deuterated).

6.3.2 Conditions for Compatibility

The FH model gives the Gibbs free energy as a function of multiple scalar variables as presented in equation 6.13. For further simplification φ_2 is substituted with $1-\varphi_1$ giving:

$$\frac{\Delta G_{\text{mix}}}{RT} = \chi\varphi(1-\varphi) + \frac{\varphi}{N_1}\ln\varphi + \frac{1-\varphi}{N_2}\ln(1-\varphi). \tag{6.16}$$

To illustrate the dependence of χ and φ, $N(=N_1=N_2)$ is fixed to 50 facilitating a surface plot of $\Delta G/RT$ versus χ and φ as presented in figure 6.5. It is noted that $\Delta G/RT$ is symmetric about $\varphi = \frac{1}{2}$. The figure indicates that a small χ-value favors mixing. If χ is kept constant, $\Delta G/RT$ vs. φ can be plotted, which is illustrated in figure 6.6.

At the local minima (the binodals[2]), the blend is stable in one phase. At the ∩-shaped part of the curve, i.e., between the two spinodals, the blend separates into two phases; this is called spinodal decomposition. The spinodals are defined at the inflection points, i.e., at $\partial^2 G/\partial\varphi^2 = 0$.

Polymer blends with concentration between φ_{B1} and φ_{S1}, and φ_{S2} and φ_{B2} are said to be metastable. This means that a direct phase separation results in increased Gibbs free

[2]Actually, the binodals are defined as the point of common tangent; however, for similar DOP they equal the local minimum [Mortensen, 2009].

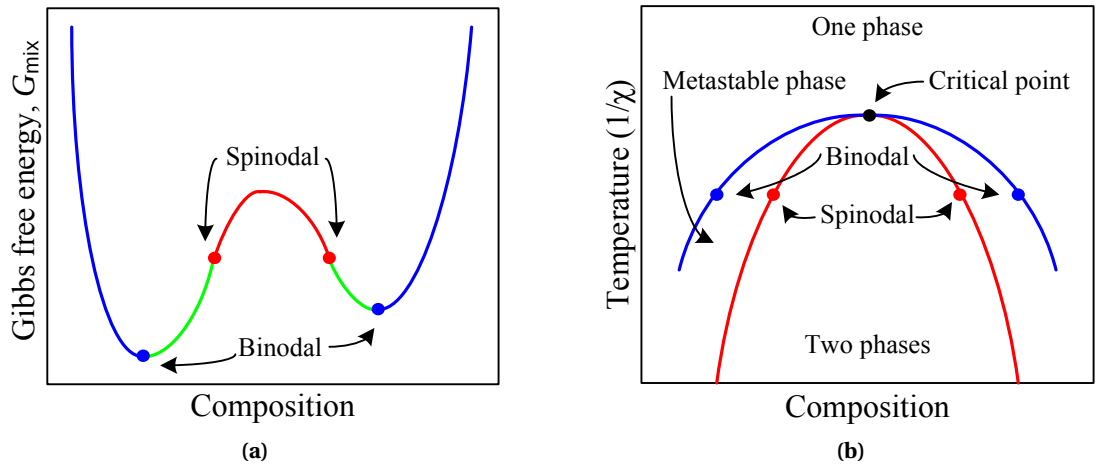

Figure 6.6: Sketch of the binodal and spinodal decomposition. (a) The change in Gibbs free energy as function of composition, also indicating binodal and spinodal transitions. (b) The Gibbs Free energy curve translated to its corresponding phase diagram. The binodal and spinodals from figure (a) is here aligned at the constant temperature [Mortensen, 2009].

energy; therefore, for phase separation to occur, the blend is required to cross an energy barrier. In this case phase separation follows a nucleation and growth mechanism.

As figure 6.5 indicates, the location of binodals and spinodals is dependent on the χ-parameter, and thereby temperature as stated in equation 6.14. As T is increased χ decreases and the binodals and spinodals approach, and when the inflection point is horizontal, all four points are located at the same temperature and concentration, see figure 6.6. The common concentration is called the critical concentration (φ_c) and is given at $\partial^3 G/\partial\varphi^3 = 0$. The corresponding interaction parameter is called the critical interaction parameter (χ_c). By differentiation of equation 6.16, φ_c and χ_c can be derived to [Doi, 1996; Mortensen, 2009]:

$$\varphi_c = \frac{\sqrt{N_1}}{\sqrt{N_1}+\sqrt{N_2}} \tag{6.17}$$

$$\chi_c = \frac{1}{2}\left(\frac{1}{\sqrt{N_1}}+\frac{1}{\sqrt{N_2}}\right)^2, \tag{6.18}$$

which for $N_1 = N_2$ reduces to $\varphi_c = 1/2$ and $\chi_c = 2/N$. The $\cap$-shaped phase diagram in figure 6.6b possess an upper critical temperature, because χ is proportional to $1/T$. This is not always the case; some blends have a lower critical temperature (LCT), while various other shapes also exist [wiley.com, 2011].

Example 6.3

Consider two commercial polymers; PE with M_w = 128,000 g/mol and PP with M_w = 237,000 g/mol. Are they compatible at 200 °C = 473 K; and if not, at what degree of polymerization are they?

The overall consideration is to determine whether $\chi_{12} < \chi_c$; thus, equation 6.14 is evaluated as function of temperature, which using data from van Krevelen and te Nijenhuis [2009] gives:

$$\chi_{PE/PP} = \frac{\sqrt{32.9\frac{cm^3}{mol}\cdot 49.1\frac{cm^3}{mol}}\cdot\frac{1}{2}\cdot\left(16.0\sqrt{MPa}-17.0\sqrt{MPa}\right)^2}{8.3144\frac{J}{mol\,K}\cdot 473K} = 0.0102, \tag{6.19}$$

where V_m is the average molar volume of PE and PP. χ_c is evaluated utilizing $N = M/M_0$, yielding

$$\chi_c = \frac{1}{2}\left(\frac{1}{\sqrt{4563}}+\frac{1}{\sqrt{5632}}\right)^2 = 3.96\cdot 10^{-4}. \tag{6.20}$$

Therefore, PE and PP are not compatible – the degree of polymerization to ensure compatibility at 200 °C is thus given as

$$\chi_{PE/PP} < 2/N \quad \Rightarrow \quad N < 2/0.0102 = 196, \tag{6.21}$$

which is equivalent to $M_{w,PE} = 5483$ g/mol and $M_{w,PP} = 8235$ g/mol. These values are comparable to the critical molecular weight which for PE is 4200 g/mol and 7600 g/mol for PP, see table 5.1 on page 54. Thus, compatible systems of PE and PP will not be used for structural elements in mechanical devices.

Therefore, in order for mixing to take place for commercial high-molecular-weight plastics, their solubility parameters would have to be virtually identical. An example of a frequently used polymer blend is ABS/PMMA. Nowadays, the search for compatible plastics is focused on plastic pairs with a negative χ-parameter, i.e., $\Delta H_{mix} < 0$ meaning that the process of mixing is exothermic. This is the case for polymers capable of forming strong dipole bonds or hydrogen bonds [Cowie and Arrighi, 2008].

Criticism of FH Theory

The FH-model from equation 6.13 with the interaction parameter defined in equation 6.14 is widely used and generally accepted as an appropriate theory for polymer compatibility – although, it is not the most sophisticated model available, but it is simple and tractable [Jones and Richards, 1999; Oh and Bae, 2010]. However, when utilizing the theory in practice, the χ-parameter is often fitted as a parameter, and not determined through equation 6.14, i.e., the FH-model is less of a theory and more a convenient parametrization of the Gibbs free energy. Moreover regarding χ, it seems obvious that the value decreases as the temperature increases ($\chi \propto T^{-1}$) resulting in a *upper critical solution temperature* (UCST) below which the polymer blend phase separates. Yet, this is not the case in practice since χ is often reported to increase with temperature, i.e., possessing a *lower critical solution temperature* (LCST) [Jones and Richards, 1999].

Thus, from an empirical point of view the FH-model is proved inadequate, but also from a theoretical viewpoint, the theory possesses potential sources of error [Jones and Richards, 1999]:

1. The model assumes unperturbed chain statistics, i.e., ideal random walk chain models. This is a good approximation for a polymer melt; however, near the critical point of phase separation or at crystallization, this assumption becomes invalid.

2. The model is a mean-field theory, thus, it does not take fluctuations of temperature or polydispersity of molecular weight into account.

3. Volume effects are neglected, i.e., no change in V_m upon mixture. In some variations of the FH-model, V_m does not change with temperature.

4. Local structure and packing are not considered, which is likely to be most important for pairs of polymers with different backbone stiffness leading to error in the entropic contribution.

Although other models have had their successes, it is to say that no single model has achieved universal applicability. Nonetheless, it is emphasized that it is difficult to predict the compatibility of two polymers using model tools, thus experimental work is necessary.

6.3.3 Helfand's Theory

Even though it seems clear from example 6.3 on page 66 that PE and PP are incompatible and will phase separate when mixed, experience has proven that strong welds are possible between the two materials [Chaffin et al., 2000; Zhang et al., 2011]. The conclusion is clear; although the materials are incompatible, some polymers from one material can diffuse across the interface and vice versa forming *entanglements*. The result is a nanometer thick interphase consisting of both materials, see figure 6.1. The interphase width can be determined using the Helfand expression for molecular weight approaching infinity, M_w [Helfand and Sapse, 1975; Lo and Narasimhan, 2005]:

$$w_\infty = \frac{2b}{\sqrt{6\chi_{12}}}. \tag{6.22}$$

Considering the FH model from equation 6.13, the compatibility increases with decreasing molecular weight, i.e., the interphase width should increase for an asymmetric interface with decreasing M_w, thereby N. Taking N into account, the interphase width is given as [Lo and Narasimhan, 2005]:

$$w = w_\infty \left[1 + \ln(2) \cdot \frac{1}{\chi_{12}} \left(\frac{1}{N_1} + \frac{1}{N_2}\right)\right], \tag{6.23}$$

which for high values of N reduces to equation 6.22. Other similar equations have also been suggested [wiley.com, 2011], which also reduces to equation 6.22 for large values of N. Fetters et al. [1994] have proposed a third equation taking variations in chain dimensions into account [Cole et al., 2003]:

$$w_\infty = 2\sqrt{\frac{b_1^2 + b_2^2}{12\chi_{12}}}. \tag{6.24}$$

Example 6.4
What is the interfacial width, w, for a weld interface of the two commercial plastics from example 6.3?

Using data from Fetters et al. [2007] and van Krevelen and te Nijenhuis [2009] and equations 6.23 and 6.24, the interfacial width in a HDPE/iPP interface can be estimated by:

$$w = 2\sqrt{\frac{(5.64\text{Å})^2 + (5.25\text{Å})^2}{12 \cdot 0.0104}} \cdot \left[1 + \ln(2) \cdot \frac{1}{0.0104}\left(\frac{1}{4563} + \frac{1}{5632}\right)\right] \tag{6.25}$$

$$= 4.4\text{nm} \cdot 1.026 = 4.5\text{nm} \tag{6.26}$$

This interfacial width is in good agreement with the TEM image in figure 6.2a, where the interfacial width is estimated to 4 nm [Chaffin et al., 2000].

Furthermore, notice that w is comparable to the tube diameter (a) and the radius of gyration between entanglements ($R_{g,e}$) from table 5.1 on page 54 and is less than R_g (16–17 nm) from example 5.1 on page 42.

Calculated values of interfacial widths, as the one shown in example 6.4, are always smaller than the widths measured experimentally with X-ray and neutron reflection. This general trend is caused by concentration fluctuations, chain end effects, distorted chain conformations, polydispersity, and initial roughness [Lo and Narasimhan, 2005; Stamm and Schubert, 1995].

The Gorga-Narasimhan Criteria

Another criteria for compatibility is suggested by Gorga and Narasimhan [2004], suggesting that entanglement formation will only take place when $N^*\chi$ is less than 2, where N^* is the effective degree of polymerization given as:

$$N^* = \frac{2N_1N_2}{N_1 + N_2}. \tag{6.27}$$

This definition is inspired from the mutual diffusion coefficient (D_m), see equation 5.49 on page 52.

6.4 Diffusion and Entanglement

In section 5.5 on page 49 the basics of self-diffusion and inter-diffusion were described. In this section the inter-diffusion will be coupled to entanglements and their role in strength development.

As figure 6.1 on page 58 indicates, when the wetting and the compatibility criterion is fulfilled, polymer diffusion proceeds. Diffusion leads to molecular entanglement, which most authors characterize as the central mechanism of weld strength development [Chaffin et al., 2000; Cole et al., 2003; Wool, 1995]. Regarding diffusion, different time domains are important to emphasize; these include Rouse relaxation time for entangled segments

(τ_e), Rouse relaxation for the whole chain (τ_R), and the reptation time (τ_{rep}), as described in sections 5.3 and 5.4 and summarized in table 5.2 on page 55. Since the welding time, particularly when dealing with laser welding, is within seconds (see section 4.3.1 on page 34), it is important to evaluate these relaxation characteristics and corresponding time domains in order to determine the major mechanism for entanglement formation [Dealy and Larson, 2006; Doi, 1996; Doi and Edwards, 1986; Wool, 1995].

Evaluations on polymer diffusion/mobility were performed by Guvendiren et al. [2010], who investigated a miscible blend of low-T_g and high-T_g polymers from a microscopic point of view. Intuitively, it is concluded that the mobility increases with decreasing molecular weight and increasing temperature above T_g. Empirically, interfacial diffusion of polymers is also evaluated utilizing tools from rheology, e.g., plate-plate shear rheometry [Bousmina et al., 1998; Yang et al., 2010]. Moreover, molecular dynamics (MD) modeling and numerical simulation tools are also exploited; however, these computational methods do have limitations when considering a welding process, which is rather widescale with respect to time and space from a molecular point of view [Guvendiren et al., 2010; Larson, 2007; Lo and Narasimhan, 2005].

Regarding entanglements, Chaffin et al. [2000] conclude that entanglement is the main reason for high-strength weld interfaces in mHDPE/miPP laminates. Quantitatively, Cole et al. [2003] have shown that the critical mechanical energy release rate for fracture (G_c) between immiscible polymers are proportional to the number of entangled segments squared (Σ^2). In order to achieve interfacial bridging entanglements with suitable anchoring, a molecular weight of 8 times M_c is required. At the interface, however, low molecular weight fractions gather, eliminating entanglement establishments [Wool, 1995]. This is often known as the *weak boundary layer*, which is further discussed in section 6.5.1 on page 73.

From a theoretical point of view, this part of the project is challenging. The theory within the area counts the famous *tube models* [Dealy and Larson, 2006; Larson et al., 2003]. A goal would be to couple these models to diffusion establishments of entanglement.

6.4.1 Inter-diffusion at Interfaces

In a welding process inter-diffusion is of interest, and implicitly the two polymers welded together can be amorphous or semi-crystalline, while they also can be similar or dissimilar. Most research has focused on similar amorphous interfaces, such as PMMA/PMMA and PS/PS [Wool, 1995]. Also dissimilar, but still compatible, amorphous polymers have been tested [Guvendiren et al., 2010].

Many techniques have been developed and utilized to directly determine inter-penetration depth at a polymer-polymer interface, and thereby estimate the mutual diffusion coefficients (D_m). These include pulsed field gradient nuclear magnetic resonance spectroscopy (PFG-NMR), X-ray microanalysis in scanning electron microscopy, neutron scattering, infrared microdensitometry, Fourier transform infrared spectroscopy (FTIR), and secondary ion mass spectroscopy (SIMS). Common for these techniques is the requirement for isotopic or chemical labeling, making them relatively complex and inappropriate in some areas of research [Karim et al., 1994; Klein, 1990; Zhao and Macosko, 2007].

An alternative method of microscopy where isotopic or chemical labeling is unnecessary is TEM, see figure 6.2 on page 58. The interfaces were microtomed to a flat face, then stained with ruthenium tetroxide (RuO_4) vapor for 6 hours and sectioned into 80 nm thick

slices. Crystalline regions almost completely exclude the RuO_4 and appear light in the figure. White streaks (about 10 nm wide) in both the PE and iPP regions correspond to chain-folded crystalline lamellae. Because the PE phases have a lower overall degree of crystallinity, see table 6.1 on page 73, they appear darker than the iPP domains [Chaffin et al., 2000]. Lo et al. [2004] have also investigated the interphase thickness at various temperatures using TEM; interphase widths were reported to range from ~0 to 49 nm, when annealing temperature was varied from 120 to 160 °C.

Rheometry

To determine D_m plate-plate shear rheometry can be used as an alternative to microscopy. Originating from Qiu and Bousmina [1999], the basic idea is to stack multiple layers of thin polymer foils in a plate-plate rheometer and apply heat. The rheometer starts in shear mode, and the strain must be kept low ($\gamma < 0.05$) in order to avoid mechanical disturbances. The viscosity of the molten stack of polymer foils can then be monitored. At first, the viscosity is relatively low due to slip at multiple polymer interfaces, but as time passes the viscosity increases due to inter-diffusion and established entanglements.

The increase in viscosity then reveals the diffusion dynamics at the interface, which often is modeled using Fick's second law. This modeling approach is excellently described by Lee et al. [2009]; Yang et al. [2010]. The *multiple stack approach* has been varied to test various polymer interfaces [Bousmina et al., 1998; Jablonski, 2003; Lamnawar and Maazouz, 2006; Zhao and Macosko, 2002, 2007]. Recent development by Zhang et al. [2012a] also made it possible to determine D_s and apparent diffusion (D_a), as well as the influence of temperature and molecular weight.

6.4.2 Entanglement Establishment

It is suggested by Chaffin et al. [2000] that the inter-diffusion depth in a polymer-polymer interface is not as important as interfacial entanglements when considering development of mechanical strength. However, the part involving formation or establishment of entanglements is poorly understood – entanglements or entanglement densities are often estimated from mechanical tests; thus, it is difficult to isolate the entanglement effect on strength development [Cole et al., 2003; Horiuchi et al., 2008; Mueller et al., 1998]. Although, it is suggested that entanglement density is directly proportional to inter-penetration depth [Gorga and Narasimhan, 2004].

Theoretical considerations regarding entanglements and interfacial bridges have been carried out by Wool [2005]. An interfacial bridge refers to a polymer crossing the interface back and forth; a polymer can therefore contain several bridges. Using scaling theory, Wool [1995] has determined the number of bridges ($p(t)$) to:

$$p(t) = 1.31\sqrt{\frac{C_\infty j}{M_0 M_c}} \cdot bN_A \cdot \sqrt{\frac{t}{\tau_{rep}}}. \tag{6.28}$$

Moreover, it is suggested that these bridging configurations only develops at certain inter-diffusion depths [Wool, 2006, 1995].

Entanglements have proved elusive in experimental studies. However, from a theoretical polymer physics point of view, entanglements are a hot topic for investigations [Ge et al., 2013].

6.5 (Co-)crystallization

Critics of the concept of molecular entanglement from diffusion claim that the theory only covers amorphous polymers. For semi-crystalline polymers, it turns out that crystallization at/near the interface is very important for strength development. Lo and Narasimhan [2005] describe this as a competition between crystallization and polymer inter-diffusion, concluding that the temperature in semi-crystalline polymer interfaces is of great importance relative to amorphous polymers.

Another important aspect is co-crystallization. Co-crystallization is the predominant force in strength development at semi-crystalline interfaces. Rastogi et al. [1998] indicate that deep inter-diffusion is not a prerequisite for strength development, when the possibility of co-crystallization is present. Crystallization across boundaries is often referred to as *trans-crystallization*, which is caused by heterogeneous nucleation at the interface [Cho et al., 2003].

Some mLLDPE/PP blends can co-crystallize, which means that their mutual crystalline phase is continuous and appears as one phase [Razavi-Nouri, 2007; Shanks et al., 2000]. Zhang et al. [2011] also report co-crystallization between an impact propylene copolymer (IPC) and a HDPE interface. In addition to this, Chaffin et al. [2000] observed that high strength welds exhibit a high degree of crystallinity in the interphase; and these findings might be correlated with the polymer catalysis, i.e., metallocene or Ziegler-Natta catalyst, which again can be coupled to the *weak boundary layer*.

It turns out in laminating processes between PE and PP that the ultimate peel strength is achieved when the laminatig temperature is just above the melting point of PP. This is because the recrystallization of PP will happen near the melting point and the temperature decrease is faster, resulting in faster material infreezing. If the lamination temperature is too high, the polymer melt will undercool and crystallize severel degrees below the melting temperature, thereby recrystallization happens at lower temperature, making the interphase width (w_∞) narrower as a result of equations 6.19 and 6.24 on page 68, which leads to weaker weld strength [Godail and Packham, 2001].

Regarding laser welding, 80 % crystallinity has been reported in the welded seam [Ghorbel et al., 2009], which is unusually high compared to a theoretical maximum crystallinity of iPP of 63 %, achieved at a 77 °C isothermal. The maximum degree of crystallinity of HDPE is 80 % (46 °C isothermal) [van Krevelen and te Nijenhuis, 2009]. It turns out that non-isothermal models for crystallization of iPP is very difficult to quantify and does not fit into the modified Avrami models [Mubarak et al., 2001]. This is a general trend for semi-crystalline polymers, and the crystallization is non-isothermal when dealing with laser welding. Experimental studies on very fast (100 K/s) cooling iPP have also been conducted [Coccorullo et al., 2003].

The above indicates that an interaction between material composition and welding process parameters exists. Process parameters can be reduced to time and temperature, while material composition refers to molecular properties, such as molecular weight, molecular weight distribution, co-monomer branching, and co-monomer branching distribution. These do not only influence dynamic properties in molten state, but also crystal formation during solidification.

6.5.1 Anchoring Lamellae

At an mPE/miPP interface, it is often observed that crystalline lamellae are located right next to the interface and that nearly no interphase is present, see figure 6.2a on page 58. Chaffin et al. [2000] observed that a thin interphase resulted in a high mechanical strength, which was explained by molecular bridges weaving back and forth at the interface and finally locked in an anchoring lamella.

Conversely, when investigating a zPE/ziPP interface, it is noted that a relatively thick layer (~10 nm) of amorphous material is gathered at the interphase, as indicated in figure 6.2b. This amorphous interface results in inferior mechanical strength, which can be explained with the *weak boundary layer* theory.

Weak Boundary Layer

Intuitively, a welded joint will fracture at its weakest link, which in many instances is the interface. This is due to a *weak boundary layer* (WBL) present at the welded surfaces. Bikerman [1968] suggested the WBL theory and argued that a molten surface tends to minimize its surface energy (γ); thus, low molecular weight, atactic fractions, and material additives with low surface energy will gather at the surface. Therefore, when two molten surfaces are brought together a relative high concentration of "trash" material is present. This mix of atactic and low molecular weight material is not able to crystallize and will then form an amorphous zone, as presented in figure 6.2b on page 58.

Inferior mechanical strength develops at the weak boundary layer since the low molecular weight fraction with $M < 8M_c$ is not able to form bridges; thereby, the main fracture mechanism is chain pullouts [Cole et al., 2003]. This is further described in section 6.6.

As indicated, the WBL theory is closely linked to the polymer synthesis, e.g., metallocene or Ziegler-Natta catalysis. The non-crystallizable fractions of polymer in different synthesis methods are outlined in table 6.1. Although, criticism of the WBL theory exists [Podlech, 2007].

Polymer	M_n [kg/mol]	PDI	crystallinity [w%]	non-crystallizable fraction [w%]
zPE	50	5.5	38±2	5.5
ziPP	57	2.4	52±2	0.5
mPE	50	2.3	41±2	<0.5
miPP	39	2.0	51±1	<0.2

Table 6.1: Crystallizability of Ziegler-Natta (z) and metallocene (m) catalyzed PE and iPP [Chaffin et al., 2000].

6.5.2 Influx Formations

When welding semi-crystalline polymers, material influxes are often observed as pictured in figure 6.7b and illustrated in figure 6.1. Influxes can be hundreds of microns in size [Godail and Packham, 2001] and result in mechanical interlocking, which is a macroscopic adhe-

sion mechanism in contrast to entanglements and anchoring lamellae [Pocius, 2002]. Klein [2011] also refer to influxes as micro-swirls.

Influx formations are directly recognized in optical microscopy, see figure 6.7b. An alternative indication of influxes is nano or micro fibrils at the fracture surface, which is indicated in figure 6.7a. The nano-sized fibrils are commonly observed in available literature [Zhang et al., 2011].

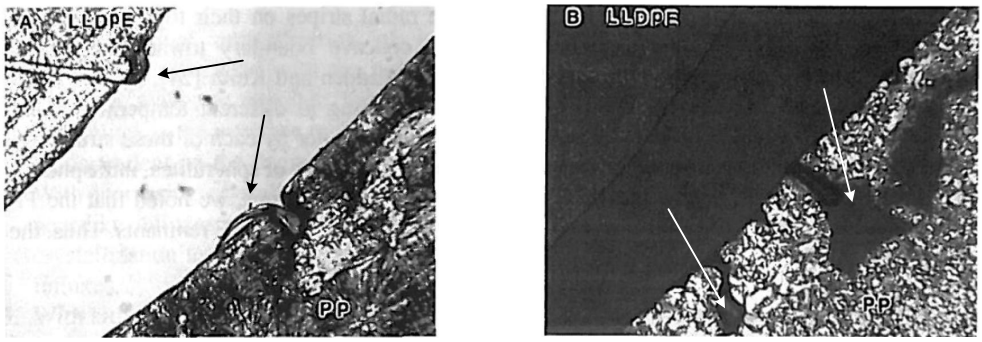

(a) (b)

Figure 6.7: Optical microscopy image of LLDPE/iPP interface. (a) a fractured interface with nano-sized fibrils. (b) an influx formation [Wool, 1995].

An explanation is that when polymers are heated and melted, the specific volume expands. This expansion results in squeeze flow along the interface, which may lead to micro-swirls at the boundary. Moreover, during re-solidification, i.e., crystallization for semi-crystalline polymers, the specific volume will shrink promoting influxes of still molten polymers [Klein, 2011; Wool, 1995]. Micro-influxes or micro-swirls result in nano-sized fibrils when fracture of the welded surfaces proceeds [Horiuchi et al., 2008]. Fracture of nano-sized fibrils exhibit characteristics of mechanical interlocking rather than chain rupture [Shanks et al., 2000; Zhang et al., 2011].

Influxes are more plausible to appear when the materials are annealed together compared to when they are quenched. On the other hand, quenching can freeze in the interfacial mixing, however, the morphological structure will be amorphous. Slow cooling might result both in a trans-crystalline interphase and influxes [Godail and Packham, 2001].

6.6 Fracture and Strength

As mentioned earlier, a necessary condition for strength development is molecular interdiffusion [Grewell et al., 2003]. When considering strength in welded joints, it is necessary to distinguish between material ultimate strength at fracture (σ_U [MPa]) and fracture energy (G_c [J/m^2]). σ_U is the maximum stress obtained in a tensile test, while G_c is known from fracture mechanics and described in the following [Osswald and Menges, 2003].

6.6.1 Fracture Mechanics

A common and relatively simple approach to analyzing failure in polymers is derived from linear elastic fracture mechanics (LEFM). The assumption of linear elasticity is only valid for

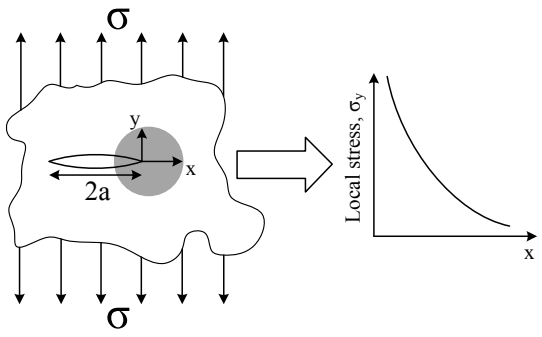

Figure 6.8: Stress near the crack tip [Osswald and Menges, 2003].

very elastic or brittle polymers, or polymers fractured at high speed.

Most polymers will fracture in a mode I crack growth, as presented in figure 6.8. For analysis of the crack tip opening, consider an internally cracked body with a crack length of $2a$ and an applied stress of σ. Close to the crack tip, the stress in the loading direction can be approximated by:

$$\sigma_y = \frac{K_{Ic}}{\sqrt{2\pi r}}, \tag{6.29}$$

where r is the distance from the crack tip and K_{Ic} is the *critical stress intensity factor* that is also known as the *fracture toughness*. K_{Ic} depends on the relative crack to component size as well as other design properties. Standard test specifications are therefore necessary [Osswald and Menges, 2003]. Hence, the critical stress intensity factor is a material property, revealing how vulnerable the material is to cracks. For instance from table 5.1 on page 54, $K_{Ic,iPP} = 3\text{MPa}\sqrt{\text{m}}$ and $K_{Ic,HDPE} = 2\text{MPa}\sqrt{\text{m}}$ meaning that more stress is required in iPP to let a crack grow. Obviously, K_{Ic} depends on temperature, morphology, polymer chain orientation, etc.

Another approach to analyze the crack growth is using Griffith's energy balance criteria [Griffith, 1920]. The derivation of Griffith's theory is presented by Wool [1995]. If the stress situation is as presented in figure 6.8, the following relation is valid for plain strain:

$$G_{Ic} = \frac{\pi \sigma_c a}{E}, \tag{6.30}$$

where σ_c is the stress required to initiate crack propagation and E is the elastic modulus. G_{Ic} is interpreted as the energy required to increase a crack with unit length in components of unit width. G_{Ic} is usually referred to as *elastic energy release rate* or *critical energy release rate*. Confusingly, *toughness* is also used which, however, is avoided in this thesis. Combining equations 6.29 and 6.30, this very important relation for plane stress appears:

$$G_{Ic} = \frac{K_{Ic}^2}{E}. \tag{6.31}$$

The Griffith model is only valid for linear elastic materials; thus, more complex models, e.g., J-integral predictions, are necessary when elaborating on viscoelastic materials such as polymers. However, it turns out that most polymers tested at moderate speed can be considered elastic [Osswald and Menges, 2003].

6.6.2 Fracture Mechanisms in Polymer Interfaces

Fracture of welded joints is caused by three main mechanisms; *disentanglement, bond rupture*, and *crazing* [Zhang and Rong, 2011]. When dealing with high-strength welds the preferred fracture mechanism is crazing, which is illustrated in figure 6.9.

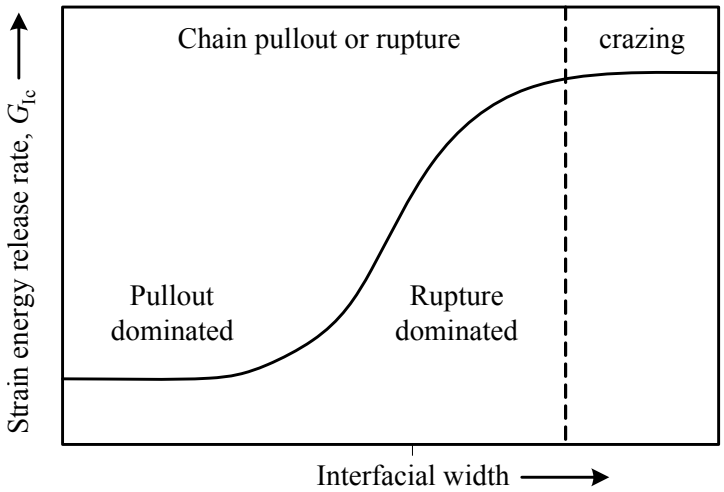

Figure 6.9: Schematic of the drastic increase in adhesion that occurs as a result of shift in failure mechanism [Cole et al., 2003].

Chain-pullout or Disentanglement

Disentanglement is the dominant fracture mechanism when dealing with small stresses for long periods of time. High fatigue toughness is therefore required to avoid this type of failure. Another word for disentanglement is chain-pullout, and Hiemenz and Lodge [2007] distinguish between *long chain pullout* and *end strand or short chain pullout*. Long chain pullout are forced reptation, i.e., an interface is pulled apart without bond rupture; and since the reptation time at room temperature is very long, this mechanism is considered highly unlikely. End strand or short chain pullouts dominate when the inter-penetration depth is on the scale of the tube diameter (a), which again is the same scale as the radius of gyration between entangled segments ($R_{g,e}$). This fracture mechanism is very weak compared to bond rupture. Thus for chain pullouts, the inter-penetration depth and entanglement establishment are very important.

Chain pullouts can be modeled using the *nail solution*, which models the polymer interface as two wooden boards held together by nails with a density (number of nails per area) of n and depth of L. From this critical mechanical energy release rate (G_{Ic}) can be estimated to [Wool, 1995]:

$$G_{Ic} = \frac{1}{2}\mu_0 v n L^2, \tag{6.32}$$

where μ_0 is the nail friction per unit length, and v is the pullout velocity. The L^2 dependence is in correspondence with equation 3.8 on page 16, since nail depth and inter-penetration depth are equivalent.

Bond Rupture

When the stresses are large, the dominant fracture mechanism becomes bond rupture of the established network. This means that the inter-penetration depth does not influence this mechanism. Therefore, the ultimate strength is not affected of the inter-penetration depth or molecular weight [Schnell et al., 1998]. However, the density of entanglements is still important for the strength in short-term tests, i.e., tests with large stresses.

Bond rupture also occur at slow rates of deformation, if the scissioned polymers are unable to disentangle. This is for instance the case when bridges are anchored in crystalline lamellae. The critical mechanical energy release rate (G_{Ic}) is correlated to the density of entanglements (Σ) as [Cole et al., 2003]:

$$G_{\mathrm{Ic}} \propto \frac{\Sigma}{\sigma_{\mathrm{cr}}}, \tag{6.33}$$

where σ_{cr} is the material crazing stress. Some theories describe this as the only mechanism in strongly welded joints [Schnell et al., 1998]; however, the theoretical strength when only assuming bond rupture is magnitudes larger than the measured; hence, molecular separation and disentanglement cannot be neglected.

Crazing

If full strength is developed, the conformation of parent material and interphase is indistinguishable and the failure will happen adjacent to the interface in the heat affected zone (HAZ). This also explains why welding of rough surfaces often result in more crack resistant welds, since the crack propagates through a tortuous path [Pocius, 2002].

Crazing happens at a threshold of certain entanglement density and above a certain maximum stress [Creton et al., 1992]. A craze is different from a crack since it contains only microvoids and also a large number of fibrils between these voids. These fibrils are crucial for the craze to sustain loadings perpendicular to the craze [Halary et al., 2011].

Dependence of Temperature and Crack Propagation Rate on G_{Ic}

The temperature dependence of G_{Ic} is complex. Increasing temperature will increase molecular movement, making disentanglement easier. On the other hand, increasing temperature will soften polymers, making them more ductile. Thus, it is difficult to make unambiguous statements. For instance, G_{Ic} of PMMA decreases with increasing temperature, while it increases for PC.

Regarding crack propagation rate, the dependence is more straightforward; an increased crack propagation rate results in an increased G_{Ic} following a potential law. At high crack propagation rates bond rupture becomes increasingly dominating, which requires more free energy compared to chain disentanglement [Halary et al., 2011; Marshall et al., 1974].

6.6.3 Mechanical Testing

The purpose of testing weld quality is to determine G_{Ic}, σ_{U}, or a third parameter describing the weld "goodness" – some just use the adhesive work (G_{a}) [Xue et al., 1998]. Various suggestions for test design exist [Wool, 1995], but in this section focus will be on test methods suited for testing laser welds, see figure 6.10. Therefore, traditional DENT tests of butt-joints

will not be evaluated [Wu and Mai, 1996]. In general, tests must be performed at low test speeds, i.e., a few millimeters per second, in order to test for inter-penetration. Otherwise, the bond rupture will be the predominant fracture mechanism.

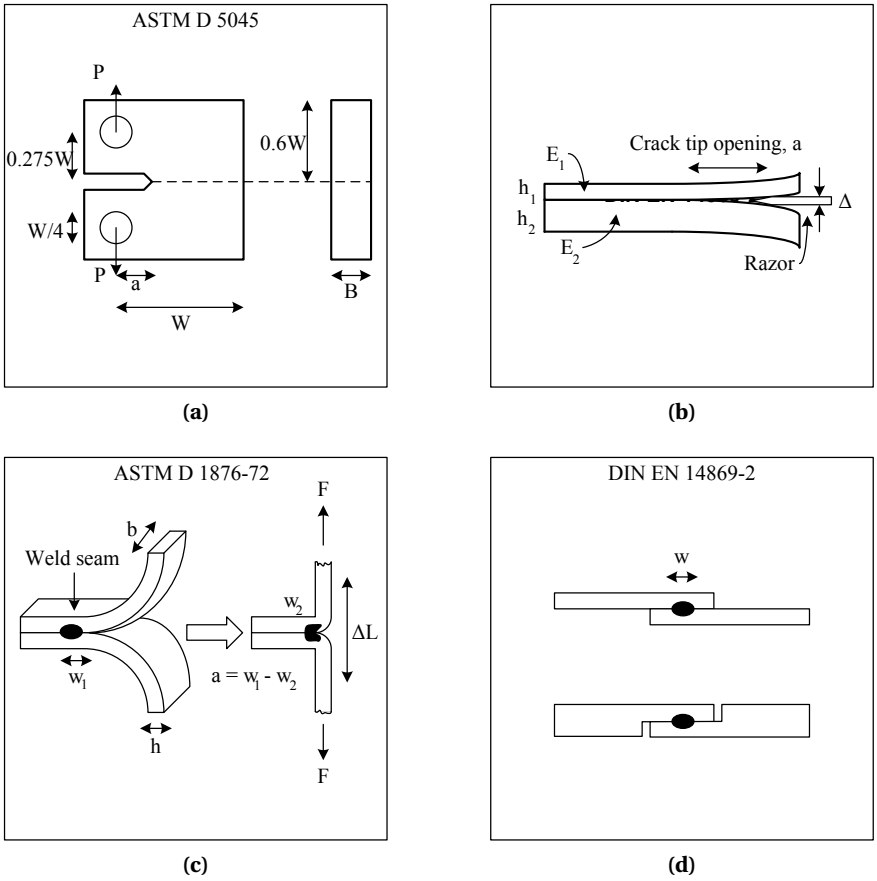

Figure 6.10: Four ways of designing specimens for weld testing (a) Compact tension test [Wool, 1995]. (b) Asymmetric double cantilever beam [Creton et al., 1992]. (c) Lap-joint peel test [Xue et al., 1998]. (d) Lap-joint shear test [Jaeschke et al., 2010].

Compact Tension Test

This method (see figure 6.10a) is ideal for determining plane strain fracture toughness (K_{Ic}) and strain energy release rate (G_{Ic}) of plastic materials. The recommended test dimensions are: $W = 2B$, $0.45 < a/W < 0.55$. A validity criterion for the test is:

$$2.5\,(K_{Ic}/\sigma_Y)^2 < B \wedge a \wedge (W-a), \tag{6.34}$$

where σ_Y is the yield stress. K_{Ic} can then be determined as

$$K_{Ic} = \left(P/BW^{1/2}\right) f(x), \tag{6.35}$$

where P is the critical load at fracture, $x = a/W$, and the function $f(x)$ is

$$f(x) = \frac{(2+x)(0.886+4.64x-13.32x^2+14.72x^3-5.60x^4)}{(1-x)^{3/2}}, \tag{6.36}$$

Note for plane strain that $G_{\mathrm{Ic}} = (1-\nu^2)K_{\mathrm{Ic}}^2/E$ [Wool, 1995].

Asymmetric Double Cantilever Beam (ADCB)

The method is utilized in this project for determination of G_{Ic} in PS/PS laser welds, thus a more detailed description is given in section 9.3.2 on page 92. In figure 6.10b the test specimen for the asymmetric double cantilever beam (ADCB) is presented. From the parameters presented in the figure, Creton et al. [1992] have derived the following formula:

$$G_{1\mathrm{c}} = \frac{3\Delta^2 E_1 h_1^3 E_2 h_2^3}{8a^4} \frac{E_1 h_1^3 C_2^2 + E_2 h_2^3 C_1^2}{\left(E_1 h_1^3 C_2^3 + E_2 h_2^3 C_1^3\right)^2}, \tag{6.37}$$

where Δ is the razor thickness, a is the crack tip opening, E is the elastic modulus, h is the cantilever thickness, and C is given as:

$$C_{\mathrm{i}} = 1 + 0.64 h_{\mathrm{i}}/a. \tag{6.38}$$

The ADCB approach is also conducted by others [Schnell et al., 1998, 1999], suggesting following relation:

$$G_{1\mathrm{c}} = \frac{3\Delta^2}{8a^4} \frac{E_1 h_1^3 E_2 h_2^3}{E_1 h_1^3 \alpha_2^2 + E_2 h_2^3 \alpha_1^2}, \tag{6.39}$$

where α is given as:

$$\alpha_{\mathrm{i}} = \frac{(1+1.92h_{\mathrm{i}}/a) + 1.22(h_{\mathrm{i}}/a)^2 + 0.39(h_{\mathrm{i}}/a)^3}{(1+0.64h_{\mathrm{i}}/a)}, \tag{6.40}$$

The big advantage of the ADCB methodology is the possibility to test weld strength of asymmetric interfaces with differences in elastic modulus. Additionally, the cantilever design is ideal to cut out from laser welded lap-joints. However, the method is not applicable to very ductile polymers, such as PE and PP.

Lap-Joint Peel Test

The basic idea of a peel test is illustrated in figure 6.10c. The peel test is good for determining the fracture strength of flexible or ductile polymers. From the figure, the strain in the adherent part is given as:

$$\epsilon = \frac{\Delta L - 2a}{2a}. \tag{6.41}$$

When elongating the peel specimen, the overall work (W) can be divided into three components; adhesive work of joint (G_{a}), plastic bending (U_{b}), and tensile elongation of the arm

(U_{arm}). W is given as the area under the force-extension curve before rupture. The adhesive work can be estimated as [Xue et al., 1998]:

$$G_{\text{a}} = \frac{1}{b}\left(\frac{\partial W}{\partial a} - \frac{\partial U_{\text{arm}}}{\partial a} - \frac{\partial U_{\text{b}}}{\partial a}\right) \tag{6.42}$$

where $U_{\text{arm}} = 2bha\int_0^{\epsilon}\sigma\, d\epsilon$. The integral can be determined from a regular tensile test and $U_{\text{b}} = bha\sigma_{\text{Y}}$. Combining this, the work of adhesion is given as:

$$G_{\text{a}} = \frac{2}{b}F(1+\epsilon) - 2h\int_0^{\epsilon}\sigma\, d\epsilon - \sigma_{\text{Y}}h \tag{6.43}$$

Note, only symmetric interfaces can be used and relatively brittle polymers cannot be tested this way.

Lap-Joint Shear Test

This method is the main test method in this thesis for quantifying weld strength, therefore, more detailed information is given in section 9.3.1 on page 92. Basically, the force required to fracture the weld (F_{U} [N]) is divided by specimen width (w [m] from figure 6.10d) resulting in measure for strength (G_{U}), i.e., a measure of force per length ([N/m]) or energy per area ([J/m^2]). The method works with both ductile and brittle polymers.

6.7 Summary

This summary of the literature survey deals with the time horizons for the different mechanisms responsible for weld strength establishments. It is intended to determine which mechanisms that are the process "bottlenecks". Based on the examples in part II, the time horizon from each step in figure 6.1 on page 58 will be reviewed. Keep in mind that the examples are based on the commercially available mHDPE from table 8.1 on page 87.

Heat development and melting: Different models exist to determine the temperature profile in a weld seam. They vary from simple one-dimensional models, which do not take phase transition and temperature dependence of materials into consideration [Klein, 2011], to 3D finite element models taking temperature and pressure variation into account [Van de Ven, 2006]. Altogether, all models agree that the maximum temperature in a weld is relatively high, e.g., more than 300 °C for HDPE. From example 4.2 on page 37, the time to melt ($t_{\text{i,melt}}$), the total melt time (t_{molten}), and the maximum temperature (T_{max}) are determined (100 W and 75 mm/s)[3]:

$$t_{\text{i,melt}} = 0.24\text{s} \tag{6.44}$$

$$t_{\text{molten}} = 5.2\text{s} \tag{6.45}$$

$$T_{\text{max}} = 282^{\circ}\text{C} < 336^{\circ}\text{C} = T_{\text{d,iPP}} < 360^{\circ}\text{C} = T_{\text{d,HDPE}}. \tag{6.46}$$

Moreover, the melting kinetics are important to consider. Rastogi et al. [2006] have proven that for UHMWPE it takes hours about to reach a homogeneous melt state where reptation and thereby diffusion is optimum.

[3] Note that this temperature development is for PP, see figure 4.10 on page 38.

Wettability: As demonstrated in example 6.1 on page 61, the work of adhesion is responsible for 64 mJ/m^2, which is far from the typical reported fracture energy of 1-3 J/m^2. Therefore, when welding plastics, this mechanism is negligible. However, the mechanism is still necessary for the subsequent diffusion, as illustrated in figure 6.1 on page 58, and from example 6.2 on page 62 the time of wetting (t_{wetting}) is determined.

$$t_{\text{wetting}} = 1.4\text{ms} \tag{6.47}$$

Compatibility: Two polymers are compatible if they appear in one phase when mixed. For polymers, it turns out that practically no polymer pairs are compatible because of the low entropic gain of mixing long chains – the difference in solubility parameter must practically be zero to ensure full compatibility. However, the maximum interphasial width (w_∞) might still be non-zero. As discussed in example 6.4 on page 69, important dimensions, such as maximum interphasial width and tube diameter (a), for the iPP/HDPE interphase are:

$$w_{\infty,\text{iPP/HDPE}} = 4.5\text{nm} \tag{6.48}$$
$$a_{\text{iPP}} = 6.9\text{nm} \tag{6.49}$$
$$a_{\text{HDPE}} = 3.6\text{nm} \tag{6.50}$$

Note that the interphasial width is comparable to the tube diameter in this case.

Chemical adhesion: Primary chemical bonds may have an important impact; however, primary bonds are only created by chemical reactions at the interface or by entanglements from diffusion. It turns out that primary bonds from reactions are rare [Beyler and Hirschler, 2002; wiley.com, 2011], and entanglement are dealt with later. Left are secondary chemical interactions, which for a HDPE/iPP interface only counts van der Waals forces. These forces are only responsible for approximately 10^{-4} J/m^2, hence, negligible [Pethrick, 2010].

Diffusion and entanglement: The mechanism dealing with molecular motion across the interface was determined to be reptation with the characteristic time τ_{rep}. After the reptation time, the polymers have inter-penetrated by a distance of $0.81R_{\text{g}}$, which according to Wool's classic theory is enough to develop full strength. In examples 5.1 on page 42 and 5.2 on page 48, R_{g} and τ_{rep} are determined to:

$$R_{\text{g}} = 16.3\text{nm} \tag{6.51}$$
$$\tau_{\text{rep}}(190^\circ\text{C}) = 0.9\text{ms} \tag{6.52}$$

This characteristic reptation time is so short that the characteristic time constants related to Rouse relaxation (τ_{e} and τ_{R}) do not influence at all – at least not for polyolefins above 190 °C; see table 5.2 on page 55.

Regarding establishment of entanglements, this is still not fully understood. However, figure 6.2 on page 58 reveals that full strength can be developed even though the interpenetration is only 4 nm. The explanation is that diffusion depth is worth nothing without entanglements – without entanglements the dominating fracture mechanism is weak pull-outs [Chaffin et al., 2000; Juhl et al., 2013].

(Co-)crystallization: For full strength development in semi-crystalline interfaces not only inter-diffusion and entanglements are necessary. Formation of crystals near the interface is also important for achieving full strength; and for asymmetric interfaces the optimum condition is the ability of co-crystallization which, however, is not necessary, as concluded from Chaffin et al. [2000] – the entanglements just need to be anchored in crystalline lamellae. Regarding laser welding, it is found that the degree of crystallinity near the interface can be as high as 80 % in iPP [Ghorbel et al., 2009]. However, there still is a lack of knowledge concerning the influence of the thermal history in the weld seam [Abed et al., 2003].

Mechanical interlocking: This mechanism is considered a dark horse, since it is intuitively valid; however, literature does not conclude any influence from this effect. Although, within adhesive technology the mechanism is often mentioned [Pocius, 2002]. In adhesive technology, rough surfaces are desired in order to optimize this effect. Roughness in heat welding is also reported to enhance strength. This is explained from the crazing possessing a more tortuous path.

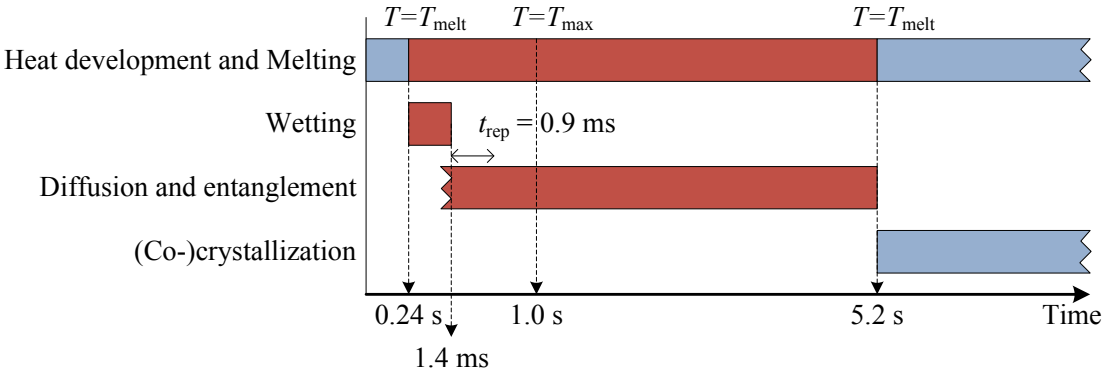

Figure 6.11: The estimated time horizons for the phenomena described in this chapter. The melt time is from a welding of HDPE/HDPE with a 100 W laser and a weld speed of 75 mm/s.

Eventually, all this is summarized in figure 6.11 and a few conclusions can be drawn:

1. From a time frame point of view, the heating and melting phase is without doubt the most important mechanism to control during welding; therefore, selection of appropriate absorbers and scatterers are important.

2. The time dependence of melting is important to investigate, e.g., it is necessary to evaluate how fast polymers can actually melt. Lasers are able to heat up the material quickly, but is the material also able to melt quickly?

3. Diffusion does not play a role when considering the strength development. As long as the melt and wetting criteria are fulfilled, the inter-penetration of $0.81R_g$ is achieved in less than a millisecond. LDPEs are also easily weldable even though its diffusion coefficient is much larger than for linear PE.

In chapter 7 three hypotheses based on this knowledge are formed.

PART III

MATERIALS AND METHODS

CHAPTER 7

HYPOTHESES

In the end of last chapter, the mechanisms of strength establishment and time domains of polymer laser welding were discussed and concluded on. Based on these conclusions and the knowledge presented in part II, three hypotheses are formed constituting the basis of the three main papers presented in part IV.

7.1 Investigation on High Strength Laser Welds of Polypropylene and High-Density Polyethylene – Hypothesis I

From the laser weld matrix in figure 1.2 on page 5, it is noticeable that relatively many types of plastics can be welded together. For instance, LDPE is easier welded than HDPE which is surprising according to the reptation theory, since LDPEs do not reptate due to their long side-chains. This also implies that diffusion is not the bottleneck in the development of weld strength, as concluded in section 6.7. Therefore, the reptation time must be very short, i.e., much shorter than the time in molten state, which for LTW is within a few seconds. Moreover, as described in section 6.4, this is often mentioned as the central mechanism, and researchers often mention the reptation time without questioning the magnitude of it. Thus, a better understanding and estimations of reptation times of industrial polymers are desired.

Moreover, the laser weld matrix reveals that HDPE and PP are non-weldable. However among others, Chaffin et al. [2000] have succeeded with high-strength weldability with two metallocene grades of HDPE and iPP utilizing heat press welding. It is still to be investigated if HDPE and PP are laser weldable.

"Reptation times can be determined from Doi and Edward's tube model theory from chapter 5. The theories are extended and aimed for determination of reptation time in section 5.4 on page 47. The approach concerns linking polymer rheology to polymer physics."

7.2 Mechanical Testing of Polystyrene/Polystyrene Laser Welds – Hypothesis II

It is a fact, and well-known to the industrial partners, that increasing line energy (E_{line}) results in increased strength until the absorbing polymer starts decomposing. On the other

hand, if τ_{rep} is within the millisecond range, other mechanisms must be responsible for increased strength. For a lap-shear joint, one simple explanation is the formation of a wider weld seam caused by increased heat input from the slower moving laser. This has been tested with optical microscopy and only a little increase in weld seam width is observed for increased line energy. Influx formations might be more profound with higher temperature gradients. The influence of these are sought minimized by welding an amorphous polymer, such as polystyrene (PS).

Another explanation for increased strength is the method of quantifying strength. This will be investigated using two different methods for testing mechanical properties; the double cantilever beam (DCM) method, see figure 6.10b, and the lap-joint shear test, see figure 6.10d on page 78. This investigation might reveal information on the influence of fracture mechanisms on mechanical strength.

"Increased line energy results in increased strength. However, since the reptation times of polyolefins are often reported very low, other mechanisms must be responsible for the increased strength. Also, does any significant difference in the quantitative testing exist?"

7.3 Predicting the Laser Weldability of Dissimilar Polymers – Hypothesis III

The equilibrium inter-penetration depth (w_∞) found using Helfand's equation is for HDPE/-iPP predicted to approximately 4.5 nm; see example 6.4 on page 69. This distance is comparable to the radius of gyration of entangled segments ($R_{g,e}$), which is approximately equal to the tube diameter (a), see table 5.1 on page 54. Therefore, entanglement formation should be possible when w_∞ is larger or at least comparable to a. This means that a large w_∞/a-ratio will result in relatively strong welds. This is tested by correlating qualitative weld strength to w_∞/a_{max} determined from considerations similar to those in example 6.4.

If a correlation exists, the ratio w_∞/a_{max} might be harnessed to predict the weldability of two polymers, e.g., by implementing polymer properties into a computer program. Note that this hypothesis only takes thermodynamics of mixing into account and not kinetic effect, i.e., it is assumed that the reptation time for all materials are very low compared to the laser welding processing time.

"Large inter-penetration depth (w_∞) and small polymer melt mesh size (a) might facilitate space for interphasial entanglements. Therefore, does a large w_∞/a_{max} imply a strong welded joint between two dissimilar polymers?"

CHAPTER 8

MATERIALS

Based on the hypothesis and figure 1.2 on page 5, seven different polymers are selected for experimentation; see table 8.1. High density polyethylene (HDPE) and polypropylene (PP) are used for hypothesis 1; see chapter 10 on page 101. Polystyrene (PS) are used for hypothesis 2; see chapter 11 on page 109. For hypothesis 3 HDPE, PP, and PS from the former two hypotheses are used along with poly(methyl methacrylate) (PMMA), poly(butylene terephthalate) (PBT), and polycarbonate (PC), i.e., a total of 6 materials; see chapter 12 on page 117.

POM is not used in the three papers, however, it is implemented in the EXPAND program and used for model validation in section 13.2 on page 129. The carbon black grade, Enasco 260G from Timcal Lmt., is chosen as an absorber for the absorbing parts of the LTW process. Note that the selected PP is a metallocene block PP, consisting of isotactic blocks and random blocks. Therefore, this specific grade is referred to as mPP.

Polymer	Grade	Manufacturer	M_w	M_n	PDI
mHDPE	mPE M 6091	Total Petrochemicals	128,000	55,100	2.3
mPP	Metocene HM562S	LyondellBasell	237,000	107,000	2.2
PMMA	EH 910	LG MMA corp.	N/A	N/A	N/A
PS	MFCD00084450	Sigma-Aldrich	192,000	N/A	N/A
POM	Delrin 100 NC010	DuPont	212,000	101.000	2.1
PBT	Pocan B 1305	Lanxess	N/A	N/A	N/A
PC	Lexan HPSR2	SABIC	N/A	N/A	N/A

Table 8.1: The seven selected materials; high density polyethylene, polypropylene, poly(methyl methacrylate), polystyrene, polyoxymethylene, poly(butylene terephthalate), and polycarbonate. See also figure 5.2 on page 55 and the Excel datasheet on the enclosed CD for further details.

CHAPTER 9

METHODS

In this chapter the methods utilized to test the hypotheses in chapter 7 are described. The methods for investigating these are presented in the three publications in part IV on page 101. This chapter will present some of the details not treated in the publications. Especially photos of the laboratory equipment are emphasized.

9.1 Preparation of Sheets for Laser Welding

Prior to laser welding, the selected materials are compounded and injection molded into sheets; including laser transmissive and laser absorbing sheets.

9.1.1 Preparation of Absorbing Sheets

Principally, the procedure of preparing carbon black containing absorbers consists of three steps; drying, melt blending, and granulation. Firstly, materials are dried in a vacuum oven after the specifications given in table 9.1. 0.4 w% CB is chosen simply because pilot experiments with this amount turned out to be successfull; see also example 4.1 on page 30.

Polymer	t_{dry} [hr]	T_{dry} [°C]	$T_{extrusion}$ [°C]	Feed rate [%]
mHDPE	—	—	180	20-25
mPP	—	—	180	20-25
PMMA	4	80	250	12
PS	2	70	240	15
PBT	4	120	245	10-15
PC	3	121	290	10-15

Table 9.1: The screw speed was fixed at 200 rpm.

After drying, the materials are mixed with 0.4 w% carbon black in a plastic bag. The dry mix is then processed in a co-rotating twin screw extruder, PRISM Eurolab 16 XL by ThermoFischer Scientific, see figure 9.1. This machinery has six heat zones configured as described in table 9.1. Throughout the process, a rotational speed of 200 rpm is maintained for the screw and an appropriate feed rate is maintained. Subsequently, the extruded material is lead through a water bath, air dried, and directly granulated by a pelletizing system. All samples are melt blended twice to ensure a good dispersion of carbon black.

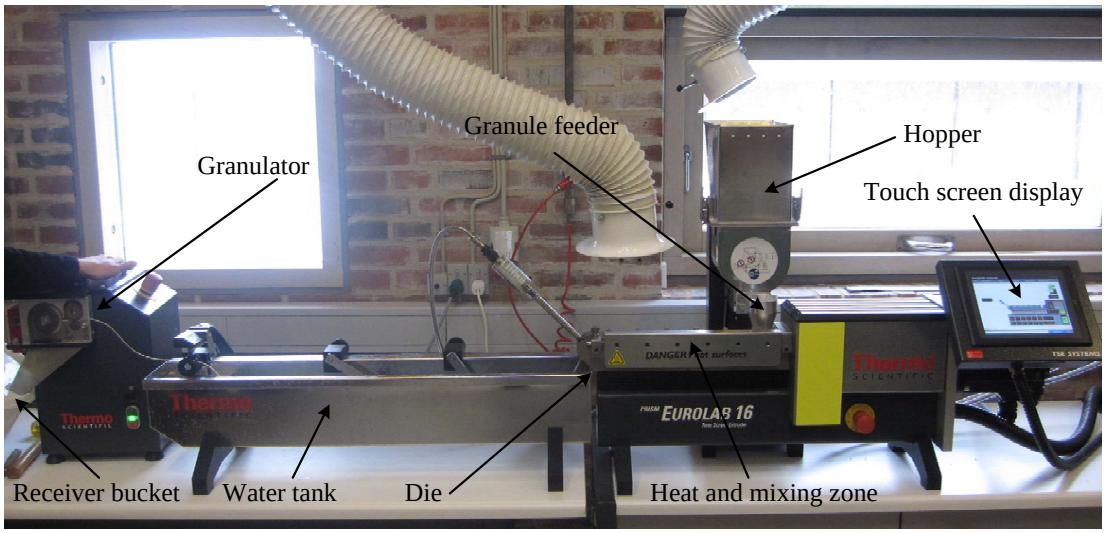

Figure 9.1: Photo of the melt compound extruder used for compounding carbon black into the selected polymers.

9.1.2 Injection Molding of Sheets

The absorbing materials containing carbon black and the pristine transparent materials are injection molded into sheets. The sheets are designed for laser transmission welding (LTW), as seen in figure 9.2 and 9.3. Four materials (PMMA, PS, PBT, PC) were injection molded at Coloplast, while mHDPE and mPP were molded by DTI.

	mHDPE	mPP	PMMA	PS	PBT	PC
Shot weight [g]	N/A	N/A	10.94	9.7	11.5	11.1
Inj. molding melt temp. [°C]	200	220	260	230	255	270
Tool temp. [°C]	50	50	65	30	70	70
Cooling time [s]	40	30	25	22	22	22
Cycle time [s]	48.3	38.3	38.2	32.2	32.2	32.8
Fill time [s]	1.71	1.31	1.63	1.86	1.87	1.98
Inj. speed [mm/s]	25	25	16.3	16.3	16.3	16.3
Holding pressure [bar]	N/A	N/A	750	400	400	700
Holding time [s]	N/A	N/A	4.0	3.5	3.5	4.0

Table 9.2: Process parameters for injection molding of sheets. mHDPE and mPP are molded at DTI in an Engel HS 1300-650 machine, while PMMA, PS, PBT, and PC are molded at Coloplast in a Engel VC 200/45 TECH machine.

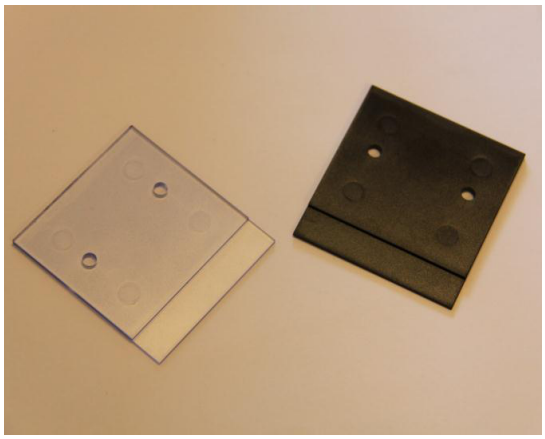

Figure 9.2: Two injection molded PC sheets.

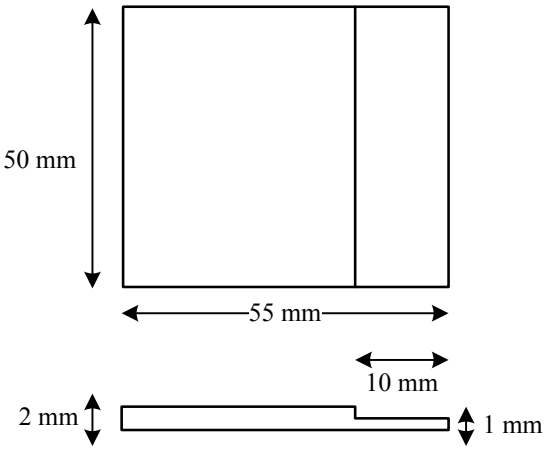

Figure 9.3: Dimensions of the sheets.

9.2 Laser Welding Experiments

Laser transmission welding (LTW) was carried out at Coloplast. The laser used was a diode laser, Laserline 300 W, with a wavelength of 808 nm equipped with an Arges scanner. The laser power was fixed to 50 W for all experiments and the energy input was altered by varying the weld speed. The sheets were welded at least 24 hours after injection molding, and no drying was used prior to welding. 5 repetitions were used in all experiments.

9.2.1 Experimental Plan

Six materials were chosen for experimentation; HDPE, PP, PMMA, PS, PBT, and PC – all in a transparent and an absorbing version. This means that (6^2 =)36 material combinations must be tested. For each material combination, if an exact process optimum must be found, the amount of experiments will be tremendous. Therefore, according to the hypothesis in chapter 7, following delimitation is stated:

aHDPE/tHDPE, aPP/tPP, aHDPE/tPP and aPP/tHDPE: The experiments involving welding of HDPE to PP and vice versa, a global maximum for weld strength was estimated, i.e., the materials were welded at various weld speeds to find the optimum line-energy. The work is summarized in the publication in chapter 10.

aPS/tPS: Also here a process optimization is performed by welding at different line-energies. The work is summarized in chapter 11.

All others: No process optimization was carried out for other material combinations. The materials were welded at different speeds and tested by hand to evaluate whether the two materials were weldable. The weld speed resulting in the strongest welding was noted, 5 repetitions carried out, and tested as described in section 9.3.1. These experiments were conducted in the end of the project, and from experience it turned out to be easy to *feel* (strength and toughness), but mostly *see* if the weld was strongly welded. In general, it is experienced that an aesthetic and uniform weld is also strong and tough. This work is summarized in chapter 12.

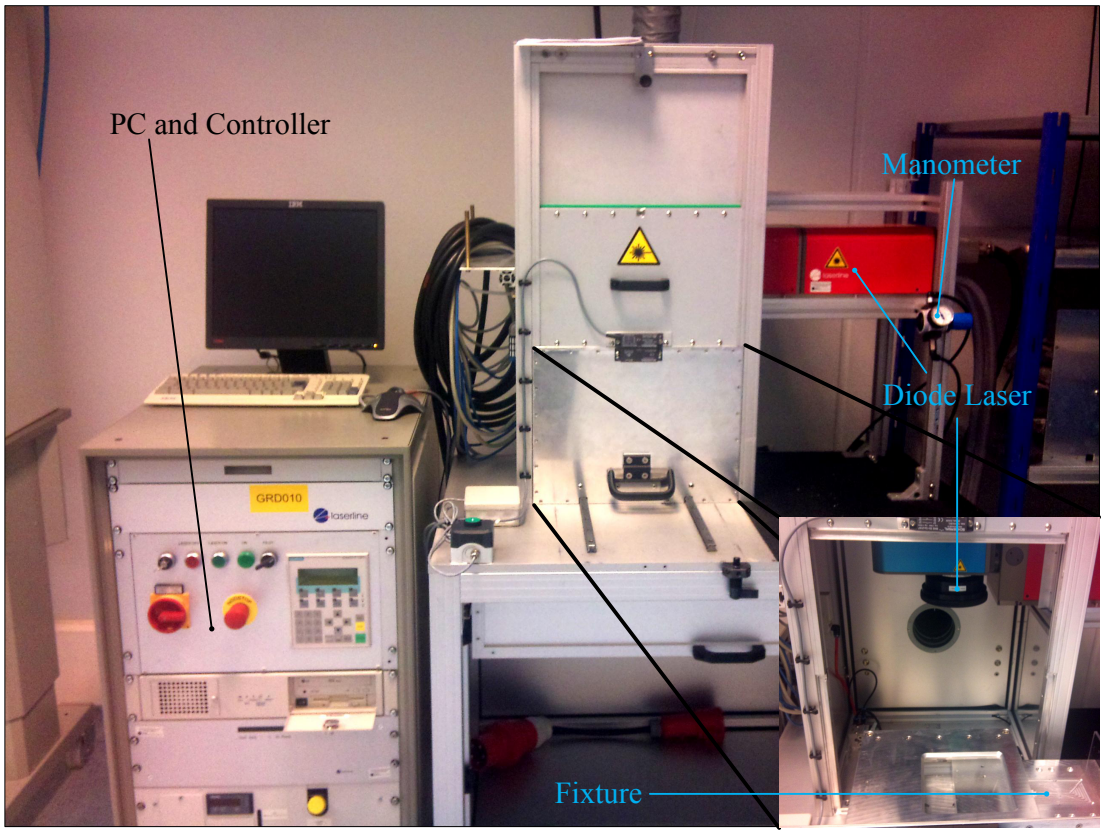

Figure 9.4: The equipment at Coloplast utilized for laser transmission welding.

9.3 Procedure for Tests and Measurements

Welded specimens were evaluated for ultimate strength (σ_U) and critical energy release rate (G_{Ic}) using mechanical testing as described in the following.

9.3.1 Lap-Joint Shear Test

The welded specimens were cut out to strips as illustrated in figure 9.5. The cut was performed with a band saw equipped with a precision blade to ensure a flawless, smooth finish of the strips. The strips were tensile tested in an Instron 5944 tensile testing machine equipped with a 2 kN load cell, see figure 9.6. For all tests, the grips were located 63 mm apart and the tests were performed with a speed of 50 mm/min. The tested stress state was shear stress and the reported strength was the force required to fracture the test specimen divided by the weld specimen length, which was approximately 10 mm; the exact length was measured with a slide gauge for each specimen.

9.3.2 Asymmetric Double Cantilever Beam (ADCB) Method

The critical energy release rate (G_{Ic}) of the polymer welds were determined using the asymmetric double cantilever beam (ADCB) method, see section 6.6.3 on page 77 for more in-

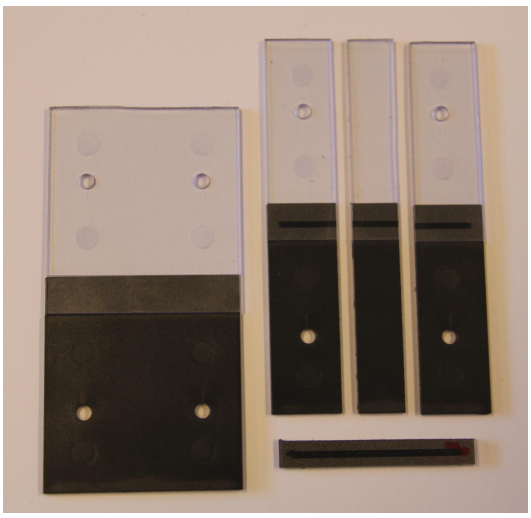

Figure 9.5: A laser welded specimen presented together with the two test specimens; a strip for lap-joint shear testing and a beam for the ADCB method.

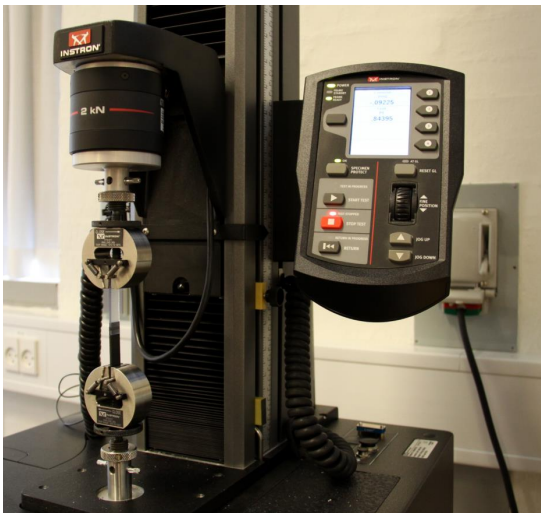

Figure 9.6: A lap-joint shear test specimen placed in the tensile testing machine.

formation. This method required the lap-joint cut into a double beam as illustrated in figure 6.10b on page 78.

The double beam was placed in an experimental setup as shown in figure 9.7. The double beam was fixed in the setup with a micro-clamp, and a double edged Stanley-razor (Δ = 0.65 mm or 0.35 mm) can cleave the specimen apart opening a crack in front of the knife. The setup was build into an Instron 5944 tensile testing machine working in compression mode, moving the knife 100 μm/s. This velocity is lower than 150 μm/s as suggested by Schnell et al. [1998]. As the razor moved, a fixed Canon EOS 50D camera (15.1 Mpx, equipped with a Canon 18–200 mm optics) captured photos of the crack length every 5 seconds. An example of such a photo is seen in figure 9.8. Using the Matlab Image Processing Toolbox on the high-resolution pictures, the crack length (a) can be determined with 10 μm accuracy.

9.3.3 Determining Elastic Modulus, E

In order to determine G_{Ic} from the ADCB method, the elastic modulus of the beam material must be known. The elastic modulus of the PS beams, measuring 50.0 × 8.80 × 1.04 mm, was determined from dynamic mechanical analysis (DMA) in a Q800 from TA Instrument. The specimen was placed in the instrument as a regular tensile test. The test speed was fixed to 100 µm/min and 5 repetitions were used. The modulus was determined to 3110 MPa ± 40.5 MPa.

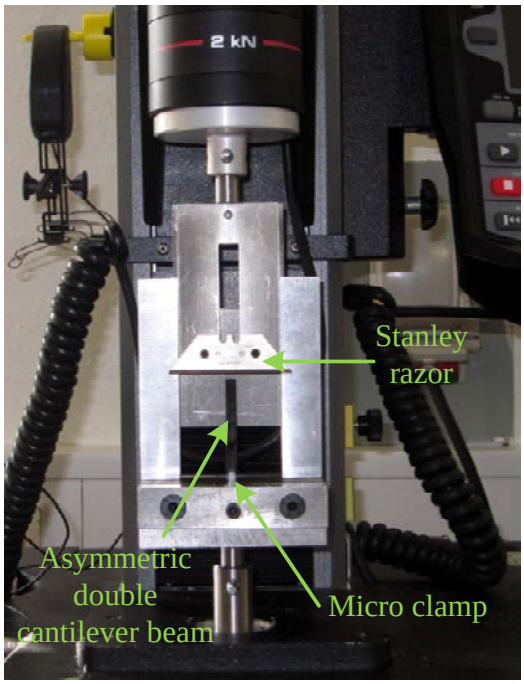

Figure 9.7: Setup of the ADCB method in the tensile testing machine.

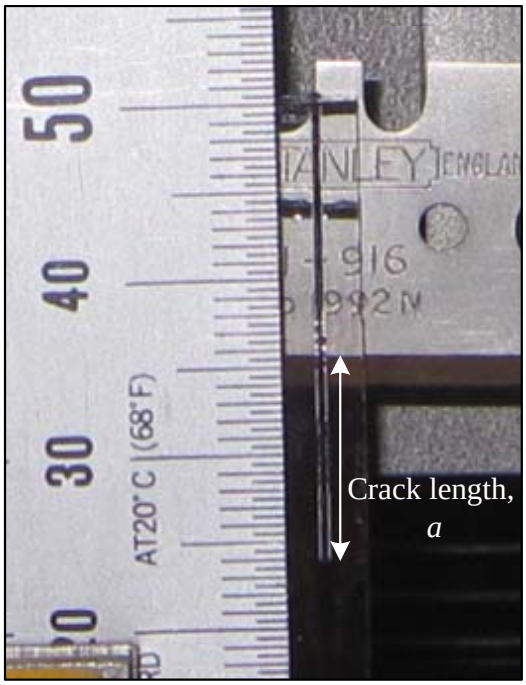

Figure 9.8: The crack tip is easily detected.

9.3.4 Rheometry

In order to determine the reptation time (τ_{rep}) and the monomeric friction coefficient (ζ) of a polymer, the zero shear viscosity (η_0) is necessary. The zero shear viscosity is determined with a Paar Physica MCR500 rheometer in a plate-plate configuration with a 25 mm disc and a gap height of 1 mm. In order to measure within the linear elastic regime, the oscillatory tests were performed with small strain amplitude, $\gamma = 0.05$. The angular frequency varied from 0.0628 to 628 rad/s. η_0 was determined as the viscosity at 0.0628 rad/s or a fitted Carreau-Yasuda model. Each specimen was melted for 5 min, the required gap height was established, and the specimen was equilibrated for another 5 min before measurement, and no repetitions were performed. When operating in oscillatory mode, the Cox-Merz rule is assumed valid. This is for instance the case for PS with a molecular weight of 182,000 g/mol [Snijkers and Vlassopoulos, 2011].

9.3.5 Differential Scanning Calorimetry (DSC)

Thermal characterization was performed using a Q2000 DSC from TA Instruments. Melting temperature (T_{melt}) and crystallization temperature (T_{melt}) of semi-crystalline polymers (HDPE, PP, POM, PBT) and glass transition temperature (T_g) of amorphous polymers (PMMA, PS, PC) were determined; see figures 9.9 and 9.10. From the injection molded sheets approximately 15 mg was cut out using a punch plier. The materials were placed in aluminum pans according to TA Instrument's Tzero series. All samples were equilibrated at 25 °C and heated/cooled at a rate of 10 K/min to a maximum temperature presented in table 9.3.

Three heating/cooling cycles are used and N_2 was used as a purge gas with a flow rate of 50 mL/min.

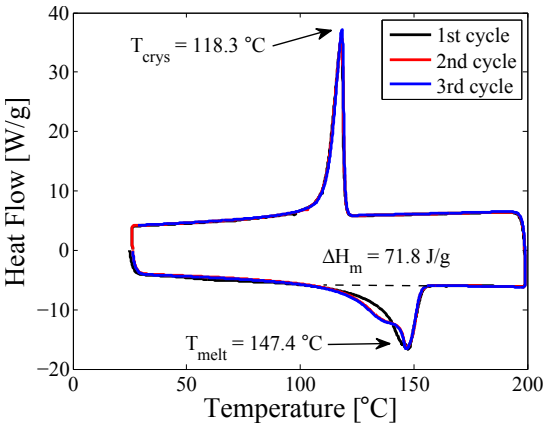

Figure 9.9: Heat flow versus temperature for semi-crystalline PP.

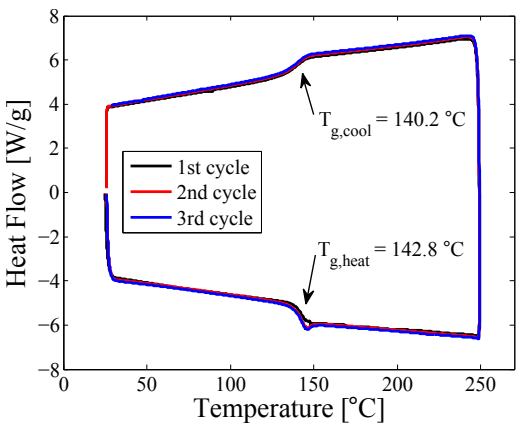

Figure 9.10: Heat flow versus temperature for amorphous PC.

Polymer	**HDPE**	**PP**	**PMMA**	**PS**	**POM**	**PBT**	**PC**
DSC T_{max} [°C]	180	200	230	200	210	250	250
T_{melt} [°C]	132.4 (132.5)	147.4 (146.9)	N/A	N/A	178.9 (N/A)	224.7 (224.7)	N/A
T_{crys} [°C]	119.2 (120.4)	118.3 (119.3)	N/A	N/A	149.1 (N/A)	201.6 (206.5)	N/A
$T_{g,heat}$ [°C]	N/A	N/A	114.6 (113.1)	104.8 (104.7)	N/A	N/A	142.8 (142.4)
$T_{g,cool}$ [°C]	N/A	N/A	111.0 (110.5)	100.4 (100.3)	N/A	N/A	140.2 (140.0)
ΔH_m [J/g]	163 (165)	71.8 (73.1)	N/A	N/A	130.1 (N/A)	46.6 (44.3)	N/A
ΔH_m^0 [J/g] [a]	285	207	N/A	N/A	170	142	N/A
α_c [%]	57.2 (57.8)	34.7 (35.3)	N/A	N/A	76.6 (N/A)	32.8 (31.2)	N/A

Table 9.3: Results from the DSC experiments. The numbers in parenthesis denote the characteristics with addition of 0.4 w% carbon black. [a] refers to [van Krevelen and te Nijenhuis, 2009].

As indicated in table 9.3 addition of 0.4 w% carbon black does not significantly alter the thermal properties – except for those of PBT, where T_{crys} varies 4.9 °C. The crystallinity is defined by:

$$\alpha_c = \frac{\Delta H_m}{\Delta H_m^0} \cdot 100\%, \tag{9.1}$$

where ΔH_m^0 is the specific heat of melting of a pure polymer crystal and ΔH_m is the melting heat given as the area between the endothermic peak during heating and the baseline.

9.3.6 Hansen Solubility Parameters (HSP)

For data input to equation 6.15 on page 64 the Hansen solubility parameters (HSPs) are essential. The method for determining HSP was originally proposed by Charles M. Hansen [Hansen, 2000]. Stated shortly, the methodology involves measuring solubility or degree of swelling in a sufficient number of liquids, having suitably different HSPs, covering as much of the Hansen space as possible. In this case 44 different standardized liquids with known HSP ($\delta_D, \delta_P, \delta_H$) are used. The Hansen SPs were determined at FORCE Technology by Daniela Bach. The HSPs were determined for all 7 polymers from table 8.1 on page 87. Results are presented in table 9.4.

In practice, a few granules from the specific polymer grade were submerged into the 44 solvents. Over a period of time, the degree of swelling was reported until no difference over time could be detected. In this case the polymers were submerged for approximately three months. The degree of swelling ranged from 1 (dissolved) to 6 (no visible effect) and the results were plotted into the software HSPiP v. 4.0.03 [Hansen, 2013], as illustrated in figure 9.11. The software fits a sphere around the "soluble" solvents, specifying the center of the sphere ($\delta_D, \delta_P, \delta_H$) and the radius ($R$, interaction radius). Polymers are usually expected to give data fits of R^2 0.95 or above. Often unusual outliers are presented within the sphere. These can be excluded in the calculation in order to obtain a better fit.

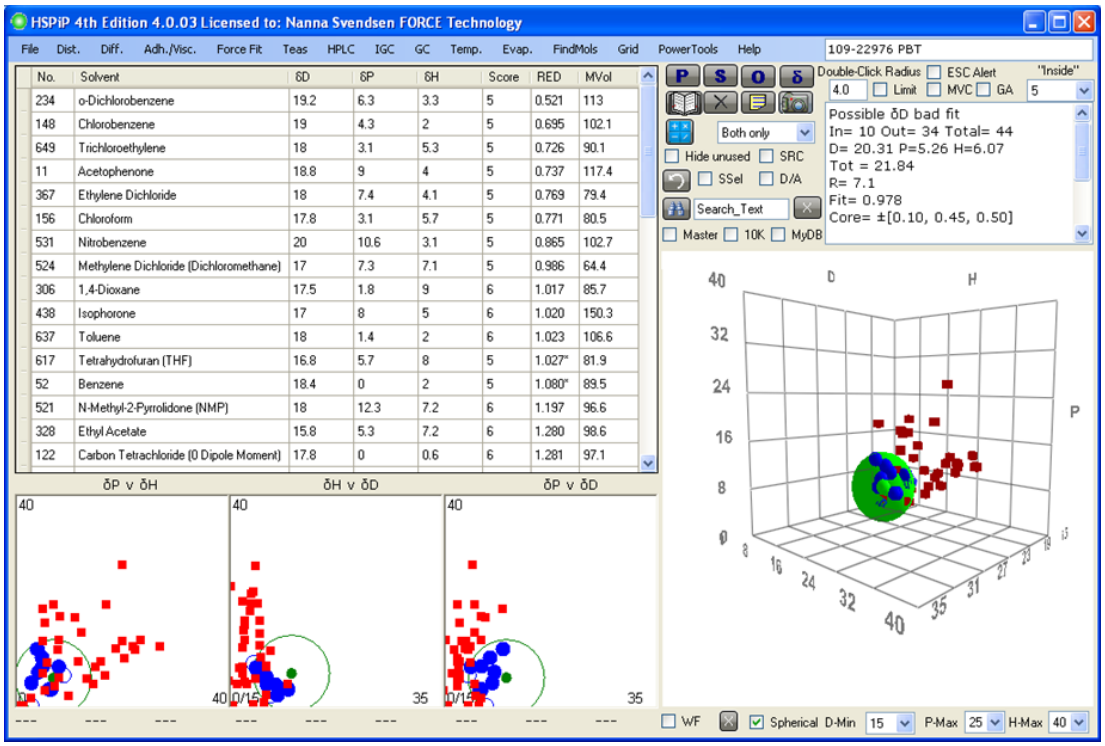

Figure 9.11: Screen shot of the HSPiP program. Here with PBT as an example.

Table 9.4 summarizes the obtained Hansen SPs and raw data is found on the CD. The Hansen SP from theory was obtained using a simple software based on group contribution methods [Hinge et al., 2002]. The experimental Hansen SPs from Hansen [2000] are data from specific grade of said polymer determined by different research groups. The methodology might therefore not be identical. Finally, the experimental HSPs determined at FORCE Technology and published by Juhl et al. [2013] are also displayed. For an overall discussion on the quality of these see section 13.3.1 on page 132.

All polymers, except HDPE, show nice fits. The bad fit from HDPE might be explained by a short incubation time in the solvents. The time can be sped up by submerging into an ultrasonic bath [Hansen and Just, 2001].

Polymer	**HDPE**	**PP**[a]	**PMMA**[a]	**PS**	**POM**	**PBT**[a]	**PC**
Hildebrand SP (th.) [$MPa^{1/2}$] [b]	16.0	17.0	19.0	19.1	20.4	20.5	23.0
Hansen SP (th.) [$MPa^{1/2}$] [c]							
δ_D	15.5	14.3	15.6	17.1	12.6	15.6	19.5
δ_P	0.0	0.0	5.4	1.0	13.5	3.7	3.1
δ_H	0.0	0.0	8.1	0.0	11.4	8.5	6.8
Hansen SP (exp.) [$MPa^{1/2}$] [d]							
δ_D	16.0	17.2	18.1	18.5	17.1	18.0	18.1
δ_P	0.8	5.6	10.5	4.5	3.1	5.6	5.9
δ_H	2.8	-0.4	5.1	2.9	10.7	8.4	6.9
Interaction radius, R	3.2	4.5	9.5	5.3	5.3	4.5	5.5
Hansen SP (exp.) [$MPa^{1/2}$] [e]							
δ_D	11.9	17.2	18.8	18.1	16.7	20.3	19.9
δ_P	5.5	3.1	12.8	9.0	4.4	5.3	10.7
δ_H	3.8	2.2	4.2	2.7	2.2	6.1	2.0
Interaction radius, R	21.8	3.7	13.0	9.8	4.1	7.1	12.3
Fit, R^2	0.46	0.99	1.00	0.98	0.94	0.98	1.00

Table 9.4: Theoretical and experimental Hildebrand and Hansen solubility parameters. [a] solvent outliers have been removed. [b] refers to [van Krevelen and te Nijenhuis, 2009], [c] refers to [Hinge et al., 2002], [d] refers to [Hansen, 2000], [e] refers to own experiments [Juhl et al., 2013].

PART IV

RESULTS AND DISCUSSION

CHAPTER 10

INVESTIGATION ON HIGH-STRENGTH LASER WELDS OF POLYPROPYLENE AND HIGH-DENSITY POLYETHYLENE – HYPOTHESIS I

Authors: Thomas Brokholm Juhl, Jesper deClaville Christensen, and Erik Appel Jensen.

Title: *Investigation on High Strength Laser Welds of Polypropylene and High-Density Polyethylene* [Juhl et al., 2013a].

Publisher: Wiley.

Journal: Journal of Applied Polymer Science.

Volume: 129.

Number: 5.

Pages: 2679–2685.

DOI: http://dx.doi.org/10.1002/app.39000

Background: This paper originates from bullet point 2 from the problem statement on page 19 and the hypothesis formulated in section 7.1 on page 85.

CHAPTER 11

MECHANICAL TESTING OF POLYSTYRENE/POLYSTYRENE LASER WELDS – HYPOTHESIS II

Authors: Thomas Brokholm Juhl, Jesper deClaville Christensen, and Erik Appel Jensen.

Title: *Mechanical Testing of Polystyrene/Polystyrene Laser Welds* [Juhl et al., 2013b].

Publisher: Elsevier.

Journal: Polymer Testing.

Volume: 32.

Number: 3.

Pages: 475–481.

DOI: http://dx.doi.org/10.1016/j.polymertesting.2013.01.009

Background: This paper originates from bullet point 3 from the problem statement on page 19 and the hypothesis formulated in section 7.2 on page 85.

CHAPTER 12

PREDICTING THE LASER WELDABILITY OF DISSIMILAR POLYMERS – HYPOTHESIS III

Authors: Thomas Brokholm Juhl, Daniela Bach, Ronald G. Larson, Jesper deClaville Christiansen, and Erik Appel Jensen.

Title: *Predicting the Laser Weldability of Dissimilar Polymers* [Juhl et al., 2013].

Publisher: Elsevier.

Journal: Polymer.

Volume: 54.

Number: 15.

Pages: 3891–3897.

DOI: http://dx.doi.org/10.1016/j.polymer.2013.05.053

Background: This paper originates from bullet point 4 from the problem statement on page 19 and the hypothesis formulated in section 7.3 on page 86.

CHAPTER 13

OVERALL DISCUSSION

This chapter will sum up the findings and tie together the three papers presented in the previous chapters. The main conclusion from the papers is that the ratio $w_\infty / a_{\max}$ could predict the laser weldability of a polymer pair. This knowledge is utilized in section 13.1 to develop a program for weldability prediction, which also is in accordance with bullet point 5 from the problem statement on page 19. The suggested model is in section 13.2 validated using a *seventh* polymer, POM. The selected POM grade is presented in table 8.1 on page 87.

In section 13.3 alternative correlations for predicting weldability are tested, e.g., difference in melting point, which is often used as a rule of thumb in industry [lpkfusa.com, 2012]. And eventually in section 13.4, a very common question from process engineers is answered; *What is best for welding; a high temperature for short time, or a low temperature for long time?*

13.1 The EXPAND Program

As pointed out in the project background in chapter 1, a generic tool for material selection is desired when considering materials for welding processes. The knowledge from this project is gathered in the EXPAND program, which is attached on the enclosed CD. The software architecture is designed with easy expansion in mind, i.e., the new materials can easily be added to the database. The program might be integrated into Aleksei Likhtmann's RepTate [reptate.com, 2013] or Charles Hansen's HSPiP software [Hansen, 2013]. As indicated in figure 13.1 the program is divided into three tabs:

Reptation: Based on the knowledge gained from chapters 5, 10, and 11, a tool to predict radius of gyration (R_g), reptation time (τ_{rep}), self-diffusion coefficient (D_s), and other relevant molecular properties; see tables 5.1 and 5.2 on page 55.

Weldability: Based on hypothesis 3 and the three papers, especially paper no. 3 (p. 117), this module can predict weldability based on theoretical Hildebrand SP or experimental Hansen SP. The module is based on material constants from table 5.1 and the Excelsheet on the CD. All seven[1] polymers from table 8.1 on page 87 can be selected.

Custom: This is similar to the *Weldability*-module; however, in this module the material properties and constants can be customized.

[1] Although the predictions involving POM are not yet validated, see section 13.2 on page 129.

13.1.1 Reptation

The *reptation*-module is based on polymer physics table values as presented in table 5.1. However, as described in section 5.3.2 on page 47, the monomeric friction coefficient (ζ) is very rarely reported in literature. Moreover, the temperature dependence of ζ is modeled using the Volger-Fulcher equation; see equation 5.30 on page 47. The Volger-Fulcher parameters for HDPE, PP, PS, and POM are presented in table 13.1.

	A	B	T_0	R^2
HDPE[a] ($140°C < T < 200°C$)	-34.56	1981	124.3	0.9925
PP[a] ($160°C < T < 210°C$)	-71.58	59,180	-869.3	0.9832
PS[b] ($200°C < T < 250°C$)	-29.54	1115	364.5	0.9936
PS[c] ($T < 160$ °C)	-24.34	1620	332.6	N/A
POM ($190°C < T < 240°C$)	-23.69	588.9	626.2	0.9960

Table 13.1: Parameters for the Volger-Fulcher equation for three selected polymers. [a] refers to [Juhl et al., 2013a], [b] refers to [Juhl et al., 2013b], [c] refers to [Majeste et al., 1998].

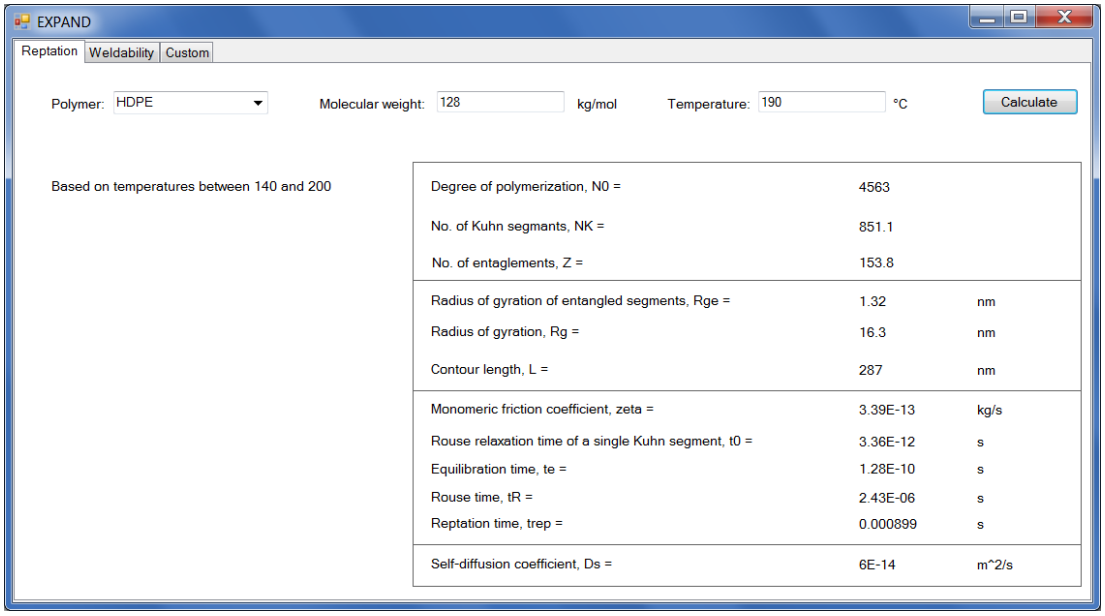

Figure 13.1: Screen shot of the *Reptation*-module of the EXPAND-program.

The data output for a HDPE with molecular weight of 128,000 g/mol at 190 °C is presented in figure 13.1. These values can be compared with examples 5.1 on page 42 and 5.2 on page 48.

Based on this knowledge it can be concluded that HDPE is easily weldable at 190 °C, since the processing time will exceed the reptation time – as in accordance with Wool's theory, see equation 3.7 on page 16. On the other hand, the reptation time of a PS having a molecular weight of 300,000 g/mol at 190 °C has a reptation time of 0.8 seconds. This is a very long reptation time for a laser welding process, and the temperature should there-

fore be increased. For instance, if the temperature is increased to 250 °C, the reptation time drops to 10 ms, which is much lower than the laser welding processing time. This is also consistent with Wool's conclusion that PS at low temperatures requires a long welding time to fully heal [Wool, 1995].

13.1.2 Weldability

This module is primarily based on paper 3 from chapter 12. Therefore, all constants and parameters necessary for predicting the weldability is presented there [Juhl et al., 2013]. Basically, the weldability is predicted from two methods; one using theoretical Hildebrand SPs and another using experimental Hansen SPs. From Juhl et al. [2013], it is to conclude that two polymers are weldable if their w_∞/a_{max} ratio is above a certain threshold. For the Hildebrand model this threshold is $w_\infty/a_{max} = 0.30$, while the threshold for the Hansen model is 0.15. The difference is explained from Hansen SP generally predicting larger values of χ due to a three-component solubility parameter compared to the one-dimensional Hildebrand SP[2]. In figure 13.2 an example of the *weldability*-module is presented for welding of PBT and PC.

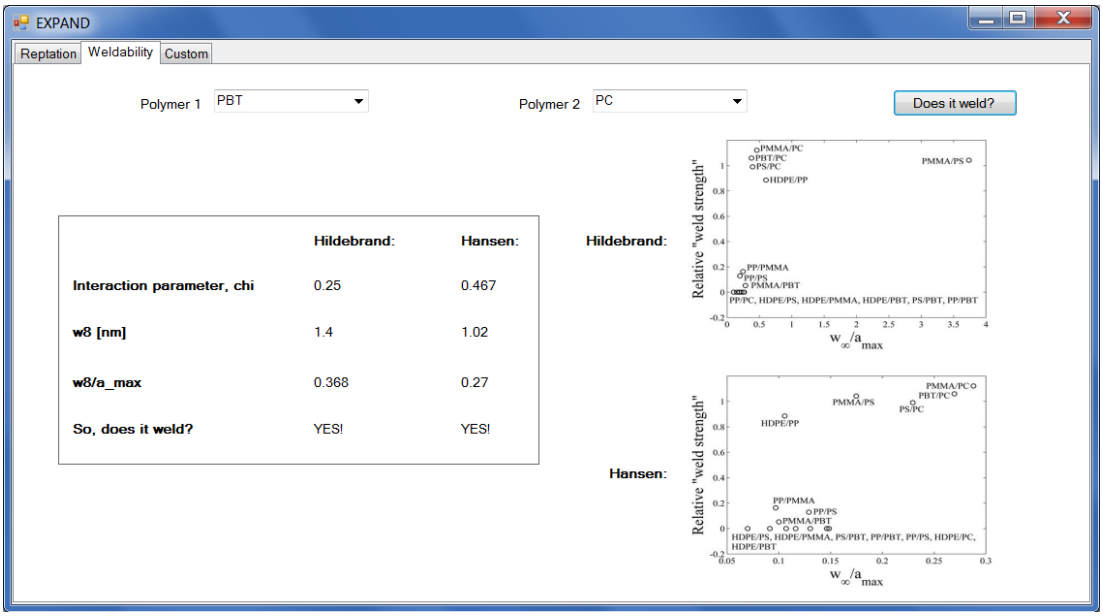

Figure 13.2: Screen shot of the *Weldability*-module of the EXPAND program.

For the Hildebrand approach two incorrect predictions exist; PMMA/PC and PS/PC, while the Hansen approach fails the prediction of HDPE/PP weldability. This means that the two methods in some cases disagree whether two polymers are weldable or not. In general, the model should be validated taking more polymer pairs into account. In section 13.2 this is done by expanding the model with polyoxymethylene (POM).

[2] The $(\delta_{x1} - \delta_{x2})^2$-part will always be positive, and for Hansen SP three parts are added together, resulting in larger χ-value, see equation 6.15 on page 64.

13.1.3 Custom

At this writing, the *weldability*-module only covers seven polymers, which is far from the number of various polymers used in the industry. Therefore, the *custom*-module facilitates weldability predictions for specific polymers simply by typing in data values. Data values for five "new" commodity plastics are presented in table 13.2: Acrylonitrile butadiene styrene (ABS), styrene-acrylonitrile (SAN), polyamide 66[3] (PA66), polyethylene oxide (PEO), and polytetrafluoroethylene[4] (PTFE). In figure 13.3 the data for PEO and PTFE are typed in, and the materials are reported to be non-weldable. Earlier research does not show examples of weldability between PEO and PTFE. Also PTFE is a high-temperature melting polymer, while PEO melts at 70 °C and decomposes at 185 °C[Matsuo et al., 1997]; therefore, weldability is highly unlikely.

Polymer	**ABS**	**SAN**	**PA66**	**PEO**	**PTFE**
δ_D [MPa$^{1/2}$] [a]	16.3	16.6	16.0	22.2	17.1
δ_P [MPa$^{1/2}$] [a]	2.7	9.8	11.0	11.2	8.1
δ_H [MPa$^{1/2}$] [a]	7.1	7.6	24.0	13.2	1.3
V_m [cm^3/mol] [b]	190.6	125.6	191.6	36.0	46.6
a [Å] [c]	N/A	N/A	N/A	37.3	52.8
b [Å] [d]	N/A	N/A	N/A	5.36	7.73
T_{crys} [°C] [b]	105$^{am.}$	105$^{am.}$	240^{sc}	55^{sc}	300^{sc}

Table 13.2: Input data for the *Custom*-module. [a] refers to [Hansen, 2000], [b] refers to [van Krevelen and te Nijenhuis, 2009], [c] refers to [Fetters et al., 2007], [d] refers to [Wool, 1995].

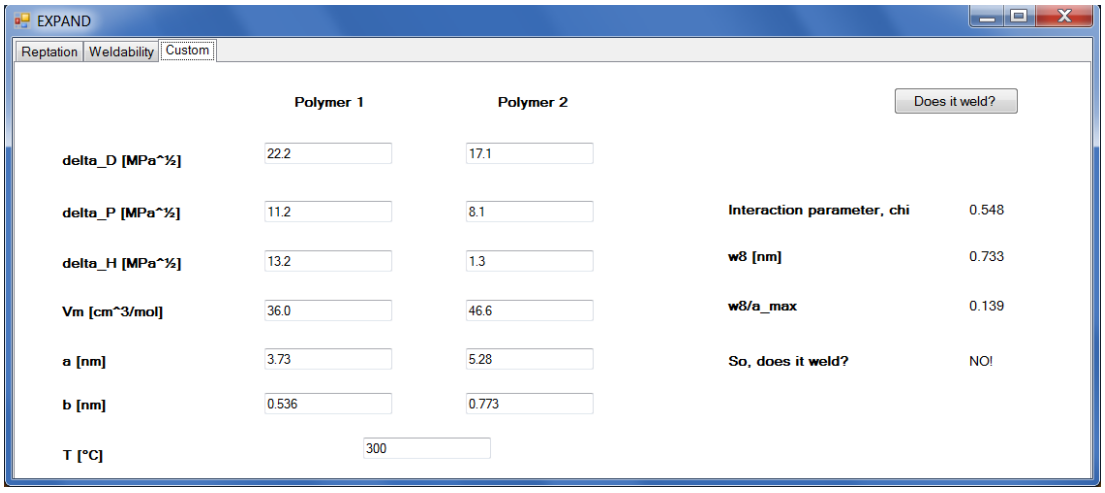

Figure 13.3: Screen shot of the *Custom*-module of the EXPAND-program for predicting weldability between PEO and PTFE.

[3] Also known as Nylon
[4] Also known as Teflon

Table 13.2 also demonstrates the limitations of this method; the data basis is relatively sparse. It was not possible to find the tube diameter (a) or the statistical segment length (b) in literature for ABS, SAN, or PA66. The explanation is that ABS and SAN are co-polymers, i.e., they consist of blocks of different homopolymers and depending on the ratio of these blocks, their physical properties alter. PA66, and in general no polyamides, has been tabulated. The sparse amount of data is especially manifested in the fact that Fetters et al. [2007] is the only reliable collected source of data.

13.2 Model Validation

The paper presented in chapter 12 [Juhl et al., 2013] investigates the weldability of six polymers. In order to verify the proposed model and the EXPAND program, the weldability of a seventh polymer (POM) is investigated. Hansen solubility parameters of POM is determined, see table 9.4 on page 97, and other relevant data of POM include; $V_m = 21.6\ cm^3/mol$, $a = 4.48$ nm, $b = 4.79$ Å, and $T_c = 146.6$ °C. If POM is added to the EXPAND program, the weldability presented in table 13.3 is predicted.

Polymer	**HDPE**	**PP**	**PMMA**	**PS**	**PBT**	**PC**
χ (Hansen)	0.182	0.00624	0.284	0.0958	0.239	0.353
w_∞ [nm] (Hansen)	1.00	5.20	0.853	1.57	0.879	1.14
w_∞ / a_{max} (Hansen)	0.223	0.753	0.122	0.184	0.196	0.254
Does it weld? (Hansen)	YES	YES	NO	YES	YES	YES
χ (Hildebrand)	0.147	0.107	0.0241	0.0221	0.000141	0.118
w_∞ [nm] (Hildebrand)	1.11	1.25	2.92	3.26	36.2	1.97
w_∞ / a (Hildebrand)	0.249	0.182	0.418	0.383	8.08	0.439
Does it weld? (Hildebrand)	NO	NO	YES	YES	YES	YES
Rel. weld strength [a]	1/3	1/3	2/3	0	0	N/A
Exp. weld strength [kJ/m^2]	0	0	0	0	0	0

Table 13.3: Weldability predictions of POM with six different polymers using the EXPAND program. [a] refers to [laserplasticwelding.com, 2012].

The POM grade presented in table 8.1 on page 87 is injection molded into sheets in accordance with Juhl et al. [2013], see figure 9.2 on page 91. The sheets were welded with $P_{laser} = 50$ W and varying laser speed – note that POM is only present in a transparent version. From the welding experiments it was clear that POM was non-weldable to any of the six other polymers. This does not at all fit the predictions of a relatively good weldability presented in table 13.3. Note that the prediction of POM possessing a good weldability can be traced back to a relatively low molar volume ($V_m = 21.6\ cm^3/mol$) leading to a low χ-value.

One explanation for the inferior experimental weldability of POM might be due to a selected grade not intended for welding, which might be caused by a weak boundary layer. However, the selected grade was a pure resin with a PDI of only 2.1; thus, the WBL explanation seems unlikely. Additionally, the industrial chart also reports limited weldability of POM [laserplasticwelding.com, 2012].

Another explanation for the incorrect predictions could be problems determining the Hansen SP of POM. Although the sphere fit was acceptable with a correlation coefficient of 0.94, only 4 of 44 solvents could dissolve the POM. This might be due to inadequate submersion time in the solvents. The submersion time of POM was around 2 months, and 4-6 months would provide a more reliable estimate of the SP. Therefore, the model is highly dependent of the input of solubility parameters, which is discussed in section 13.3.1 on page 132.

13.3 Alternative Correlations

Typically, polymer weldability is predicted by differences in melting points, e.g., a melting point difference of less than 20 °C will result in weld compatibility. Using the welding strength data from Juhl et al. [2013], various plots are created to see if any correlation between weld strength and material properties exist. A simple linear correlation is used. The plots are presented in figures 13.4 to 13.9 and a data summary is presented in table 13.4.

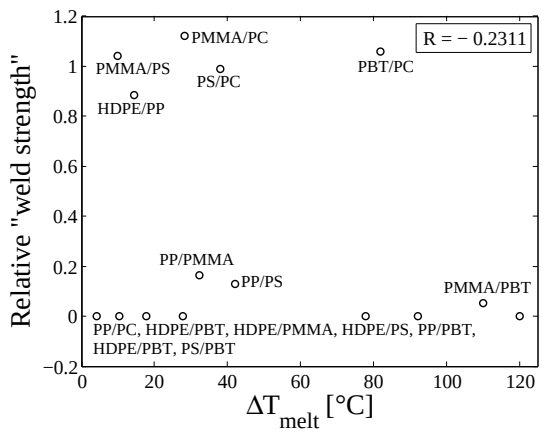

Figure 13.4: Weld strength versus difference in glass transition or melting temperature.

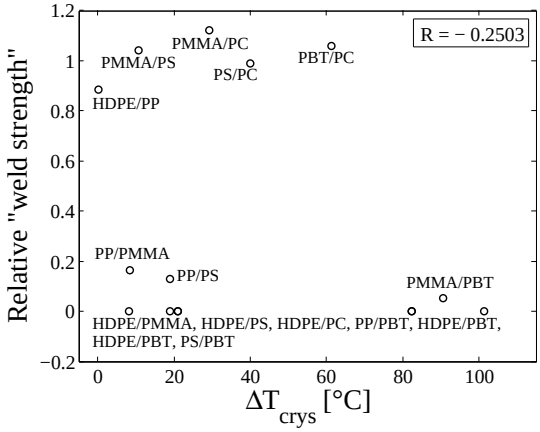

Figure 13.5: Weld strength versus difference in glass transition or crystallization temperature.

Figure	x-axis	R	Outliers	Weldable when?
13.4	ΔT_{melt}	-0.2311	5 of 5	N/A
13.5	ΔT_{crys}	-0.2503	4 of 5	< 8.2 °C
13.6	δ^2-part	-0.5381	2 of 5	< 9.8 MPa
13.7	w_∞	0.7553	2 of 5	> 11 Å
13.8	$w_\infty / R_{\text{g,e,max}}$	0.7146	2 of 5	> 0.42
13.9	$w_\infty / a_{\text{max}}$	0.7787	1 of 5	> 0.15

Table 13.4: Data summary of the plots presented in figures 13.4 to 13.9.

Common for the plots is the relative weld strength (y-axis). The relative weld strength is defined as the strongest of the dissimilar welds (A/B or B/A) relative to the weakest of the similar welds (A/A or B/B) as in correspondence with Juhl et al. [2013]. Five polymer pairs

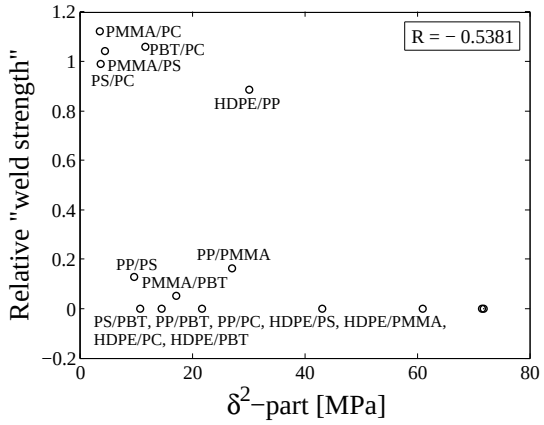

Figure 13.6: Weld strength versus the δ^2-part from equation 6.15 on page 64.

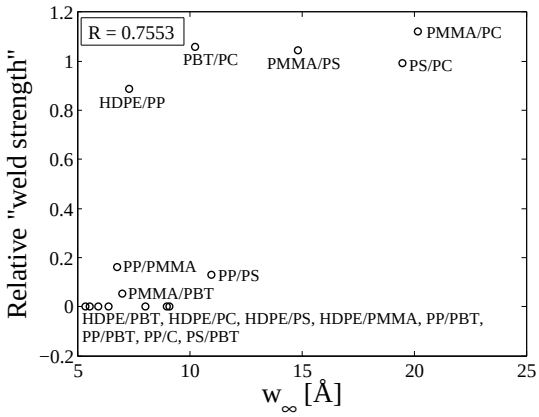

Figure 13.7: Weld strength versus the equilibrium inter-penetration depth from equation 6.22 on page 68.

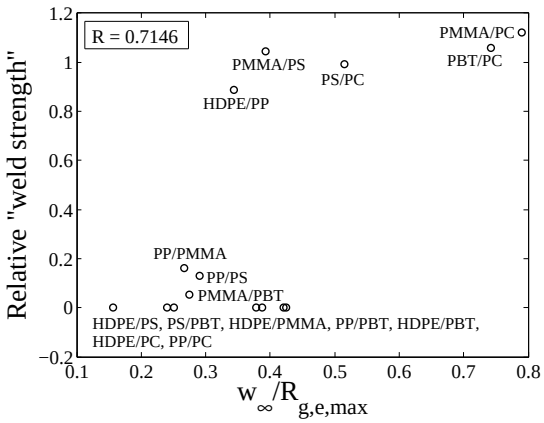

Figure 13.8: Weld strength versus the ratio w_∞ to the maximum radius of gyration of entangled segments.

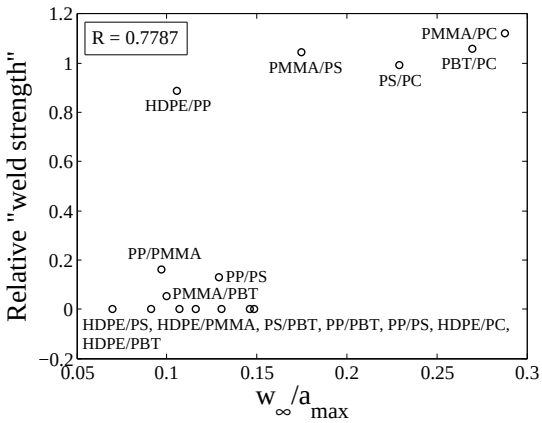

Figure 13.9: Weld strength versus the ratio w_∞ to the maximum tube diameter.

are considered weldable, namely HDPE/PP, PMMA/PS, PMMA/PC, PS/PC, and PBT/PC. The other 10 pairs are considered non-weldable. What in table 13.4 is referred to as “outliers” is the number of weldable polymer pairs not fulfilling the threshold set by the non-weldable polymer pairs with the lowest x-value for figures 13.4, 13.5, and 13.6; and largest x-value for figures 13.7, 13.8, and 13.9.

As seen in figures 13.4 and 13.5 the melting or crystallization point cannot predict the weldability of a polymer pair. One big error in the comparison of melting and crystallization points is that the semi-crystalline melting point, defined from the endothermic peak (T_{melt}), is compared with the amorphous glass transition (T_g); see section 9.3.5 on page 94. If only the glass transitions are compared and the melting points are compared, the correlation will only be constituted of three polymer pairs. However, it is a general trend that all amorphous polymer pair combinations (PMMA/PS, PMMA/PC, and PS/PC) are weldable.

Regarding the correlation plots from figures 13.6 to 13.9, only 1 to 2 outliers are present; thus, these values can all be utilized for weld strength predictions:

δ^2-part: A δ^2-part-value, i.e., $\left((\delta_{D1}-\delta_{D2})^2+\frac{1}{4}(\delta_{P1}-\delta_{P2})^2+\frac{1}{4}(\delta_{H1}-\delta_{H2})^2\right)$, less than 9.8 MPa will indicate weldability. For Hildebrand SP a rule of thumb suggests compatibility when $(\delta_1-\delta_2)^2<4$ MPa [Brydson, 1989]. Using Hildebrand SP, this model predicts weldability when $(\delta_1-\delta_2)^2<2.25$ MPa with 2 of 5 outliers.

w_∞: Instead of dividing the equilibrium inter-penetration depth (w_∞) with the maximum mesh size (a_{max}) as suggest in hypothesis 3 on page 86, w_∞ alone is capable of predicting weldability when w_∞ is larger than 1.1 nm.

$w_\infty/R_{g,e,max}$: The maximum radius of gyration of an entangled segment ($w_\infty/R_{g,e,max}$) is by Wool [1995] also used as a measure for the polymer melt mesh size. In general, $w_\infty/R_{g,e}$ is larger than the tube diameter (a), therefore $w_\infty/R_{g,e,max}$ is closer to w_∞ resulting in ratios around 1. However, the correlation to weld strength is worse than when only w_∞ is used as x-axis data.

w_∞/a_{max}: Offhand, this quantity constitutes the best correlation to the weld strength with only one outlier. This ratio is also exploited in the EXPAND program as described in section 13.1.

It is important to note that the correlation coefficients (R) in table 13.4 are from a linear regression analysis, which seems inconvenient, since weldability rather appears as a step-function. Therefore, one should be careful with concluding that the w_∞/a_{max} ratio constitutes the best model for predicting weld strength.

All things considered, this model seems superior to old rules of thumb. Instead of a vast amount of experiments as required to the establish weldability charts, this model relies on polymer physics data and is especially sensitive to the solubility parameter input.

13.3.1 Solubility Parameter Input

It turns out that the solubility parameter is the critical input parameter, and the model relies on the validity of these. In table 9.4 on page 97 four different estimates of solubility parameters are presented. In paper 3 [Juhl et al., 2013], the weld strength was correlated to w_∞/a_{max} based on theoretical Hildebrand SP from van Krevelen and te Nijenhuis [2009] and experimentally determined Hansen SP. These inputs work quite well and are also utilized in the EXPAND *Weldability*-module as presented in section 13.1.2. If other methods for estimating solubility parameters are used, other results will be obtained. These are summarized in table 13.5. The plots are not presented, but possess the same appearance as figures 13.4 to 13.9.

First of all, theoretical Hansen SP estimated from group contribution methods [Hinge et al., 2002] cannot predict weldability at all – note the correlation coefficient of 0.0407 and 4 of 5 outliers. Likewise, the Hansen SPs from Hansen [2000] result in 4 of 5 outliers. This might be due to data being determined by different research groups, meaning that different solvents and methods might have been used. Therefore, this method suggests a very systematic approach for determination of solubility parameters.

Solubility parameter	R	Outliers	Weldable when?
Hildebrand (theory) [a]	0.4211	2 of 5	$w_\infty/a_{\max} > 0.28$
Hansen (theory) [b]	0.0407	4 of 5	$w_\infty/a_{\max} > 0.48$
Hansen (experiment) [c]	0.4126	4 of 5	$w_\infty/a_{\max} > 0.32$
Hansen (experiment) [d]	0.7787	1 of 5	$w_\infty/a_{\max} > 0.15$

Table 13.5: Summary of weld strength versus $w_\infty/a_{\max}$ for the four different estimates of solubility parameters presented in table 9.4 on page 97. [a] refers to [van Krevelen and te Nijenhuis, 2009], [b] refers to [Hinge et al., 2002], [c] refers to [Hansen, 2000], [d] refers to [Juhl et al., 2013].

13.4 High Temperature or Long Melting Time?

During the project period, this question has without comparison been asked the most by external collaborators; *What is best; a high temperature for short time, or a low temperature for long time?* And unfortunately, the answer is not trivial. First of all, the temperature needs to be as high as possible without exceeding the decomposition temperature, thereby lowering the reptation time; see equation 5.31 on page 47. Likewise, the time in molten state should be as long as possible to ensure an optimum inter-diffusion; as in correspondence with equation 5.51 on page 52. The influence of time and temperature is best illustrated with an example from laser welding.

Example 13.1
Using the Rosenthal approximation from section 4.3.2 on page 35, laser welding with similar line energy will result in similar temperature development, assuming the high speed approximation. What have not been considered is the contour laser welding process compared to the quasi-simultaneous welding process, e.g., is it preferable to weld once (contour) with a line energy of 1 J/mm or weld five times with a line energy of 0.2; and what about the laser repetition interval?

To answer the question, four Rosenthal models similar to the simulations in figure 4.10 on page 38 are simulated. The Rosenthal model is found in the Matlab script `laserweld` and model inputs are presented in table 13.6. Fixed input parameters include: $P_{\text{laser}} = 100$ W, $y_{1/e} = 0.25$ mm, $z_{1/e} = 30$ µm, all data is in a distance of 0.65 mm from the laser spot center; just as in example 4.2 on page 37, although this example uses PS with $M_w = 192,000$ g/mol and not PP. Again as in example 4.2 on page 37, the models are not validated experimentally and therefore only highlight the trends of the temperature development.

In figures 13.10 to 13.13 the four simulations are presented, and the maximum temperature ($T_{\max}$) and the time above the glass transition temperature (T_{molten}) is presented in table 13.6. Note the discontinuity in the temperature development when the laser beam passes the origin. This is caused by the model singularity for small values of t, which is best seen in figure 13.10, where the temperature in the limit for t approaching zero gives 40 °C, which is 20 °C above the assumed room temperature. For faster weld speeds the singularity is less pronounced.

t_{molten} does only deviate from 6.06 s to 6.47 s, while T_{max} deviates from 166 °C to 224 °C. The reptation time at these temperatures are 0.0114 s and 8.09 s, respectively, which are both longer than t_{molten}. Therefore, it can be concluded that a quasi-simultaneous laser welding with a line energy of 0.2 J/mm with five repetitions of 1 s intervals is not sufficient for welding PS with a molecular weight of 192,000 g/mol.

On the other hand, if the intervals are only 0.5 s, $\tau_{rep,max}$ will decrease to 0.109 s, which is sufficient for welding; see figure 13.12. Therefore to answer the question, a rule of thumb is that high temperature is more important than time. This conclusion is based on the temperature sensitivity of τ_{rep}, e.g., for PS τ_{rep} roughly drops a decade when the temperature increases 20 °C. Also from an industrial engineering point of view, low cycle times are preferable.

Figure	**13.10**	**13.11**	**13.12**	**13.13**
v_{laser} [mm/s]	100	300	500	500
No. of repetitions	1	3	5	5
Δt [s]	N/A	1	1	0.5
t_{molten} [s]	6.06	6.25	6.47	6.28
T_{max} [°C]	224	193	166	196
$\tau_{rep,max}$ [s]	0.0114	0.158	8.09	0.109

Table 13.6: Summary of figures 13.10 to 13.13. Δt is the repetition interval for quasi-simultaneous welding, while t_{molten} refers to the time the weld seam temperature is above $T_{g,PS}$.

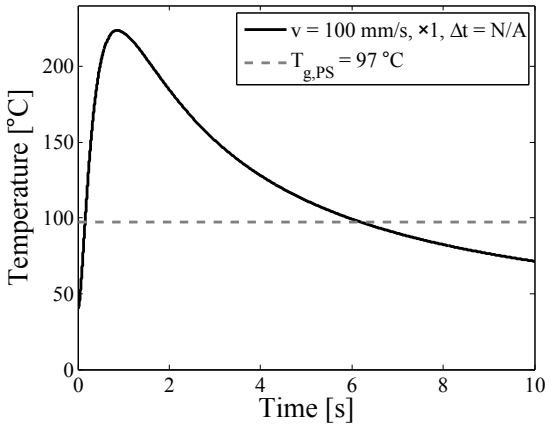

Figure 13.10: Temperature development in a regular contour laser welding process.

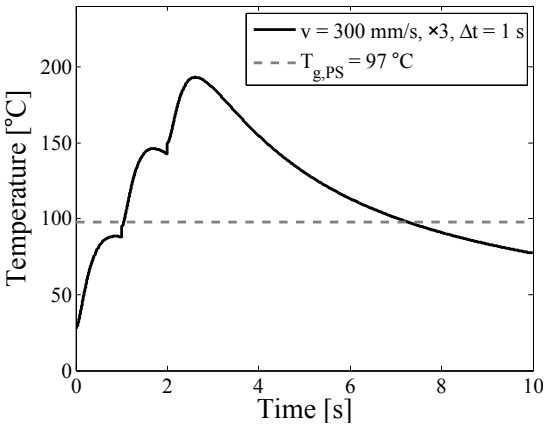

Figure 13.11: Temperature development in a quasi-simultaneous laser welding process with five repetitions and 1 second intervals.

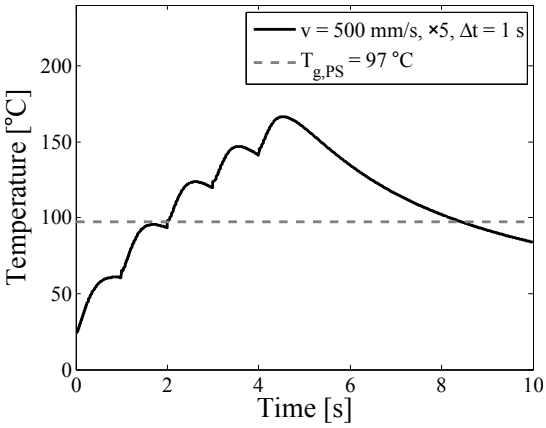

Figure 13.12: Temperature development in a quasi-simultaneous laser welding process with five repetitions and 1 second intervals.

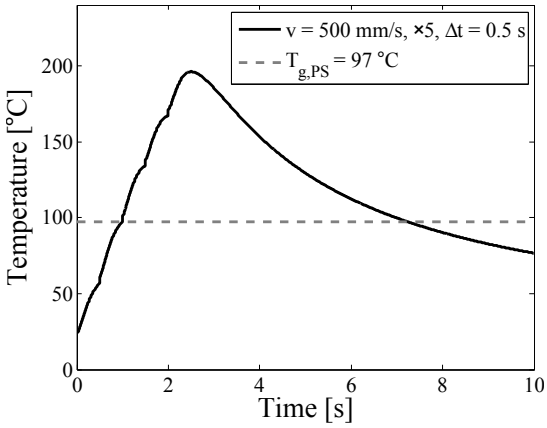

Figure 13.13: Temperature development in a quasi-simultaneous laser welding process with five repetitions and 0.5 second intervals.

As concluded in example 13.1, the reptation time decreases faster with increasing temperature than the molten time increases with increasing temperature. Therefore, high temperature is more important than long welding time. This conclusion does, however, not take other mechanisms responsible for weld strength development into account. Especially the neglection of crystallization is a problem for the consideration, since high quality crystals best occur at temperatures only slightly larger than the highest melting temperature of the two polymers [Godail and Packham, 2001]. This is of course not relevant for this example where amorphous PS is considered. Moreover, the time perspective of melting and wetting is neglected.

Eventually, the overall conclusion is that the polymer laser welding process is very complex and many parameters can be varied; see page 31. Example 13.1 was just a specific example with fixed process design, joint design, and materials; and it cannot be concluded that contour welding is better than quasi-simultaneous welding.

PART V

CONCLUDING REMARKS

CHAPTER 14

CONCLUSION

The initial problem stated: "What is decisive for strength development in polymer weld interfaces, and can this knowledge be exploited to expand the weldability of plastics?". In the following, the project is concluded with the initial problem in mind.

Essentially, based on a literature survey, five different mechanisms were identified for weld strength development. These are *melting*, *wetting*, *compatibility*, *diffusion and entanglements*, and *(co-)crystallization*. Each mechanism is necessary for the next step to occur, e.g., polymer-polymer *compatibility* is essential for subsequent *diffusion and entanglement* formation. The time horizon for each mechanism was estimated for *melting*, *wetting*, and *diffusion* to be fractions of a second at relatively high temperatures. Lowering the melt temperature 10-50 °C would increase the reptation time one decade of magnitude. Therefore, as a rule of thumb, higher temperature is more significant than long welding time.

Moreover, polymer weldability might be dramatically deteriorated when incorporating additives or other substances with low molecular weight into the polymer matrix. The low molecular weight fractions will migrate towards the surface due to the minimizing of the surface energy. The surface is then dominated by relatively short molecules eliminating entanglement establishment. This also promotes the selection of polymers with a relatively narrow molecular weight distribution, e.g., metallocene catalyzed polymers.

Three hypotheses were formed constituting the basis of the three papers presented in chapters 10, 11, and 12, respectively:

1. The first hypothesis is concerned with the estimation of reptation time (τ_{rep}) based on polymer rheology and physical models.

   A simple method to estimate the reptation time (τ_{rep}) of a polymer melt at a given temperature and molecular weight was suggested. The method was based on Doi and Edward's tube model and coupled the reptation time to zero shear viscosity (η_0). For instance, the reptation time for mHDPE of 128,000 g/mol at 190 °C was estimated to 0.9 ms, i.e., much shorter than the usual reported time in molten state during the welding process. Therefore, reptation dynamics were not the limiting mechanism when welding HDPE. Short τ_{rep} was also reported for PP and POM. Furthermore, laser weldability between HDPE and PP, both metallocene catalyzed, with 89 % of the strength of a HDPE/HDPE weld was achieved [Juhl et al., 2013a].

2. The second hypothesis departed from the different fracture mechanisms in polymer weld lines, and how these influence the final mechanical strength and toughness.

Opposite to HDPE, PP, and POM, the reptation time and temperature of PS seemed to be an issue when welding with lasers. For instance, t_{rep} of PS (M_w = 300,000 g/mol and T = 190 °C) was estimated to 0.8 s, which was comparable to t_{molten}. Therefore, laser welding of PS turned out to be very sensitive to temperature; in this case equivalent to laser weld speed (v_{laser}). This was investigated using two methods of mechanical testing; a simple lap-shear test and double cantilever beam (DCB) test. Using the lap-shear test, the mechanical strength was reported constant (21 J/m^2) with laser line energy (E_{line}); while the DCB method displayed a $\cap$-function with E_{line}. This was explained with the DCB method taking the time dependent chain pull-outs into account. The DCB method also proved promising for mechanical evaluation of relatively brittle and dissimilar polymer pairs [Juhl et al., 2013b].

3. The third hypothesis stated that the ratio between the equilibrium inter-penetration depth and the maximum tube diameter of two welded polymers (w_∞ / a_{max}) will imply weldability between dissimilar polymers.

   In short, the ratio w_∞ / a_{max} of a welded polymer pair correlated with the relative lap-shear mechanical strength. Using Hildebrand solubility parameters to determine w_∞, weldability existed when $w_\infty / a_{max} > 0.28$; and when utilizing experimental Hansen SP for the estimation, weldability existed when $w_\infty / a_{max} > 0.15$. The model using experimentally determined Hansen solubility parameters provided optimum results with only one outlier – the HDPE/PP combination, which was due to problems determining the Hansen SP of HDPE. Weldability predictions from the w_∞ / a_{max}-ratio were far more superior to older rules of thumb, e.g., difference in melting or crystallization point. The results also implied that full-developed strength is already achieved when the polymers have inter-diffused a scale of radius of gyration of an entangled segment ($R_{g,e}$) and not a scale of R_g as suggested by Wool [1995] [Juhl et al., 2013].

Finally, the attained knowledge was used to develop a computer program for predicting weldability of plastics. The program is named EXPAND and is attached on the enclosed CD. All things considered, the knowledge of polymer welding and especially polymer laser welding is now expanded, i.e., it is now possible to predict the weldability of two polymers based on the chemical and physical properties instead of the current trial-and-error approach.

CHAPTER 15

PERSPECTIVES

As mentioned in the introduction to this thesis: "Polymer interfaces and polymer welds are ubiquitous". This means that the findings of this work is not limited to laser welding of plastics, but can also be harnessed in the understanding and improvement of injection molding, self-healing materials, 3D printing, etc.

As depicted from the conclusion in the previous chapter, this three-year project concludes primarily on strength establishment and material compatibility in relation to polymer welding. The considerations and findings are not only interesting from a scientific point of view, but also from an industrial and technological viewpoint. In the following sections the project perspectives are evaluated with regard to academia/science and industry/technology.

Furthermore, this thesis has only covered a fraction of all challenges within the subject of understanding polymer welding. Suggestions for future work are therefore also presented.

15.1 Scientific Perspectives

The topic of understanding weldability of plastic is a broad interdisciplinary science, among others including theoretical physics, chemical engineering, mechanical engineering, and materials science. Therefore, the future path within this field of research will be to link these sciences even further together. Plausibly not all of them at once, but if two could be coupled and investigated, many small steps might provide a better overall understanding of polymer welding. The main contribution from this thesis is the coupling between physical and chemical properties and mechanical strength; and in general a better understanding of polymer weldability.

Concrete topics, interesting from a scientific point of view, include the influence of influx formations, see figure 6.1 on page 58. Also a better understanding of the influence of the interfacial crystal morphology on mechanical strength is needed. This might be investigated by understanding the weldability between amorphous and semi-crystalline polymers, e.g., PC and PBT, which have been proven fully weldable. The variation in interfacial crystallinity can be accomplished by altering the laser welding input mode, e.g., contour or quasi-simultaneous welding. Also the effect of deformation speed for mechanical testing needs to be further investigated.

As more data on weldability and material properties of more polymers enter the database, a better picture of weldability is obtainable. Therefore, instead of a step function predicting weldability for $w_\infty / a_{\max}$ larger than a certain threshold, the weldability function

might instead prove to be an S-curve when more details in the boundary between weldable and non-weldable materials are provided. Moreover, a better measure for solubility is preferable – the theoretical Hildebrand SP and the experimental Hansen SP might be improved to give a better prediction of the interaction parameter.

For the research hot topic of nanomaterials and self-healing materials, the findings are also of interest. The understanding of self-healing polymers might be explained by self-reptation near or slightly below the polymer glass transition temperature [Boiko et al., 2004; Zhang and Rong, 2012].

15.2 Technological Perspectives

Besides from the scientific outcome, this project also involves technological findings and progression, which may be harnessed in an industrial context. First of all, the understanding of strength development in polymer weld interfaces may ease the material selection process for design and manufacturing engineers. It might also boost the creativity for combining materials which typically never are welded together. Likewise, when developing new materials, solubility parameters may be tailored to fulfill the requirements for weldability to a specific material.

In general from a material science point of view, the knowledge regarding wetting, welding, and strength establishment might be utilized to improve the adhesion of regular thermosetting composites. Also within the area of polymer nanocomposites the knowledge of entanglements might generate new ideas for improving strength and other relevant material properties. Add to this that the research and development within polymer-polymer blends might be able to benefit from the findings.

Regarding the spin-off software, the perspectives are promising – even on short terms. By now, the program includes seven polymers which is only a fraction of all polymer materials. However, the seven selected polymers (HDPE, PP, PMMA, PS, POM, PBT, PC) cover a vast majority of the world marked. Furthermore, the program database is easy to expand with new materials, which again should be validated, as seen in section 13.2 on page 129. It is still important that the model is validated by experiments, as known from computational solid mechanics, CFD, and molecular dynamics.

BIBLIOGRAPHY

Abed, S., P. Laurens, C. Carretero, J. Deschamps, and C. Duval (2003). Diode laser welding of polypropylene: Investigations of the microstructures in the welded seam. In I. Miyamoto, K. Kobayashi, K. Sugioka, R. Poprawe, and H. Helvajian (Eds.), *First international symposium on high-power laser macro-processing*, Volume 4831 of *Proceedings of the society of photo-optical instrumentation engineers (SPIE)*, pp. 77–81.

Acherjee, B., A. S. Kuar, S. Mitra, and D. Misra (2012a). Effect of carbon black on temperature field and weld profile during laser transmission welding of polymers: A FEM study. *Optics and Laser Technology 44*(3), 514–521.

Acherjee, B., A. S. Kuar, S. Mitra, and D. Misra (2012b). Modeling of laser transmission contour welding process using FEA and DoE. *Optics and Laser Technology 44*(5), 1281–1289.

Agrawal, G., R. Wool, W. Dozier, G. Felcher, J. Zhou, S. Pispas, J. Mays, and T. Russell (1996). Interdiffusion of polymers across interfaces. *Journal of Polymer Science Part B – Polymer Physics 34*(17), 2919–2940.

Akcasu, A. Z., G. Naegele, and R. Klein (1995). Remarks on the "fast" and "slow" mode theories of interdiffusion. *Macromolecules 28*(19), 6680–6683.

Ashby, M. F. and D. R. H. Jones (2012). *Engineering Materials 1 – An Introduction to Properties, Application, and Design*. Butterworth-Heinemann.

Bachmann, F. and U. Russek (2003). Laser welding of polymers using high power diode lasers. In F. Dausinger, V. Konov, V. Baranov, and V. Panchenko (Eds.), *Laser processing of advanced materials and laser microtechnologies*, Volume 5121 of *Proceeding of the society of photo-optical intrumentation engineers (SPIE)*, pp. 385–398.

bedreinnovation.dk (2013). Metal-plast svejsning. http://2012.bedreinnovation.dk/aktivitet/metal-plast-svejsning.

Beyler, C. L. and M. M. Hirschler (2002). *Thermal Decomposition of Polymers*, Chapter 7. National Fire Protection Association.

Bikerman, J. J. (1968). *The Science of Adhesive Joints* (2nd ed.). Academic Press.

Binder, K. (1983). Collective diffusion, nucleation, and spinodal decomposition in polymer mixtures. *Journal of Chemical Physics 79*(12), 6387–6409.

blueprinter.dk (2013). Affordable 3d printer with new selective heat sintering technology. http://www.blueprinter.dk/shs.html.

Boiko, Y. M., A. Bach, and J. Lyngaae-Jørgensen (2004). Self-bonding in an amorphous polymer below the glass transition: A T-peel test investigation. *Journal of Polymer Science Part B-Polymer Physics 42*(10), 1861–1867.

Bousmina, M., H. Qiu, M. Grmela, and J. Klemberg-Sapieha (1998). Diffusion at polymer/polymer interfaces probed by rheological tools. *Macromolecules 31*(23), 8273–8280.

Bower, D. I. (2002). *An Introduction to Polymer Physics*. Cambridge.

Branson (2008). *Polymers: Characteristics and Compatibility for Ultrasonic Assembly*. Branson Ultrasonics Corporation. http://www.branson-plasticsjoin.com/pdf/PW-01CharComp.pdf.

Brochard, F., J. Jouffroy, and P. Levinson (1983). Mutual diffusion of short polymer-chains among long chains. *Journal de Physique Letters 44*(12), 455–460.

Brydson, J. A. (1989).

Casco Nobel (1992). *Limhåndbogen*. Casco Nobel A/S.

Chaffin, K. A., J. S. Knutsen, P. Brant, and F. S. Bates (2000). High-strength welds in metallocene polypropylene/polyethylene laminates. *Science 288*(5474), 2187–2190.

Chernyy, S., B. Jensen, K. Shimizu, M. Ceccato, S. Pedersen, A. Zelikin, K. Daasbjerg, and J. Iruthayaraj (2013). Surface grafted glycopolymer brushes to enhance selective adhesion of hepg2 cells. *Journal of Colloid and Interface Science*.

Chien, R., S. Chen, H. Peng, P. Su, and C. Chen (2004). Investigations on the weldline tensile strength of thin-wall injection molded parts. *Journal of Reinforced Plastics and Composites 23*(6), 575–588.

Cho, K., D. Kim, and S. Yoon (2003). Effect of substrate surface energy on transcrystalline growth and its effect on interfacial adhesion of semicrystalline polymers. *Macromolecules 36*(20), 7652–7660.

Coccorullo, I., R. Pantani, and G. Titomanlio (2003). Crystallization kinetics and solidified structure in iPP under high cooling rates. *Polymer 44*(1), 307–318.

Cole, P., R. Cook, and C. Macosko (2003). Adhesion between immiscible polymers correlated with interfacial entanglements. *Macromolecules 36*(8), 2808–2815.

Cowie, J. M. G. and V. Arrighi (2008). *Polymers: Chemistry and Physics of Modern Materials* (3rd ed.). CRC Press.

Creton, C., E. J. Kramer, C. Y. Hui, and H. R. Brown (1992). Failure mechanisms of polymer interfaces reinforced with block copolymers. *Macromolecules 25*(12), 3075–3088.

de Gennes, P. G. (1971). Reptation of a polymer chain in the presence of fixed obstacles. *Journal of Chemical Physics 55*(2), 572–579.

Dealy, J. M. and R. G. Larson (2006). *Structure and Rheology of Molten Polymers – From Structure to Flow Behavior and Back Again*. Hanser.

Debondue, E., J. E. Fournier, M. F. Lacrampe, and P. Krawczak (2004). Weld-line sensitivity of injected amorphous polymers. *Journal of Applied Polymer Science 93*(2), 644–650.

Doi, M. (1996). *Introduction to Polymer Physics*. Oxford: Clarendon Press.

Doi, M. and S. F. Edwards (1986). *The Theory of Polymer Dynamics*. Oxford University Press.

dsm.com (2011). New advances in polymer laser welding. http://www.dsm.com/nl_NL/downloads/dep/laser_welding_handbook.pdf.

Fetters, L. J., D. J. Lohse, and R. H. Colby (2007). *Chain Dimensions and Entanglement Spacings*, Chapter 25. Springer New York.

Fetters, L. J., D. J. Lohse, D. Richter, T. A. Witten, and A. Zirkel (1994). Connection between polymer molecular weight, density, chain dimensions, and melt viscoelastic properties. *Macromolecules 27*(17), 4639–4647.

Fink, I. L. (2001). *Varmekontaktsvejsning af folie og sprøjtestøbt emne*. Ph. D. thesis, Technical University of Denmark.

Flory, P. J. (1942). Thermodynamics of high polymer solutions. *Journal of Chemical Physics 10*(51), 51–61.

Ge, T., F. Pierce, D. Perahia, G. S. Grest, and M. O. Robbins (2013). Molecular dynamics simulations of polymer welding: Strength from interfacial entanglements. *Physical Review Letters 110*, 098301.

Ghorbel, E., G. Casalino, and S. Abed (2009). Laser diode transmission welding of polypropylene: Geometrical and microstructure characterisation of weld. *Materials & Design 30*(7), 2745–2751.

Godail, L. and D. Packham (2001). Adhesion of ethylene-octene copolymers to polypropylene: Interfacial structure and mechanical properties. *Journal of Adhesion Science and Technology 15*(11), 1285–1304.

Gorga, R. and B. Narasimhan (2004). Fracture behavior at partially miscible polymer interfaces. *Polymer Engineering and Science 44*(5), 929–939.

Graessley, W. (1980). Some phenomenological consequences of the Doi-Edwards theory of viscoelasticity. *Journal of Polymer Science Part B: Polymer Physics 18*(1), 27–34.

Graham, R. S. (2002). *Molecular modelling of entangled polymer fluids under flow*. Ph. D. thesis, University of Leeds.

Grewell, D., T. Jerew, and A. Benatar (2003). Diode Laser Microwelding of Polycarbonate and Polystyrene. pp. 1039–1044.

Grewell, D. A., A. Benatar, and J. B. Park (Eds.) (2003). *Plastics and Composites Welding Handbook*. Hanser.

Griffith, A. A. (1920). The phenomena of rupture and flow in solids. *Philospical Transactions of the Royal Society of London A221*, 163.

Guvendiren, M., R. L. McSwain, T. E. Mates, and K. R. Shull (2010). Welding kinetics in a miscible blend of high-T_g and low-T_g polymers. *Macromolecules 43*(7), 3392–3398.

Hadriche, I., E. Ghorbel, N. Masmoudi, and G. Casalino (2010). Investigation on the effects of laser power and scanning speed on polypropylene diode transmission welds. *International Journal of Advanced Manufacturing Technology 50*(1-4), 217–226.

Haire, K. and A. Windle (2001). Monte carlo simulation of polymer welding. *Computational and Theoretical Polymer Science 11*(3), 227–240.

Halary, J. L., F. Lauprêtre, and L. Monnerie (Eds.) (2011). *Polymer Materials – Macroscopic Properties and Molecular Interpretations* (1st ed.). John Wiley & Sons.

Hansen, C. (2013). Hansen solubility parameters – hspip v. 4.0.03. http://www.hansen-solubility.com/.

Hansen, C. M. (2000). *Hansen Solubility Parameters – a User's Handbook* (2nd ed.). CRC Press.

Hansen, C. M. and L. Just (2001). Prediction of environmental stress cracking in plastics with hansen solubility parameters. *Industrial & Engineering Chemistry Research 40*(1), 21–25.

Helfand, E. and A. M. Sapse (1975). Theory of unsymmetric polymer-polymer interfaces. *Journal of Chemical Physics 62*(4), 1327–1331.

Hiemenz, P. and T. Lodge (2007). *Polymer Chemistry* (2nd ed.). CRC Press.

Hinge, M., M. H. Alm, A.-S. Ravn, and A. N. Thraner (2002). Characteristics of a polymer-polymer interface. Eighth semester project, Aalborg University.

Hopmann, C. and M. Weber (2013). Joining of dissimilar materials. *Kunststoffe International 3*, 17–21.

Horiuchi, S., A. Nakagawa, Y. Liao, and T. Ougizawa (2008). Interfacial entanglements between glassy polymers investigated by nanofractography with high-resolution scanning electron microscopy. *Macromolecules 41*(21), 8063–8071.

Ilie, M., J.-C. Kneip, S. Mattei, A. Nichici, C. Roze, and T. Girasole (2007). Through-transmission laser welding of polymers – temperature field modeling and infrared investigation. *Infrared Physics & Technology 51*(1), 73–79.

industrial lasers.com (2012). Laser based polymer welding in medical device manufacturing. http://www.industrial-lasers.com/articles/2010/07/laser-based-polymer.html.

Jablonski, E.L., G. R. N. B. (2003). Interdiffusion and phase behavior at homopolymer/random copolymer interfaces. *Polymer 44*(3), 729–741.

Jaeschke, P., D. Herzog, H. Haferkamp, C. Peters, and A. S. Herrmann (2010). Laser transmission welding of high-performance polymers and reinforced composites - a fundamental study. *Journal of Reinforced Plastics and Composites 29*(20), 3083–3094.

Jeon, H., J. Lee, and N. Balsara (1998). Predictions of the thermodynamic properties of multicomponent polyolefin blends from measurements on two-component systems. *Macromolecules 31*(10), 3328–3339.

Jiang, G., H. Wu, B. Yan, S. Guo, and J. Huang (2009). Reinforcement of Solid-Melt Interfaces for Semicrystalline Polymers in a Sequential Two-Staged Injection Molding Process. *Journal of Polymer Science Part B – Polymer Physics 47*(11), 1112–1124.

Jones, R. A. L. and R. W. Richards (1999). *Polymers at Surfaces and Interfaces*. Cambridge University Press.

Jud, K., H. H. Kausch, and J. C. Williams (1981). Fracture mechanics studies of crack healing and welding of polymers. *Journal of Materials Science 16*, 204–210.

Juhl, T. B. (2013). Forståelse og forbedring af lasersvejsning af plast. *Plast Panorama* (6), 14–15. http://techmedia.swiflet.com/tm/pla/76/14/.

Juhl, T. B., D. Bach, R. G. Larson, J. d. Christiansen, and E. A. Jensen (2013). Predicting the laser weldability of dissimilar polymers. *Polymer 54*(15), 3891–3897.

Juhl, T. B., J. d. Christiansen, and E. A. Jensen (2013a). Investigation on high strength laser welds of polypropylene and high-density polyethylene. *Journal of Applied Polymer Science 129*(5), 2679–2685.

Juhl, T. B., J. d. Christiansen, and E. A. Jensen (2013b). Mechanical testing of polystyrene/polystyrene laser welds. *Polymer Testing 32*(3), 475–481.

Karim, A., G. P. Felcher, and T. P. Russell (1994). Interdiffusion of polymers at short times. *Macromolecules 27*(23), 6973–6979.

Kausch, H. H. and M. Tirrell (1989). Polymer interdiffusion. *Annual Review of Materials Science 17*(19), 341–377.

Kawaguchi, D., A. Nelson, Y. Masubuchi, J. P. Majewski, N. Torikai, N. L. Yamada, A. R. Siti Sarah, A. Takano, and Y. Matsushita (2011). Precise analyses of short-time relaxation at asymmetric polystyrene interface in terms of molecular weight by time-resolved neutron reflectivity measurements. *Macromolecules 44*(23), 9424–9433.

Klein, J. (1990). The interdiffusion of polymers. *Science 250*(4981), 640–646.

Klein, R. (2011). *Laser Welding of Plastics*. Weinheim: Wiley.

Klæstrup, J. (2011). Welding of plastics – analytical mathematical solutions. Lecture notes from a consortium meeting.

Lamnawar, K. and A. Maazouz (2006). Rheological study of multilayer functionalized polymers: characterization of interdiffusion and reaction at polymer/polymer interface. *Rheologica Acta 45*(4), 411–424.

Larson, R. G. (2007). Looking inside the entanglement "tube" using molecular dynamics simulations. *Journal of Polymer Science: Part B: Polymer Physics 45*, 3240–3248.

Larson, R. G. (2012). Discussion on polymer physics.

Larson, R. G., T. Sridhar, L. G. Leal, G. H. McKinley, A. E. Likhtman, and T. C. B. McLeish (2003). Definitions of entanglement spacing and time constants in the tube model. *Journal of Rheology 47*(2), 809–818.

laserplasticwelding.com (2012). Material compatibility chart. http://www.laserplasticwelding.com/material-compatibility-chart.

laserplasticwelding.com (2013). Laser plastic welding.
http://www.laserplasticwelding.com/.

Lee, P. C., H. E. Park, D. C. Morse, and C. W. Macosko (2009). Polymer-polymer interfacial slip in multilayered films. *Journal of Rheology 53*(4), 893–915.

Likhtmann, A. (2011). Viscoelasticity and molecular rheology. Notes from the Dynacop summer school in Capri.

LinkedIn.com (2013). Laser plastic welding – cross-linking at polymer interfaces as explanation for mechanical strength. http://tinyurl.com/d3jw5o5.

Lo, C., F. Laabs, and B. Narasimhan (2004). Interfacial adhesion mechanisms in incompatible semicrystalline polymer systems. *Journal of Polymer Science Part B: Polymer Physics 42*(14), 2667–2679.

Lo, C. T. and B. Narasimhan (2005). A new kinetic model for interdiffusion at semicrystalline polymer interfaces. *Polymer 46*(7), 2266–2275.

Lo, C. T., S. Seifert, P. Thiyagarajan, and B. Narasimhan (2004). Phase behavior of semicrystalline polymer blends. *Polymer 45*, 3671–3679.

lpkf.com (2012). Laser plastic welding – innovative joining technology for the electronics industry.
http://www.lpkf.com/newsletter/rapid-pcb-prototyping/2009/december/203.htm.

lpkfusa.com (2012). Laser plastic welding – design guidelines manual.
http://www.lpkfusa.com/lq/articles.htm.

Majeste, J., J. Montfort, A. Allal, and G. Marin (1998). Viscoelasticity of low molecular weight polymers and the transition to the entangled regime. *Rheologica Acta 37*(5), 486–499.

Mark, J. E. (Ed.) (2007). *Physical Properties of Polymers Handbook* (2nd ed.). Springer.

Marshall, G., L. Coutts, and J. Williams (1974). Temperature effect in fracture of pmma. *Journal of Materials Science 9*(9), 1409–1419.

Matsuo, Y., K. Tahara, and Y. Sugie (1997). Structure and thermal properties of poly(ethylene oxide)-intercalated graphite oxide. *Carbon 35*(1), 113–120.

Mayboudi, L. S., A. M. Birk, G. Zak, and P. J. Bates (2010). Finite volume model for laser-soot interaction for a laser transmission welding process. *Journal of Laser Applications 22*(1), 22–28.

Mortensen, K. (2009). Small Angle Neutron Scattering (SANS). Notes for Graduate Course in Polymer Physics and Course in Neutron Scattering.

Mubarak, Y., E. Harkin-Jones, P. Martin, and M. Ahmad (2001). Modeling of non-isothermal crystallization kinetics of isotactic polypropylene. *Polymer 42*(7), 3171–3182.

Mueller, C., G. Capaccio, A. Hiltner, and E. Baer (1998). Heat sealing of LLDPE: Relationships to melting and interdiffusion. *Journal of Applied Polymer Science 70*(10), 2021–2030.

nobelprize.org (2011). The nobel prize in physics 1991. http://nobelprize.org/nobel_prizes/physics/laureates/1991/index.html.

novonordisk.com (2013). Simple screw-on needle with automatic safety shield feature. http://www.novonordisk.com/diabetes/public/needles/novofine_autocover/novofineautocover-default.asp.

Oh, S. Y. and Y. C. Bae (2010). Molecular thermodynamics approach for polymer-polymer miscibility. *European Polymer Journal 46*(6), 1328–1333.

Osswald, T. A. and G. Menges (2003). *Materials Science of Polymers for Engineers* (2nd ed.). Carl Hanser Verlag.

Packham, D. E. (Ed.) (2005). *Handbook of Adhesion* (2nd ed.). John Wiley & Sons.

Paul, D. R. and L. M. Robeson (2008). Polymer nanotechnology: Nanocomposites – a review. *Elsevier Vol. 49*, p. 3187–3204.

Pecorini, T. and K. Seo (1996). Predicting weld strength in amorphous polymers. *Plastics Engineering 52*(6).

Pethrick, R. A. (2010). *Polymer Science and Technology for Engineers and Scientists*. Whittles Publishing.

Pierce, F., D. Parahia, and G. S. Grest (2011). Dynamics of polymers across an interface. *A Letters Journal Exploring the Frontiers of Physics 95*, 1–5.

Pizzi, A. and K. L. Mittal (Eds.) (2003). *Handbook of Adhesive Technology* (2nd ed.). Marcel Dekker.

plasticsengineering.org (2011). Polymer degradation during contour laser transmission welding. http://www.plasticsengineering.org/industries/node/4836.

Pocius, A. V. (2002). *Adhesion and Adhesives Technology*. Hanser Verlag.

Podlech, M. K. A. (2007). *Development of a Novel PE/PET Composite Materials using Functionalized PE*. Ph. D. thesis, Aalborg University.

polymerwelding.com (2013). New insights of polymer welding processes. http://polymerwelding.com/.

Qiu, H. and M. Bousmina (1999). New technique allowing the quantification of diffusion at polymer polymer interfaces using rheological analysis: Theoretical and experimental results. *Journal of Rheology 43*(3), 551–568.

Rastogi, S., L. Kurelec, and P. Lemstra (1998). Chain mobility in polymer systems: On the borderline between solid and melt. 2. crystal size influence in phase transition and sintering of ultrahigh molecular weight polyethylene via the mobile hexagonal phase. *Macromolecules 31*(15), 5022–5031.

Rastogi, S., D. Lippits, G. Peters, R. Graf, Y. Yao, and H. Spiess (2006). Heterogeneity in polymer melts from melting of polymer crystals. *Nature Materials 5*(6), 507.

Razavi-Nouri, M. (2007). Properties of polypropylene and metallocene-prepared polyethylene blends: Crystallization behavior and interaction parameter. *Polymer Testing 26*(1), 108–115.

reptate.com (2013). Rheology of entangled polymers: Toolkit for analysis of theory & experiment. http://reptate.com/.

Rotheiser, J. (2009). *Joining of Plastics – Handbook for Designers and Engineers* (3rd ed.). Hanser.

Rouse, P. E. (1953). A theory of the linear viscoelastic properties of dilute solutions of coiling polymers. *Journal of Chemical Physics 21*(7), 1272–1280.

Schnell, R., M. Stamm, and C. Creton (1998). Direct correlation between interfacial width and adhesion in glassy polymers. *Macromolecules 31*(7), 2284–2292.

Schnell, R., M. Stamm, and C. Creton (1999). Mechanical properties of homopolymer interfaces: Transition from simple pullout to crazing with increasing interfacial width. *Macromolecules 32*(10), 3420–3425.

Shanks, R. A., J. Li, and L. Yu (2000). Polypropylene-polyethylene blend morphology controlled by time-temperature-miscibility. *Polymer 41*(6), 2133–2139.

Snijkers, F. and D. Vlassopoulos (2011). Cone-partitioned-plate geometry for the ares rheometer with temperature control. *Journal of Rheology 55*(6), 1167–1186.

Stamm, M. and D. Schubert (1995). Interfaces between incompatible polymers. *Annual Review of Materials Science 25*, 325–356.

Swallowe, G. M. (Ed.) (1999). *Mechanical Properties and Testing*. Kluwer Acedemic Publishers.

Van de Ven, J. D. (2006). *Laser transmission welding of thermoplastics*. Ph. D. thesis, University of Minnesota.

van Krevelen, D. W. and K. te Nijenhuis (2009). *Properties of Polymers* (4th ed.). Elsevier.

van Meerveld, J. (2004). A method to extract the monomer friction coefficient from the linear viscoelastic behavior of linear, entangled polymer melts. *Rheologica Acta 43*(6), 615–623.

Vega, J. F., S. Rastogi, G. W. M. Peters, and H. E. H. Meijer (2004). Rheology and reptation of linear polymers. Ultrahigh molecular weight chain dynamics in the melt. *Journal of Rheology 46*(3), 663–678.

Vingaard, M. (2009). *Surfaces of Injection Moulded Amorhpous Polymers*. Ph. D. thesis, Aalborg University.

von Bulow, J. F., K. Bager, and C. Thirstrup (2009). Utilization of light scattering in transmission laser welding of medical devices. *Applied Surface Science 256*(3), 900–908.

wiley.com (2011). *Properties and Behavior of Polymers – Two-volume Set*. John Wiley & Sons. http://onlinelibrary.wiley.com/book/10.1002/0471440264.

Willett, J. and R. Wool (1993). Strength of incompatible amorphous polymer interfaces. *Macromolecules 26*(20), 5336–5349.

Wool, R. (2006). Adhesion at polymer-polymer interfaces: a rigidity percolation approach. *Comptes Rendus Chimie 9*(1), 25–44.

Wool, R. P. (1995). *Polymer Interfaces – Structure and Strength*. Munich: Hanser Publishers.

Wool, R. P. (2001). A material fix. *Nature 409*(6822), 773–774.

Wool, R. P. (2005). *Fundamentals of Fracture in Bio-Based Polymers*, Chapter 6.

Wool, R. P. (2008). Self-healing materials: A review. *Soft Matter 4*(3), 400–418.

Wu, J. and Y. Mai (1996). The essential fracture work concept for toughness measurement of ductile polymers. *Polymer Engineering and Science 36*(18), 2275–2288.

Wu, S. (2001). *Polymer Interface and Adhesion*. Marcel Dekker.

Xue, Y.-Q., T. A. Tervoort, and P. J. Lemstra (1998). Welding behavior of semicrystalline polymers. 1: The effect of nonequilibrium chain conformations on autohesion of UHMWPE. *Polymer Engineering and Science 31*, 3075–3080.

Yang, L., T. Suo, Y. Niu, Z. Wang, D. Yan, and H. Wang (2010). Effects of phase behavior on mutual diffusion at polymer layers interface. *Polymer 51*(22), 5276 – 5281.

Yokomizo, K., Y. Banno, T. Yoshikawa, and M. Kotaki (2013). Effect of molecular weight and molecular weight distribution on weld-line interface in injection-molded polypropylene. *Polymer Engineering & Science*.

Zhang, C.-h., R.-f. Chen, F. Chen, Y.-g. Shangguan, Q. Zheng, and G.-h. Hu (2011). Study on high weld strength of impact propylene copolymer/high density polyethylene laminates. *Chinese Journal of Polymer Science 29*, 497–505.

Zhang, G., J. Qiu, L. Shao, and X. Fu (2011). Molecular interdiffusion of hauling theory between dissimilar polymers based on novel USW. In Wang, CH and Ma, LX and Yang, W (Ed.), *Advanced Polymer Science and Engineering*, Volume 221 of *Advanced Materials Research*, pp. 289–294.

Zhang, H., K. Lamnawar, and A. Maazouz (2012a). Rheological modeling of the diffusion process and the interphase of symmetrical bilayers based on PVDF and PMMA with varying molecular weights. *Rheologica Acta 51*(8), 1–21.

Zhang, H., K. Lamnawar, and A. Maazouz (2012b). Rheological modeling of the mutual diffusion and the interphase development for an asymmetrical bilayer based on PMMA and PVDF model compatible polymers. *Macromolecules 46*(1), 276–299.

Zhang, H. and R. Wool (1989). Concentration profile for a polymer – polymer interface 1. identical chemical composition and molecular weight. *Macromolecules 22*(7), 3018–3021.

Zhang, M. Q. and M. Z. Rong (2011). Theoretical consideration and modeling of self-healing polymers. *Journal of Polymer Science Part B: Polymer Physics*, 1–13.

Zhang, M. Q. and M. Z. Rong (2012). Theoretical consideration and modeling of self-healing polymers. *Journal of Polymer Science Part B: Polymer Physics 50*(4), 229–241.

Zhao, R. and C. W. Macosko (2002). Slip at polymer-polymer interfaces: Rheological measurements on coextruded multilayers. *Journal of Rheology 46*(1), 145–167.

Zhao, R. and C. W. Macosko (2007). Polymer-polymer mutual diffusion via rheology of coextruded multilayers. *AIChE Journal 53*(4), 978–985.

Zhou, Y. (Ed.) (2008). *Microjoining and Nanojoining*. Woodhead Publishing.

Zoubeir, T. and G. Elhem (2011). Numerical study of laser diode transmission welding of a polypropylene mini-tank: Temperature field and residual stresses distribution. *Polymer Testing 30*(1), 23–34.

www.m-tech.aau.dk

ISBN: 87-91464-54-4

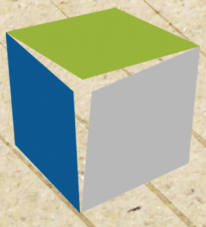

Materials Science and Engineering Group
Department of Mechanical and Manufacturing Engineering
Faculty of Engineering and Science
Aalborg University
Denmark